ASTROCYTE-DERIVED NITRIC OXIDE IN MANGANESE NEUROTOXICITY: FROM CELLULAR AND MOLECULAR MECHANISMS UNDERLYING SELECTIVE NEURONAL VULNERABILITY IN THE BASAL GANGLIA TO POTENTIAL THERAPEUTIC MODALITIES

A Dissertation

by

XUHONG LIU

Submitted to the Office of Graduate Studies of
Texas A&M University
in partial fulfillment of the requirements for the degree of

DOCTOR OF PHILOSOPHY

December 2005

Major Subject: Toxicology

ASTROCYTE-DERIVED NITRIC OXIDE IN MANGANESE NEUROTOXICITY: FROM CELLULAR AND MOLECULAR MECHANISMS UNDERLYING SELECTIVE NEURONAL VULNERABILITY IN THE BASAL GANGLIA TO POTENTIAL THERAPEUTIC MODALITIES

A Dissertation

by

XUHONG LIU

Submitted to the Office of Graduate Studies of
Texas A&M University
in partial fulfillment of the requirements for the degree of

DOCTOR OF PHILOSOPHY

Approved by:

Co-Chairs of Committee,	Ronald B. Tjalkens
	Evelyn Tiffany-Castiglioni
Committee Members,	Louise C. Abbott
	Rajesh C. Miranda
Chair of Toxicology Faculty	Robert C. Burghardt

December 2005

Major Subject: Toxicology

ABSTRACT

Astrocyte-derived Nitric Oxide in Manganese Neurotoxicity:

From Cellular and Molecular Mechanisms

Underlying Selective Neuronal Vulnerability in the Basal Ganglia

to Potential Therapeutic Modalities. (December 2005)

Xuhong Liu, M.D., Harbin Medical University;

M.S., Harbin Medical University

Co-Chairs of Advisory Committee: Dr. Ronald B. Tjalkens
Dr. Evelyn Tiffany-Castiglioni

Chronic exposure to manganese (Mn) causes the neurodegenerative movement disorder, manganism. A mouse model was developed to elucidate mechanisms involved in the etiology and progression of injury. Twelve-week old female C57Bl/6J mice were exposed to $MnCl_2$ (100 mg/kg/day) by oral gavage daily for 8 weeks. After the experiment striatal dopamine (DA) content was decreased with the manifestation of hypoactivity. A distinct population of neurons was vulnerable to the effects of Mn, including enkephalin (ENK)-positive projection neurons, interneurons expressing neuronal nitric oxide synthetase (nNOS/NOS1), and choline acetyltransferase (ChAT)-expressing interneurons. Activation of surrounding astrocytes occurred with expression of inducible nitric oxide synthase (iNOS/NOS2) and production of nitric oxide (NO)/peroxynitrite ($ONOO^-$). Activated astrocytes were detected primarily near the microvasculature in both the striatum and globus pallidus (GP). It is suggested that Mn

exposure may damage the blood-brain barrier (BBB) and induce astrocytosis and NOS2 expression, subsequent NO production may cause the death of adjacent neurons.

This hypothesis was also tested in an *in vitro* co-culture model. Differentiated pheochromocytoma cells (PC12 cells) were co-cultured with primary astrocytes and exposed to Mn and inflammatory cytokines. Mn and cytokines induced NOS2 expression and NO production in astrocytes, which correlated with apoptosis of PC12 cells. Apoptosis of PC12 cells was prevented by overexpression of a phosphorylation-deficient mutant of IκBα that inhibited NOS2 expression in astrocytes. It is concluded that Mn-and cytokine-dependent apoptosis in PC12 cells requires astrocyte-derived NO and nuclear factor κB (NF-κB)-dependent expression of NOS2.

To explore possible means of interdicting this inflammatory process in astrocytes, a noval pharmacologic ligands of the peroxisome proliferator-activated receptor gamma (PPARγ) agonist, 1,1-Bis(3'-indolyl)-1-(p-trifluoromethylphenyl) methane (DIM-C-pPhCF_3) were used in the same co-culture system. DIM-C-pPhCF_3 protected PC12 cells from apoptosis through inhibition of NOS2 expression in astrocytes after Mn and cytokines exposure. By contrast, the PPARγ antagonist, 2-chloro-5-nitrobenzanilide (GW9622), had the opposite effect, increasing both NO production in astrocytes and neuronal injury. It is concluded that PPARγ is involved in the regulation of NOS2 expression in astrocytes and that agonists of PPARγ may represent a potential treatment method for Mn neurotoxicity.

DEDICATION

This dissertation is dedicated

to my incredible parents, Ms Mingqing Fu and Dr Jiayin Liu,

with their unconditional love, I have the courage to face all the difficulties to live in a new world and explore a new career in my life

to my beloved husband, Jijun Zhou,

whose unselfish love and patience

has made all the difference and who has made my life full of hope and color

to my dear daughter, Evelyn Zhou,

who grows with it and

has made my life so meaningful

to my brother, Xudong Liu ,whose brotherly love has protected

and saved me from many hurdles in life

ACKNOWLEDGEMENTS

Successful completion of the research that comprises this dissertation is not a singular effort but involves the dedicated support of many individuals. For this reason, I wish to acknowledge my dissertation advisor, Dr. Ronald Tjalkens, for his continual, patient mentoring and for providing a friendly and exciting research environment filled with possibilities, as well as for his open and enthusiastic character encouraging me to overcome the difficulties. Additionally, Dr. Evelyn Tiffany-Castiglioni has always been a great co-mentor, who not only gave me knowledge but also offered me a great opportunity to study a new area under a different culture and language and most importantly a chance to face challenge. Western blot and co-culture techniques which I learned in her lab added great value to my research. I am also indebted to the considerable help and expertise of Dr. Louise Abbott, who directed the behavior, neuroanatomy and immunohistochemistry in animal studies and Dr. Thomas Champney, who helped with dopamine and GABA detection in mouse striatum and also Dr. Jack Nation, who directed the behavior study of animals; Dr. Les Dees, who directed animal dosing. I also appreciate Dr. Stephen Safe, Dr. Western Porter, Dr. Bill Hanneman, Dr. Yongchang Qian and Dr. David Brenner at Columbia University for experimental and technical support. For sure, I would not forget Dr. Rajesh Miranda's great advice on our research which has contributed to the big progress we made toward the final conclusions.

Also I want to thank my lab-mates: Jennifer Faske, Tyler Wright, Julie Buffington, and other graduate students: Robin Johnson, Carolyn Broccardo who have provided me with all kinds of support during my years in graduate school.

NOMENCLATURE

5-HT:	5-hydroxytryptamine (serotonin)
5-HTP:	5-hydroxytryptophan
ACh:	acetylcholine
ACTR:	activator of the thyroid and retinoic acid receptors
ADP:	adenosine diphosphate
AIB-1:	amplified in breast carcinoma
ATF:	activating transcription factor
ATP:	adenosine triphosphate
BBB:	blood–brain barrier
BH_4:	tetrahydrobiopterin
CaM:	calmodulin
CB:	calcium-binding protein calbindin
CBP:	CREB-binding protein
cGMP:	cyclic guanosine monophosphate
ChAT:	choline acetyltransferase
CO:	carbon monoxide
CREB:	cyclic AMP response element binding protein
CSF:	cerebrospinal fluid
DA:	dopamine
DBD:	DNA binding domain

DCT1: divalent cation transporter-1

DIM-C-pPhCF$_3$: 1,1-Bis(3'-indolyl)-1-(p-trifluoromethylphenyl)methane

DMT-1: divalent metal transporter-1

DOPAC: 3,4-dihydroxyphenylacetic acid

dUTP: deoxyuridine triphosphate

DYN: dynorphin

EAA: excitatory amino acid

ECM: extracellular matrix

EDTA: ethylenediaminetetraacetic acid

ENK: enkephalin

ERK: extracellular signal-regulated kinase

ETC: electron transport chain

FAD: flavin-adenine dinucleotide

FMN: flavin-mononucleotide

GABA: gamma-aminobutyric acid

GAD: glutamic acid decarboxylase

GAPDH: glyceraldehyde-3-phosphate dehydrogenase

GC: guanylate cyclase

GFAP: glial fibrillary acidic protein

GLAST: glutamate/aspartate transporter

GP: globus pallidus

Gpe: external segment of the globus pallidus

Gpi:	internal segment of the globus pallidus
GRIP-1:	glucocorticoid receptor interaction protein
GS:	glutamine synthetase
GSH:	glutathione
GW9622:	2-chloro-5-nitrobenzanilide
HAT:	histone acetyltransferase
HPLC:	high performance liquid chromatography
ICP-MS:	inductively-coupled plasma-mass spectrometry
IKK:	IκB kinase
IL-1:	interleukin-1
LDH:	lactate dehydrogenase
MMT:	methylcyclopentadienyl manganese tricarbonyl
Mn:	manganese
MnSOD:	mitochondrial superoxide dismutase
MRI:	magnetic resonance imaging
NAD:	nicotinamide adenine dinucleotide
NADH:	nicotinamide adenine dinucleotide, reduced form
NADPH:	nicotinamide adenine dinucleotide phosphate, reduced form
NADPH-d:	nicotinamide adenine dinucleotide phosphate-diaphorase
NCoA-1:	nuclear receptor coactivator-1
NCoA-2:	also known as TIF-2 or GRIP-1
NF-κB:	nuclear factor κB

NMDA:	*N*-methyl-D-aspartate
NO:	nitric oxide
NOS:	nitric oxide synthase
NOS1, nNOS:	neuronal nitric oxide synthase
NOS2, iNOS:	immunologic nitric oxide synthase
NOS3, eNOS:	endothelial nitric oxide synthase
NPY:	neuropeptide Y
Nramp2:	natural resistance associated macrophage protein 2
$ONOO^-$:	peroxynitrite
p/CAF:	CBP associated factor
p/CIP:	p300/CBP cointegrator-associated protein (also known as RAC-3, AIB-1, ACTR, and TRAM-1)
PARP:	poly (ADP-ribose) polymerase
PAS:	para-aminosalicylic acid
PC12 cells:	pheochromocytoma cells
PD:	Parkinson's disease
PDZ domain:	PSD-95 discs large/ZO-1 homology domain
PEPCK:	phosphoenolpyruvate carboxykinase
PET:	positron emission tomography
PPARγ:	the peroxisome proliferator-activated receptor γ
PSD-95:	post synaptic density protein 95
PT:	permeability transition

PV:	pavalbumin
RAC-3:	receptor-associated coactivator-3
RXRs:	retinoid X receptors
SNc:	substantia nigra pars compacta
SNr:	substantia nigra pars reticulata
SOD:	superoxide dismutase
SOM:	somatostatin
SP:	substance P
SRC-1:	steroid receptor-coactivator-1
STN:	subthalamic nucleus
TCA:	tricarboxylic acid
TdT:	Terminal deoxynucleotidyl Transferase
Tf:	transferrin
TH:	tyrosine hydroxylase
TIF-2:	transcriptional intermediate factor-2
TPN:	total parenteral nutrition
TUNEL:	terminal deoxynucleotidyl transferase-mediated dUTP-biotin nick-end labeling
Ψm:	mitochondrial membrane potential

TABLE OF CONTENTS

Page

Page

LIST OF FIGURES

FIGURE Page

CHAPTER I

INTRODUCTION

The Basal Ganglia Function: Physiology and Pathophysiology

Anatomy of the Basal Ganglia

The basal ganglia are a group of grey matter structures lying at the base of the forebrain surrounding the thalamus and hypothalamus involved in the control of movement and cognition. They are composed of three groups of nuclei: (1) the caudate nucleus, putamen and ventral striatum, which together are referred to as the striatum; (2) the GP or pallidum, which comprises an internal and an external segment, as well as a ventral extension; and (3) the closely related subthalamic nucleus (STN) and substantia nigra (SN) (Parent, 1996).

The human striatum is composed of both projection neurons (Golgi type I cells) and interneurons (Golgi type II cells) (Parent, 1996). The projection neurons greatly outnumber interneurons in the striatum (Graveland and DiFiglia, 1985). Despite their relatively small number, interneurons have been shown to exert a powerful control on the activity of projection neurons in the striatum.

There are two types of spiny striatal projection neurons which use GABA as their main neurotransmitter (Oertel et al., 1983), but also coexpress a number of neuroactive peptides. One type of neurons expresses substance P (SP) and dynorphin (DYN), the

---

This thesis follows the style of Journal of Neuroscience.

other type of projection neurons expresses ENK. The physiological role of the various neuroactive peptides remains to be established.

The striatal interneurons can be grouped into two broad categories according to their cell diameters: (1) the medium aspiny interneurons, and (2) the giant aspiny interneurons (DiFiglia et al., 1976). The medium interneurons have been further divided into three subcategories on the basis of their neurochemical content. The first type displays intense immunoreactivity for GABA and/or its synthesizing enzyme glutamic acid decarboxylase (GAD) and also contains pavalbumin (PV) (Cowan et al., 1990). The second type displays immunoreactivity for somatostatin (SOM) (Desjardins and Parent, 1992), neuropeptide Y (NPY), and contains the enzyme nicotinamide adenine dinucleotide phosphate-diaphorase (NADPH-d) or NOS1 (Smith and Parent, 1986). These neurons form approximately 2% of the total neuronal population and may use NO for interneuronal communication (Selden et al., 1994). A third type of interneurons, more recently discovered, expresses calretinin (CR) (Cicchetti et al., 1998). The giant interneurons display immunoreactivity for ChAT, the enzyme that synthesizes acetylcholine (ACh), and are thus considered as the cholinergic neurons of the striatum. These neurons are also enriched in acetylcholinesterase (AChE) (Eckenstein and Sofroniew, 1983) and represent approximately 1–2% of the total cell population of the human striatum (Holt et al., 1996). A significant proportion of these neurons also expresses CR in humans (Cicchetti et al., 1998). Double-antigen localization studies showed that virtually all large CR+, cholinergic neurons express SP (neurokinin-1) receptors (SPR) in monkey and human striatum (Parent et al., 1995). They are major

targets of SP+ fibers derived principally from the GABA+/SP+ projection neurons in human and rat striatum (Gerfen, 1991). Electron microscope studies have shown that cholinergic striatal interneurons also receive inputs from the substantia nigra pars compacta (SNc) dopaminergic neurons, as well as from glutamatergic neurons of the intralaminar thalamic nuclei and cortical neurons (Dimova et al., 1993; Contant et al., 1996; Sidibe and Smith, 1999). Cholinergic interneurons also express high levels of δ opioid receptors (Mansour et al., 1994b).

The striatum is subdivided into two major compartments — the striosomes (or patches) and the extrastriosomal matrix. The AChE-poor striosomes represented approximately 10–20% of the total striatal volume and are embedded in an AChE-rich matrix (Graybiel and Ragsdale, 1978). The striosomes are also characterized by low tyrosine hydroxylase (TH) and high ENK immunoreactivity. Calcium-binding protein calbindin (CB) is one of the most reliable chemical markers of the matrix. In addition, immunoreactivity for PV is mainly confined to the matrix in human and other species. By contrast, CR+ neuropil appears more intense in the striosomes than in the matrix (Prensa et al., 1999).

Hypothesis of Basal Ganglia Function

Lesions of the basal ganglia in humans lead to motor disorders that range from hypokinesia (e.g., PD) to hyperkinesia (e.g., hemiballismus and chorea). Furthermore, the basal ganglia circuits are thought to be involved in psychotic disorders, such as schizophrenia, and mediate behavioral effects of drugs of abuse. Therefore, it is important to understand how basal ganglia control motor movement and cognitive

function through the feedback loop from the cerebral cortex through the striatum to the pallidum to the thalamus and back to the cerebral cortex.

The striatum is the major recipient structure of the basal ganglia. It receives inputs from (1) cerebral cortex (glutamic acid); (2) intralaminar nuclei of the thalamus (glutamic acid); (3) SNc (DA); (4) the raphe nuclei (5-HT); and (5) portions of the lateral amygdala (Parent and Hazrati, 1995). The internal segment of the globus pallidus (GPi) and substantia nigra pars reticulata (SNr) are the two major output structures of the basal ganglia.

The striatum receives direct excitatory cortical inputs mediated by glutamate, and projects to GPi and SNr, through two major inhibitory projection systems, the direct and indirect pathways. The direct pathway arises from GABA+/SP+ striatal neurons, and projects monosynaptically to the GPi/SNr. The indirect pathway arises from GABA+/ENK+ striatal neurons, and projects first to the external segment of the globus pallidus (GPe), GPe neurons then in turn inhibit STN and GPi/SNr. GPi and SNr neurons can inhibit neurons in the thalamus sending excitatory inputs back to the cortex, thus closing the so-called cortico-striato-pallido-thalamo-cortical loop (Figure 1.1) (Parent and Hazrati, 1995). The STN can also receive direct cortical projections, especially from the frontal lobe (Alexander and Crutcher, 1990), then send excitatory projections to GPi and SNr which will in turn projects to the thalamus and cortex, forming the cortico-subthalamo-pallido-thalamo-cortical loop (Parent and Cicchetti, 1998).

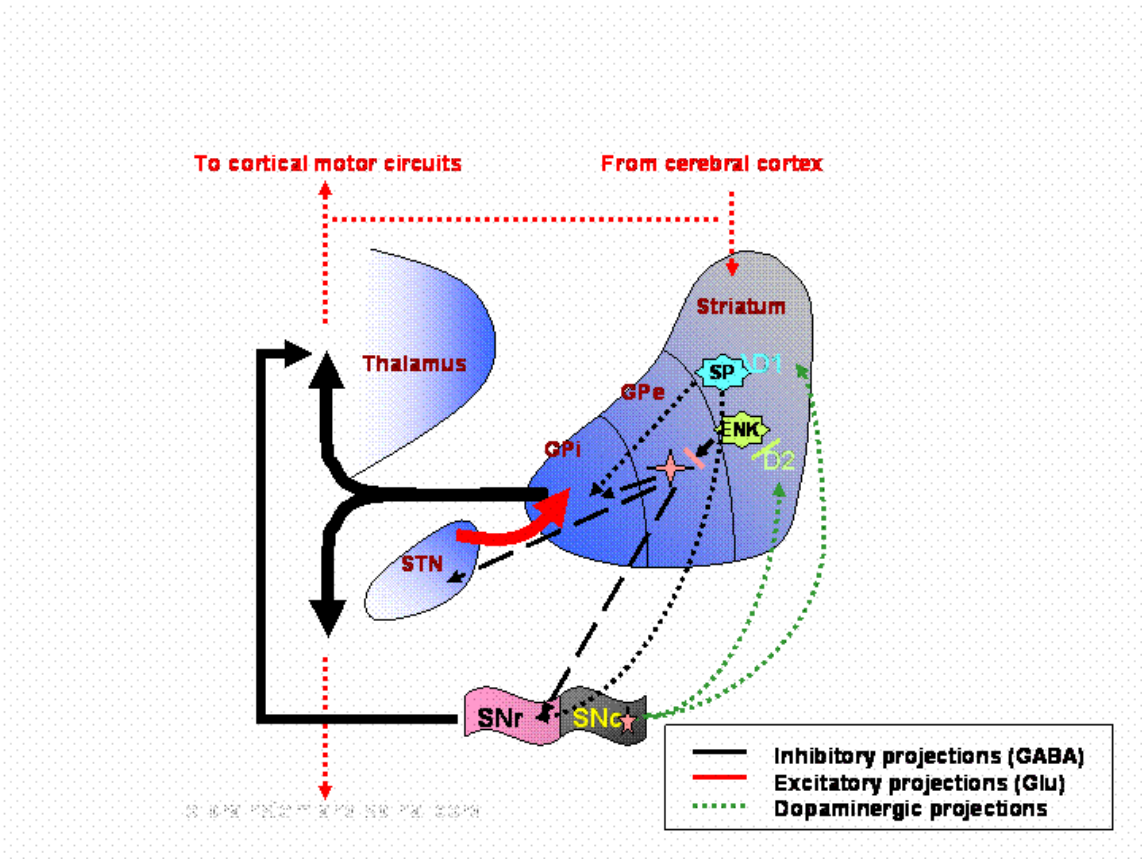

Figure 1.1. Cortico-striato-pallido-thalamo-cortical Loop. Figure adapted from (Wichmann and DeLong, 1996; DeLong, 2000).

DA input from SNc can differentially affect striatal projection neurons based on the DA receptor subtypes (Gerfen et al., 1990). DYN/SP+ neurons of the direct pathway express D1 receptor and their activity can be enhanced by DA; whereas indirect pathway ENK+ neurons express D2 receptor and are inhibited by DA (Gerfen and Young, 1988). Activation of the direct pathway results in reduction of tonic inhibitory basal ganglia output, therefore, disinhibition of thalamocortical neurons and facilitation of movement. By contrast, activation of indirect pathway leads to increased basal ganglia output and suppression of movement. The overall effect of striatal DA release is to reduce basal

ganglia output, leading to increased activity of thalamocortical projection neurons (Wichmann and DeLong, 1996).

Besides the above motor circuit concerned with learned movement, there are also three other circuits related with the basal ganglia. Cognitive circuit is concerned with motor intentions (from prefrontal cortex to the head of caudate nucleus, through putamen, GP and ventral anterior nucleus of the thalamus, then back to the premotor cortex and prefrontal cortex); limbic circuit is concerned with emotional aspects of movement (from inferior prefrontal cortex, through the nucleus accubens and ventral pallidum, with return via the mediodorsal nucleus of the thalamus to the inferior prefrontal cortex); and oculomotor circuit is concerned with voluntary saccades (from the frontal eye field and posterior parietal cortex, through the caudate nucleus and SNr, to the ventral anterior nucleus of the thalamus, then back to the frontal eye field and prefrontal cortex) (FitzGerald and Folan-Curran, 2002).

Interaction between Different Neurotransmitters

Properly regulated balance between DA and ACh within the striatum is of fundamental importance for extrapyramidal motor control (Graybiel et al., 1994). DA exerts a tonic inhibitory effect on ACh release via D2-like DA receptors on cholinergic interneurons. ENK can also inhibit ACh release by δ receptors (Mulder et al., 1984). On the contrary, glutamate and SP represent the major excitatory drive to increase ACh release (Pisani et al., 2003).

One study shows that the specific function of DYN and ENK is to dampen excessive activation of these neurons by DA and other neurotransmitters. Levels of these

opioid peptides are elevated by repeated, excessive activation of these pathways, which appears to be an adaptive or compensatory response (Steiner and Gerfen, 1998). Opioid peptide DYN could inhibit DA release by the following mechanisms: a. DA neurons express kappa receptors (Mansour et al., 1994a). Released in the SN from terminals of striatonigral neurons (You et al., 1994), DYN could act on inhibitory kappa receptors on DA neurons to inhibit nigrostriatal activity and DA release in the striatum (Reid et al., 1988). b. DYN in the striatum may also play a role in ACh-regulated DA release (Gauchy et al., 1991). Via their presynaptic localization, stimulation of kappa opioid receptors also directly inhibits calcium-dependent glutamate release. Opioid peptide ENK is an endogenous ligand of δ and μ opioid receptors, which are expressed in the striatum (Mansour et al., 1994b). Cholinergic interneurons seem to express high levels of δ receptors (Mansour et al., 1994b), which inhibit ACh release (Mulder et al., 1984). Striatal δ-opioid agonist can stimulate DA and glutamate release. Glutamate and DA depresses striatal preproenkephalin mRNA levels (Ravenscroft and Brotchie, 2000). Some experimental studies show that ENK can decrease GABA release in the GPe from the same terminals while DYN reduces glutamate release in GPi. Both effects reduced stimulation of Gpi and SNr which in turn will have less inhibitory effect on cortico-thalamic traffic and possibly reduce akinesia (Maneuf et al., 1995; Henry and Brotchie, 1996).

DA can stimulate action potential- and calcium- dependent glutamate release from striatal terminals arising from the prefrontal cortex (McGinty, 1999). By way of their postsynaptic localization, muscarinic receptors directly stimulate glutamate release

and inhibit the response of medium spiny neurons to D1 receptor stimulation but will stimulate ENK+ neurons (Ferre et al., 1997). *N*-methyl-D-aspartate receptor (NMDAR) stimulation increases striatal NO synthesis, either directly or via stimulation of ACh release by interneurons, leading to muscarinic activation of NOS1-positive cells.

Parkinson's Disease, Parkinsonism and Manganism

Parkinson's Disease (PD) and Parkinsonism

In 1817 British physician James Parkinson first described a motor disorder that now bears his name (Parkinson, 2002). PD or paralysis agitans is a progressive neurodegenerative disorder and has an unknown etiology. Risk for development of PD is attributed primarily to age but also to interaction between the environment and an individual's specific genotype (Paganini-Hill, 2001). Postmortem studies have established degeneration of nigrostriatal DA as the hallmark of PD (Kish et al., 1988). The main anatomic and biochemical characteristic of PD is the loss of dopaminergic neurons in the SNc. Neuronal loss decreases striatal DA concentrations, a process thought to underlie the clinical manifestation of the disease. Fluorodopa positron emission tomography (PET) is abnormal in PD and shows reduced striatal uptake particularly in the posterior putamen (Calne and Snow, 1993).

In addition to PD, a spectrum of disorders of the basal ganglia is termed as parkinsonism. Parkinsonism is a clinical syndrome dominated by disorders of movement similar to PD which consists of akinesia, rigidity, tremor, and postural abnormalities. The use of the term akinesia often encompasses akinesia itself (loss of movement), bradykinesia (slowness of movement), and hypokinesia (reduced movement). Akinesia

can be caused by neurodegenerative disorders (multiple system atrophy, progressive supernuclear palsy, corticobasal degeneration, dementia with Lewy bodies, Alzheimer's disease, pallidal degeneration, rigid variant of Huntington's disease, Pick's disease) or various secondary causes (antidopaminergic drugs induced, arteriosclerotic pseudoparkinsonism, hydrocephalus, postencephalitis, post-trauma, space-occupying lesions, toxin-induced: MPTP, CO, **Mn**, post anoxic encephalopathy and Wilson's disease) (Bogousslavsky and Fisher, 1998).

Disorders that affect the SNc (such as PD) can be differentiated from those affecting the striatum or GP (such as most of parkinsonism) by their clinical picture and response to L-DOPA of patients (Olanow, 1992; Hughes et al., 2001). Patients with damage confined to the SNc have a clinical feature characterized by resting tremor and a good response to L-DOPA. On the other hand, patients with damage involving the striatum or GP tend to have early speech, gait and balance dysfunction without resting tremor and with little, if any, response to L-DOPA.

Manganism and PD

Manganism, like other parkinsonian disorders, resembles PD in its late phase, but has several distinguishing features (Beuter et al., 1994; Calne et al., 1994; Pal et al., 1999). Although generalized bradykinesia and rigidity are found in both syndromes, dystonia is a neurological sign attributed to the damage of the GP in manganism (Calne, Chu et al. 1994) and is only minimally observed in PD patients. Other features of manganism that differ from PD include less frequent resting tremor, a propensity to fall backward and "cock walk", little or no sustained response to L-DOPA therapy, and

normal fluorodopa uptake, as observed by PET (Calne, Chu et al. 1994; Pal, Samii et al. 1999).

Physiology of Manganese

Physiological Functions of Manganese

Mn, a trace mineral that functions both as an enzyme activator and as a component of metalloenzymes (an enzyme that contains a metal ion in its structure), was first shown to be an essential nutrient in 1931 (Kemmerer et al., 1931). Mn is a co-factor for a large number of enzymes and enhances catalysis by binding either to the enzyme or substrate. Mn can be replaced in many of these interactions by other divalent metal ions, particularly Mg^{2+}. An exception is the Mn-specific activation of glycolsyltranserferases, which are important in bone formation. Another example is phosphoenolpyruvate carboxykinase (PEPCK), the enzyme that catalyzes the conversion of oxaloacetate to phosphoenolpyruvate. A third example is glutamine synthetase (GS), an enzyme involved in the biosynthesis of glutamine from the excitatory amino acid neurotransmitter glutamate (Keen et al., 1999).

Mn also functions as a constituent of the following metalloenzymes: arginase, a cytosolic enzyme in the liver responsible for creating urea, a component of urine; pyruvate decarboxylase, an enzyme that participates in the metabolism of blood sugar; and Mn-dependent mitochondrial superoxide dismutase (MnSOD), an enzyme with antioxidant activity that protects tissues from the damaging effects of free radicals (Crowley et al., 2000; Keen et al., 2000; Takeda, 2003).

Mn can also interact with the cell surface integrin receptor (vitronectin receptor, CD29) and extracellular matrix (ECM) proteins (Gailit and Ruoslahti, 1988; Hemler, 1990; Smith and Cheresh, 1990; Reichardt and Tomaselli, 1991; Humphries, 1996) in an RGD (Arg/Gly/Asp)-dependent process. Many studies have revealed that the vitronectin receptor upon binding to Mn and ECM can regulate attachment, tumorigenicity, differentiation, proliferation, and migration of cells (Yanai et al., 1991; Lein et al., 2000). Also, through its interaction with the vitronectin receptor, Mn can stimulate several different signal transduction pathways in the cell, including the mitogen activated protein (MAP) kinases, extracellular signal responsive kinase 1 and 2 (ERK1 and 2), and the stress activated kinase, p38 (Yanai et al., 1991; Roth et al., 2000).

Absorption and Distribution of Mn under Physiological Conditions

Under normal conditions about 1-5% of dietary Mn is absorbed into the body by the gastrointestinal tract (Davidsson et al., 1988; Davis et al., 1993). Studies in animals indicate that most of the Mn is transported into the liver, a depot of Mn, via the portal vein and is eliminated through biliary excretion (Ballatori et al., 1987). As such, it would not reach the brain or other systemic tissues in significant amounts. The molecular details of oral Mn absorption are not well understood. It has been reported that dietary Mn, which might be divalent, can be oxidized to trivalent Mn, probably by ceruloplasmin (Archibald and Tyree, 1987; Aschner and Aschner, 1991). Transferrin (Tf) , the principal Fe-carrying protein of the plasma, is a plasma carrier protein for trivalent Mn (Aisen et al., 1969), and Tf-bound Mn is mainly detected in the bloodstream after oral administration of Mn (Davidsson et al., 1989). There is also evidence suggesting an

active transport process (Garcia-Aranda et al., 1983), as well as a simple passive diffusion-like process (Bell et al., 1989). Furthermore, there are many factors that have been found to affect Mn absorption, including dietary Mn levels (Britton and Cotzias, 1966; Malecki et al., 1996), dietary levels of various minerals (Davidsson et al., 1991; Lai et al., 1999; Planells et al., 2000), age and developmental state of the infant (Keen et al., 1986), and especially iron status. There seems to be an inverse relationship between body iron stores and Mn absorption, perhaps due to competition for the same transport machinery, Tf. Several studies have demonstrated that Fe deficiency increases transport of orally administered Mn into the body as well as delivery to the brain (Erikson et al., 2002).

Absorption of Mn via the lungs has only recently been investigated and it seems to depend largely on particle solubility. $MnCl_2$ or $MnSO_4$ which are soluble salts, can be quickly taken into the bloodstream. Insoluble MnO_2 given at similar doses is very slowly absorbed and at much lower overall levels (Roels et al., 1997; Dorman et al., 2001).

Physiological Mn concentrations in serum are in the range of 0.8-2.1 μg Mn/L (~20nM) (Keen et al., 2000). Thermodynamic modeling of Mn^{2+} in serum suggests it exists in several forms, including an albumin or β1-globulin-bound species (84%), as a hydrated ion (6.4%) and in 1:1 complexes with HCO_3^- (5.8%), $citrate^{3-}$ (2.0%) and other small molecular weight ligands (1.8%) (Foradori et al., 1967; Harris and Chen, 1994). Free plasma and tissue Mn concentrations tend to be extremely low (Cotzias et al., 1968). A small percentage of trivalent Mn in serum is found 100% complexed to Tf (Aisen et al., 1969; Harris and Chen, 1994).

Distribution of Mn to the body tissues is fairly homogeneous. An increased concentration of Mn is found in tissues rich in mitochondria and pigmentation. Bone, liver, pancreas, and kidney tend to have higher Mn levels than other tissues (Rehnberg et al., 1980).

Delivery and Distribution of Mn in the Central Nervous System (CNS)

Transport of Mn into the CNS

Several reports implicate three sites of Mn entry into the brain: cerebral capillary endothelial cells of the BBB (Rabin et al., 1993), the choroid plexuses into cerebrospinal fluid (CSF) and then into the brain (Murphy et al., 1991) and the olfactory nerve (Brenneman et al., 2000). At physiological serum Mn concentrations, Mn influx is reported to be non-saturable and occurs primarily through the capillary endothelium of the BBB, while Mn influx at high plasma concentrations is saturable and occurs primarily via the CSF (Murphy et al., 1991; Rabin et al., 1993). The chemical speciation of Mn also affects its diffusion and transport into the brain. Although Mn can assume numerous oxidation states (11 in total, ranging from 3- to 7+), in mammalian tissues it is found in only three oxidation states (2+, 3+ and 4+) (Archibald and Tyree, 1987; Keen et al., 2000). It is unclear yet whether there is a predominant Mn species crossing the BBB, and if so, the identity of that species. One recent study suggests that Mn citrate may be a significant chemical species of Mn transferred across the BBB, Mn bound to small molecular weight ligands in plasma can enter the brain more rapidly than the hydrated Mn ion (Crossgrove et al., 2003).

The mechanism by which Mn is transported into the CNS at physiological plasma level remains controversial. There are two distinct but related mechanisms: a Tf-dependent and a Tf-independent pathway. Which of the two uptake mechanisms functionally predominates is unknown, but the transport mechanism is likely to be cell-type specific and may depend on the quantity of Tf receptors (TfRs) on the cell surface (Roth and Garrick, 2003).

Several lines of evidence strongly suggest that trivalent Mn is transported by Tf through the brain capillary endothelium. For instance, TfRs are present on the surface of cerebral capillaries (Pardridge et al., 1987) and endocytosis of Tf is known to occur in these capillaries. Also high concentrations of TfRs are located in the nucleus accumbens and caudate putamen, which provide efferent fibers to areas rich in Mn (ventral pallidum, the GP and SN), suggesting that these sites may accumulate Mn via Tf-mediated axonal transport (Sloot and Gramsbergen, 1994). In addition, Fe and Mn compete for the same carrier transport system. Plasma Fe overload significantly decreases uptake of Mn across the BBB, whereas Fe deficiency is associated with increased CNS burden of Mn (Aschner and Aschner, 1990). It is noteworthy that Tf-complexed Mn is exclusively present in the trivalent oxidation state (Aisen et al., 1969). Although the Tf-dependent transport is presumably responsible for much of the uptake of Mn, several critical steps within this pathway have not been definitively shown to occur during Mn import into cells. For example, a requirement for acid-dependent release of Mn from the Tf/TfR complex and the subsequent reduction of Mn by ferric reductase or a comparable enzyme within endosomes have not been demonstrated. Thus,

additional studies are needed to characterize fully the mechanism for Mn uptake by the Tf-dependent pathway (Roth and Garrick, 2003). In addition, Tf is not required to achieve or maintain normal brain Mn levels in mice with very low plasma Tf levels (Malecki et al., 1999), suggesting that Tf-independent mechanisms can maintain brain Mn homeostasis. Some studies show that the Tf-dependent route of Mn brain entry appears to play a limited role in total Mn uptake (Malecki, 2001a).

In the absence of Tf, carrier-mediated Mn transport has been demonstrated in cultured brain endothelial cells (Aschner et al., 2002b; Crossgrove et al., 2003), in Caco-2 cells from the apical, but not basolateral, side (Leblondel and Allain, 1999) and in astrocytes (Aschner et al., 1992). However, none of these studies has identified the transporter(s) at the BBB or on many other cell membrane surfaces. It has been hypothesized that the transmembrane divalent metal transporter-1 (DMT-1, a.k.a. divalent cation transporter [DCT1], natural resistance associated macrophage protein 2 [Nramp2], transporter family gene name: SLC11A2) plays a role in brain Mn uptake. DMT-1 has a very broad substrate specificity and is likely the major transmembrane protein responsible for the uptake of a variety of divalent cations, including Fe^{2+}, Mn^{2+}, Cd^{2+}, Co^{2+}, Ni^{2+}, Cu^{2+}, and Pb^{2+} (Gunshin et al., 1997). Mn has a relatively high affinity for DMT-1. There is evidence that DMT-1 transports Mn^{2+} at the cell membrane or translocates it from endocytosed vesicles (Chua and Morgan, 1997). Studies on the function of DMT-1 have been greatly assisted by the use of the Belgrade rat and the microcytic mouse which possess identical G185R mutations that result in an inactive form of DMT-1 (Fleming et al., 1997b; Fleming et al., 1998b). The fact that both Fe and

Mn uptake in brain are decreased in the Belgrade animals (Farcich and Morgan, 1992; Burdo et al., 1999; Zywicke et al., 2002) strongly suggests that DMT-1 is critical for the transport of both metals. This hypothesis is controversial, however, as a recent study suggests that DMT-1 is not a major mechanism of the carrier-mediated uptake of Mn into brain at the BBB (Crossgrove and Yokel, 2004). In addition to DMT-1, there is also evidence of Mn transport via voltage regulated Ca^{2+} channels (Lucaciu et al., 1997; Kannurpatti et al., 2000). Increased uptake of Mn by depolarization of cell membranes can be prevented by several Ca^{2+} channel blockers. Similarly, increased transport of Mn has also been demonstrated when glutamate binds to its Ca^{2+}-coupled receptor (Kannurpatti et al., 2000). It is reasonable to assume that opening of the Ca^{2+} gated channel may augment Mn uptake with the potential for enhanced cytotoxicity (Roth and Garrick, 2003).

Delivery of inhaled Mn to the brain is likely to occur through direct intra-axonal transport via the olfactory system (Tjalve and Henriksson, 1999; Dorman et al., 2002). The nasal route of uptake was reported to account for more than 90% of Mn taken up into the rat olfactory bulb following acute inhalation exposure for up to 8 days (Brenneman et al., 2000). However, the significance of the contribution of this pathway to Mn toxicity is not clear (Tjalve et al., 1996; Dorman et al., 2002). Furthermore, the physiological and anatomic differences between human and rodent nasal and brain complicate the interpretation of comparative studies. Thus, additional studies are necessary to evaluate the importance of the olfactory route of entry of Mn in humans.

Regional Distribution of Mn in the CNS

Distribution of Mn in the brain is not homogeneous and even different from species to species. Magnetic resonance imaging (MRI) techniques show that, in exposed humans and macaque monkeys, Mn concentrations are highest in the striatum, GP, and SNr (Eriksson et al., 1992; Nagatomo et al., 1999). An analysis by flameless atomic absorption spectrometry showed that Mn concentrations are higher in the striatum, GP, SN and white matter of the cerebral cortex in the human brain of control cases. However, in chronic Mn poisoning cases, Mn concentrations are increased in the grey matter of the cerebral cortex and are decreased in the basal ganglia (Yamada et al., 1986). In contrast, the results from rodents are more variable, with significant elevation in cerebellar Mn content (Takeda et al., 1994). A very recent study showed that, after dietary Fe deprivation, Mn accumulated in the GP, hippocampus, and SN of rat brain which are normally rich in Fe (Erikson et al., 2002). Still, considerable evidence also suggests that Mn intoxication preferentially affects the GP. For instance, systemically administered radiolabeled Mn primarily accumulates in the GP (Dastur DK, 1968). Also, several reports indicate that Mn intoxication in humans and animal models is associated with pathologic changes that are most pronounced in the GP: loss of neurons, decreased numbers of myelinated fibers and gliosis (Pentschew et al., 1963; Yamada et al., 1986). These different conclusions may, in part, be explained by the relative sensitivity of the analytical techniques that are used (i.e., direct chemical analysis of brain Mn by atomic absorption spectrometry or neutron activation analysis or MRI).

Cellular Uptake and Subcellular Distribution of Mn in the CNS

After luminal secretion from capillary endothelial cells and choroidal epithelial cells, Mn exists as non-Tf-bound and Tf-bound forms in the extracellular fluid in the brain. Mn^{3+} binds to Tf which is secreted from oligodendrocytes (Connor et al., 1990). Tf-bound Mn appears to be taken up via receptor-mediated endocytosis by neurons which express TfRs on the surface (Moos, 1996). There is also the possibility that DMT-1 is involved in neuronal uptake of Mn^{2+} and/or low molecular weight ligand-bound Mn (Gunshin et al., 1997). Non-Tf mediated uptake of Mn is observed in glial cell cultures (Takeda et al., 1998a). Additionally, astrocytes in the CNS have been shown to possess a high-affinity plasma membrane transporter for Mn^{2+} that facilitates uptake of this divalent metal (Aschner et al., 1992). The Mn levels are highest in mitochondria and cytosol, and lowest in myelin and nuclei. After chronic Mn treatment *in vivo*, the largest increases in Mn are noted in nuclei and mitochondria. Such observations suggest that mitochondria and nuclei may be subcellular targets for Mn neurotoxicity (Lai et al., 1999).

Mn Neurotoxicity-Manganism

Sources of Mn Exposure

Although Mn is essential for normal physiological functions, overexposure to Mn can cause a disorder known as manganism or Mn-induced parkinsonism. In 2000, the Institute of Medicine at the National Academy of Sciences established the Tolerable Upper Intake Level (UL) for Mn at 11 mg for adults (National Academy of Sciences, 2001). Overexposure may result from dietary, metabolic and environmental sources.

Grains, tea, and green leafy vegetables contain the highest amounts of dietary Mn as reported in the Total Diet Study (Pennington and Schoen, 1996). Soy-based infant formulas tend to have more Mn than human milk, and this causes many concerns (Lonnerdal, 1994; Krachler and Rossipal, 2000).

Individuals receiving total parenteral nutrition (TPN) are at higher risk for Mn toxicity, because the normal mechanisms of Mn metabolism are bypassed (i.e., the gut), and 100% of the Mn in the TPN solution enters the body as compared to approximately 5% of that taken orally. There have been reported intoxications from TPN solutions containing 0.1 mg Mn/day (Bertinet et al., 2000). Several papers have also revealed that patients with chronic liver failure exhibit increased serum and brain levels of Mn and display some of the behavioral symptoms and neurodegenerative features of Mn intoxication (Hauser et al., 1994; Krieger et al., 1995). Because Mn is normally eliminated in bile, any condition that compromises normal liver function could potentially lead to Mn intoxication (Papavasiliou et al., 1966).

Environmental contaminants may also provide sources of overexposure to Mn. Mn is used in the manufacture of dry batteries, steel, aluminum, welding metals and contained in a widely used organochemical fungicide (Maneb) and also animal feed and pigments (Keen and Leach, 1988; Keen et al., 2000). In addition, combustion emissions from power plants, iron and steel foundries and coke ovens make significant contributions to the concentration of Mn in air (Lioy, 1983). Workers from manganese mines, mills and foundries were reported to develop manganism since 1837 (Couper, 1837; Yamada et al., 1986; Huang et al., 1989). The gasoline additive,

methylcyclopentadienyl manganese tricarbonyl (MMT), is a controversial source of additional airborne Mn which has been used in Canada for more than 10 years as a replacement for lead as an antiknock agent. Its use in the United States is still under debate (Kaiser, 2003). Upon combustion in automobile engines, MMT yields a complex mixture of phosphate, sulfate, and oxide forms of Mn. However, studies have shown that the air Mn content in Canadian cities with the most traffic is near or below the current inhalation reference concentration (RfC) for inhalable Mn, which is 0.05 μg Mn/m^3, as set by the United States Environmental Protection Agency (Loranger and Zayed, 1997; Clayton et al., 1999).

Clinical Features of Manganism

Manganism is characterized by psychiatric symptoms and extrapyramidal manifestations. Chronic exposure to high levels of inhalable Mn (>1-5 mg Mn/m^3) is the most frequently observed cause of manganism (Mergler et al., 1994) and was first recognized by Couper in 1837 among workers engaged in the grinding of Mn ores (Couper, 1837). Cases of Mn poisoning have also been reported in families exposed to Mn through contaminated well-water (Kawamura, 1941). The early phase of psychiatric symptoms of manganism is also called "manganese madness" or "locura manganica" and is characterized by emotional liability, mania, compulsive or violent behavior, hallucinations, disturbance of sleep, and eating and sexual disturbances but few, or subtle, motor effects. A later phase ("established" phase), is dominated by motor symptoms such as bradykinesia, rigidity, and dystonia (prolonged muscle contractions) (Rodier, 1955). A particularly characteristic finding is the so-called "cock walk", in

which patients strut on their toes, with elbows flexed and the spine erect. It is noteworthy that patients can develop the motor deficits of manganism without having experienced any phase of manganese madness (Huang et al., 1989) and patients with manganism may develop increasing neurologic dysfunction long after cessation of exposure (Huang et al., 1993).

Functional Imaging of Manganism

MRI and PET are helpful techniques for diagnosis of manganism. The GP of humans exposed to parenteral Mn show a characteristic bilateral, symmetrical signal hyperintensity on T1 weighted MRI (Lucchini et al., 2000), which is in accordance with elevated blood serum Mn concentrations in most cases (Rosenstock et al., 1971; Huang et al., 1989; Pal et al., 1999). PET with [^{18}F]-6-fluoro-L-dopa (6-FD) uptake provides an index of prestriatal dopaminergic function (Martin et al., 1989), while [^{11}C] raclopride (RAC) is a PET marker for postsynaptic (D2 receptor) dopaminergic function (Farde et al., 1989). Cerebral glucose metabolism can be revealed by ^{18}F-2-fluoro-2-deoxyglucose (FDG) PET (Reivich et al., 1979). In patients with manganism 6-FD uptake was normal, RAC binding was in the low normal range in the putamen and FDG scans revealed a widespread decline in cortical glucose metabolism (Wolters et al., 1989; Shinotoh et al., 1997; Pal et al., 1999).

Neurochemical and Neuropathological Changes in Manganism

Neurochemical changes of manganism are observed prior to neuropathological ones (Neff et al., 1969). A severe reduction in DA levels in the caudate nucleus, putamen and SN, a distinct reduction of noradrenaline in hypothalamus and normal serotonin (5-

HT) in these areas was reported in a patient dying with chronic manganism (Bernheimer et al., 1973).

The pathologic changes in human manganism are mainly in the GP, especially the medial segment where neuronal loss and reactive gliosis occur. A less severe degeneration occurs in the putamen, caudate nucleus and SNr (Yamada et al., 1986). Damage involving the STN has also been reported and, less frequently, the SNc (Scholten, 1953; Calne et al., 1994). Mn accumulates in multiple brain regions including the basal ganglia, frontal cortex, pre-optic area, and hypothalamus, indicated by flameless atomic absorption spectrometry analytical determination in autopsy samples (Yamada et al., 1986).

Experimental Manganism

The data from nonhuman primates, but not from rodents, are similar to those obtained from humans with manganism (Calne et al., 1994), except that the key feature of reactive gliosis observed in monkeys is the presence of Alzheimer type II astrocytosis (Pentschew et al., 1963; Olanow et al., 1996). Ultrastructural studies in rats report that reactive astrocytes and microglia surround degenerating neurons and contain increased numbers of large secondary lysosomes, indicative of an active phagocytic process (Bikashvili et al., 2001). However, rodent studies have yielded variable results concerning regional brain Mn distribution and neurochemical and neuropathological responses to Mn exposure (Brenneman et al., 1999; Newland, 1999). Further, the behavioral changes observed in Mn-poisoned humans are not replicable in rodents,

which further confounds interpretation of results from those studies in assessing the consequences of human exposure (Aschner et al., 1999).

Treatment of Manganism

Treatment includes removing Mn from the body by chelation with ethylenediaminetetraacetic acid (EDTA) or other compounds for early cases and symptomatic improvement using drugs such as L-DOPA (levodopa). There are conflicting reports about the efficacy of these treatments, the reasons for which may include different routes of Mn exposure, as well as differences in severity, duration, and stage of Mn poisoning when the treatment is given. The effectiveness of chelating agents such as EDTA is probably limited to the early cases of manganism without structural neurological lesions and extrapyramidal signs and symptoms (Pal et al., 1999). Although EDTA was reported to cause significant improvement in patients with manganism for two and a half years (Penalver, 1957), this improvement was not maintained and poor responses were also seen in some patients (Cook et al., 1974). In addition, repeated use of EDTA may cause nephrotoxicity (Levine, 1970). Patients with chronic manganism must tolerate higher doses of L-DOPA than patients with PD to gain improvement in rigidity, tremor and facial expressions (Rosenstock et al., 1971; Huang et al., 1989). However, in the cases with absence of rigidity or dystonia or both, L-DOPA seems ineffective (Cook et al., 1974). The absence of a sustained response to L-DOPA is considered as a criterion for distinguishing manganism from PD (Lu et al., 1994). Other therapies reported to be effective are 5-hydroxytryptophan (5-HTP) (Mena et al., 1970) and para-aminosalicylic acid (PAS) (Ky et al., 1992). However, their mechanisms of

action are unclear. Because of the lack of a clearly effective therapy for manganism, preventive measures are necessary to avoid exposure and neurological examinations to detect early signs of exposure are required for high risk populations.

Cellular Mechanisms of Manganism

Any satisfactory hypothesis concerning mechanisms of Mn neurotoxicity should be able to explain the selective vulnerability of the GP and the chronic progression of clinical symptoms even after cessation of Mn exposure (Pal et al., 1999). Several aspects of possibilities have been studied in the past; however, the final conclusion has not been reached. Several potential mechanisms for Mn-induced neurotoxicity will be briefly considered in the following sections: oxidative stress, mitochondrial damage, excitotoxicity, neurotransmitter dysfunction and interation with Fe. In addition, specific direct effects of Mn on neurons leading to cell death and on astrocyte functions will be considered.

Mn and Oxidative Stress

Experimental evidence supports the role of Mn both as a powerful pro-oxidant and antioxidant, depending upon valence state, cellular localization, and protein binding (Kono et al., 1976; Donaldson et al., 1981). There are reports that Mn^{2+} suppresses lipid peroxidation by its antioxidant properties both in vivo (Donaldson et al., 1982) and *in vitro* (Tampo and Yonaha, 1992). Mitochondria also rely heavily on Mn^{2+} for antioxidant protection as it is the critical cofactor for MnSOD (HaMai et al., 2001). In astrocytes, Mn^{2+} is essential for the function of GS which converts the excitatory neurotransmitter glutamate to glutamine, which is safely shuttled back to neurons in a metabolite

trafficking loop. Proper functioning of this enzyme is important to protect neurons from excitotoxicity (Boksha et al., 2000; Weber et al., 2002).

However, excess Mn^{2+} can be oxidized to higher valence forms, which are associated with oxidative stress induced neurotoxicity (Desole et al., 1997; Stokes et al., 2000). There is evidence that stimulaton of cultured astrocytes with Mn^{2+} results in oxidative stress accompanied by decreases in antioxidant enzyme activities (Chen and Liao, 2002). There are several mechanisms of reactive oxygen species (ROS) formation in neurons after Mn exposure. For example, there is a significant increase in the expression of TfR mRNA and cellular ^{59}Fe net uptake by cultured neurons, but not astrocytes. These findings suggest that Mn may contribute to neuronal cytotoxicity by elevating intracellular free Fe levels (Zheng and Zhao, 2001). Excess intracellular Fe can actively participate in generation of Fe-mediated ROS, leading to neuronal cell death (Youdim et al., 1993). Several studies show that TfR is expressed in neurons and to a lesser extent in astrocytes. The rather low base-level of TfR may partially explain the insensitivity of astrocytes to Fe cytotoxicity (Zheng and Zhao, 2001). In addition, Mn can also catalyze the oxidation of DA and other catecholamines in neurons, which can generate ROS, such as superoxide anion, hydroxyl radical, and hydrogen peroxide. These ROS are believed to cause neurotoxicity and neuronal death (Graham, 1984). Ali et al. (1995) demonstrated dose-related increases in ROS production in rat caudate nucleus after in vivo Mn exposure (Ali et al., 1995). Tyree and Archibald (1987) have postulated that trivalent Mn is the neurotoxic cation of concern. *In vitro* trivalent Mn can oxidatively destroy DA, epinephrine, norepinephrine, and their precursor dopa, but the

presence and relative abundance of this valence state in brain remains to be determined (Archibald and Tyree, 1987). Desole et al. also provided evidence for Mn-induced oxidative stress via xanthine oxidase (Desole et al., 1994). The production of ROS in neurons exposed to Mn may also due to the indirect consequence of the toxic actions of Mn on the mitochondria, as a number of mitochondria toxicants have been shown to promote formation of ROS (Kitazawa et al., 2002; Samavati et al., 2002). Mn is transported into the mitochondria via the high-capacity, low-affinity Ca^{2+}-uniporter, whereupon it inhibits Na^{+}-dependent Ca^{2+} efflux from brain mitochondria, promoting an increase in matrix Ca^{2+} levels and subsequent oxidative stress (Gavin et al., 1990). Other sources of ROS caused by accumulation of Mn include depletion of intracellular thiols (Eriksson and Heilbronn, 1983), inhibition cellular antioxidant defense mechanisms (Liccione and Maines, 1988) and increased expression of cytochrome P-450 enzymes with superoxide radical formation (Liccione and Maines, 1989).

Mn and Mitochondria

The similarity between the neuropathology of manganism and the neuropathology of patients intoxicated with known mitochondrial toxicants such as cyanide or carbon monoxide (CO) (both of which have a predilection for the GP) forms the basis for suspecting Mn to be a mitochondrial toxicant (Beal, 1992). As mentioned, Mn accumulates in mitochondria via the calcium uniporter and is transported out of mitochondria mainly via the slow Na^{+}-independent efflux mechanism, which is an active (energy-requiring) process. Mn inhibits Ca^{2+} efflux, thereby promoting a Ca^{2+} permeability transition (PT) and collapsing the mitochondrial membrane potential (Ψm),

which will eventually cause rupture of the mitochondria and cell death (Gavin et al., 1999). On the subcellular level, Mn^{2+} is most concentrated in mitochondria (Maynard and Cotzias, 1955) and is postulated to spontaneously give rise to Mn^{3+}. Even in trace amounts, Mn^{3+} can cause formation of ROS (HaMai et al., 2001), which can damage components of the electron transport and oxidative phosphorylation machinery of the mitochondria and in turn subject the cells to energy failure (Gavin et al., 1992; Calabrese et al., 2001). It has also been suggested that Mn toxicity of PC12 cells could be the result of either a direct or indirect effect on complex I activity, mediated by oxidative stress (Galvani et al., 1995). Gavin *et al.* showed that the ATPase complex is inhibited at very low levels of mitochondrial Mn and that complex I is inhibited at higher Mn concentrations (Gavin et al., 1999). It has also been shown that Mn^{3+} is more effective at inhibiting complex I (Archibald and Tyree, 1987; Ali et al., 1995; Chen et al., 2001). In another study, treatment of striatal neurons with Mn showed dose-dependent loss of Ψm and complex II activity (Malecki, 2001b). Collectively, these results indicate that Mn may trigger neuronal cell death secondary to energy depletion caused by mitochondrial dysfunction. Mitochondrial dysfunction would in turn result in free radical damage to mitochondrial DNA. Together with the slow clearance of Mn from mitochondria, a progressive loss of function may continue. This chain of events may partially explain why human manganism continues to progress despite withdrawal from exposure (Brouillet et al., 1993).

Mn and Excitotoxicity

Glutamate excitotoxicity in neurons is associated with increased influx of Na^+ and Ca^{2+} ions that cause mitochondrial Ca^{2+} overload, loss of ATP production, and cell death. Increased intracellular Na^+ and Ca^{2+} causes cell swelling and eventually cell lysis. In addition, Ca^{2+} overload leads to stimulation of numerous Ca^{2+}–activated enzymes that degrade cellular structual proteins and produce ROS. ROS inhibits excitatory amino acid (EAA) transporter function limiting removal of excess extracellular glutamate, thus producing increased NMDAR stimulation, with further production of ROS and greater inhibition of EAA transport. This feed-forward NMDAR- and Ca^{2+} mediated cycle will eventually lead to cell death. Furthermore, elevated extracellular glutamate inhibits the uptake of cystine, a precursor of glutathione (GSH), thus decreasing intracellular GSH levels and antioxidant function (Choi, 1992; Sonnewald et al., 2002).

It has been shown that Mn neurotoxicity may be due to an indirect excitotoxic event caused by increased extracellular glutamate levels (Brouillet et al., 1993). As Mn is concurrently released with glutamate from glutamatergic neuron terminals (Takeda et al., 2002), the hyperactivity of corticostriatal neurons observed in the course of Mn intoxication may partially contribute to the elevated extracellular glutamate levels (Centonze et al., 2001). In the brain, both Mn uptake (Aschner et al., 1992) and glutamate uptake predominantly occur in astrocytes (Aschner et al., 2001). Therefore, it is also critical to address the relationship between Mn and glutamate uptake system in astrocytes in order to fully understand Mn induced excitotoxicity in the CNS. The glutamate uptake process occurs via glutamate transporters which are sodium/potassium-

dependent membrane proteins. Among them, glutamate transporter and glutamate/aspartate transporter (GLAST) are the prominent astrocytic transporters (Kondo et al., 1995; Danbolt, 2001), intracellularly transporting both glutamate and aspartate. A previous study showed that overnight exposure of cultured rat astrocytes to Mn caused a 30% decrease in glutamate uptake (Hazell and Norenberg, 1997). A later study showed that exposure to 500 mM $MnCl_2$ led to decreased mRNA levels of GLAST (Erikson and Aschner, 2002). Therefore, decreased glutamate uptake in astrocytes is linked to decreased GLAST mRNA after Mn exposure. Thus, the excitotoxicant effect of increased extracellular glutamate is also associated with Mn-induced glutamate uptake inhibition in astrocytes (Desole et al., 1997; Miele et al., 2000; Stokes et al., 2000; Montes et al., 2001).

Mn and Neurotransmitter Dysfunction

As mentioned above, Mn and glutamate are concurrently released from glutamatergic neuron terminals (Takeda et al., 2002), the abnormal excitation of striatal neurons in the course of Mn intoxication may be due to hyperactivity of corticostriatal neurons, a presynaptic mechanism upstream of calcium-entry-triggered events (Centonze et al., 2001). In this light, the strong D2-DA-receptor mediated inhibitory control of corticostriatal transmission reported in Mn treated rats may represent an adaptive change aimed at counteracting abnormal glutamate release (Calabresi et al., 2001). The enhancement of excitatory transmission in the striatum is an early event in the course of Mn poisoning and plays a pathogenic role in the development of further striatal damage. This might explain why motor symptoms appear after emotional symptoms, as abnormal

inhibitory dopaminergic control on corticostriatal glutamatergic inputs has been previously proposed to play a critical role in schizophrenia (Carlsson and Carlsson, 1990).

Evidence for anterograde axonal transport of Mn was indicated in the GABAergic striato-nigral and/or dopaminergic nigro-striatal pathways (Takeda et al., 1998b). The axonal transport of Mn in these circuits seems to reflect the association with neuronal activity (Sloot and Gramsbergen, 1994). Takeda reported that levels of gamma-aminobutyric acid (GABA) in the perfusate were remarkably decreased during perfusion with Mn in the striatum (Takeda et al., 2003). A novel finding recently was that the Mn concentration in the striatum was negatively correlated with the GABA concentration (Erikson and Aschner, 2003). The inhibitory action of low Mn concentrations against GABAergic neuron activity seems to be important to understand the abnormal excitation of striatal neurons during Mn intoxication, which may be associated with hyperactivity of corticostriatal fibers (Centonze et al., 2001).

It has been demonstrated that Mn^{2+} permeates presynaptic voltage-dependent Ca^{2+} channels and induced DA release from depolarized nerve terminals (Narita et al., 1990). Altered glutamatergic and GABAergic function also can contribute to altered striatal DA release. For example, increased glutamate in the SN can increase striatal DA release via NMDARs (Castro and Zigmond, 2001; Page et al., 2001). It is also been found that the striatum is sensitive to a modest increase in Mn concentration (~40% increase compared to control) which leads to a decrease in GABA levels. This disturbance in GABAergic inhibitory firing into the SN may lead to increased striatal

DA levels. Therefore, the neurotoxic effects of Mn on striatal DA may be indirectly mediated via abnormal striatal glutamate and/or GABA metabolism (Erikson and Aschner, 2003).

Another study, however, showed that low cumulative Mn exposure increased striatal GABA but not DA in a pre-Parkinson's rat model (Gwiazda et al., 2002). Motor dysfunction in the absence of measurable effects on striatal DA has also been observed at low Mn cumulative doses both in monkeys (Olanow et al., 1996) and rodents (Witholt et al., 2000). These results suggest that initial motor deficits might not be due to Mn effects on the dopaminergic nigro-striatal system, but possibly in the GABAergic and/or other circuits of the basal ganglia (Gwiazda et al., 2002).

The influence of Mn on TH activity is of importance. Bonilla showed an initial increase in the enzyme activity and then a decrease at later stages. The initial increase in the enzyme activity may thus account for an early increase in the levels of DA and norepinephrine, while the decrease in the enzyme activity at later stages may be the cause of a decrease in the levels of these amines after chronic exposure (Bonilla, 1980).

Mn and Fe

The co-accumulation of Fe and Mn in the same brain region (the GP) after Mn exposure raises the concern that Fe may be a contributing factor facilitating neuronal cell loss during Mn intoxication since Fe deposition is also found in degenerative brain areas of other neurological disorders, including Alzheimer's, Parkinson's, and Huntington's disease (Shoham and Youdim, 2000; Berg et al., 2001; Thompson et al., 2001). Fe is capable of generating ROS via the Fenton reaction, leading to oxidative stress, lipid

peroxidation, and eventually cell death. In addition, Fe can have both a direct and an indirect influence on the transport of Mn and other divalent metals in that it is capable of regulating expression of a number of the key proteins involved in metal transport such as Tf and DMT1 (Oates et al., 2000; Moos et al., 2002; Roth et al., 2002b).

Mn and Neuronal Cell Death

Several *in vitro* studies in PC12 cells show that Mn induced both apoptotic and necrotic cell death depending on the intracellular ATP level (Roth et al., 2000; Hirata, 2002; Roth et al., 2002a). There is strong evidence that Mn elicits caspase-dependent apoptosis in PC12 cells that is blocked by Bcl-2 under conditions in which ATP levels remained unchanged (Hirata, 2002). Many enzymes of classical signaling pathways associated with apoptosis are activated in cells treated with Mn, such as the JNK and p38 protein kinases, caspase- 3-dependent cleavage of poly(ADP ribose) polymerase (PARP), ERK et al. (Desole et al., 1996; Hirata, 2002). However, apoptosis only partially explains the cytotoxic actions of Mn, because inhibitors of several classic apoptotic markers, including the caspase family of proteases and p38 kinase, fail to prevent cytotoxicity (Roth et al., 2000). Therefore, other cytotoxic events must account for the observed decrease in cell viability provoked by Mn. As previously mentioned, Mn can disrupt mitochondria function and the subsequent depletion of ATP will ultimately cause necrotic cell death (Roth et al., 2000; Chen and Liao, 2002), which is likely to be the prevailing mechanism responsible for Mn-induced cell death, even when apoptotic signaling is initiated.

Mn Neurotoxicity and Astrocytes

Astrocytes are postulated to be the principal repository for Mn in the CNS following the demonstration that GS, for which Mn is a required cofactor, is located mainly in this cell type (Martinez-Hernandez et al., 1977). Spin resonance studies show that GS is an octameric protein that can bind up to 8 Mn ions per octamer (Wedler and Denman, 1984) and as a result it is considered that 80% of brain Mn is associated with GS (Wedler et al., 1982), which catalyzes the conversion of glutamate and ammonium to glutamine, driven by the hydrolysis of ATP (Derouiche and Frotscher, 1991).

The level of astrocytic Mn is hypothesized to regulate GS activity (Wedler et al., 1994). Although the question has not been studied *in vivo*, *in vitro* animal studies show that Mn has a complex effect on GS activity. Mn activates GS in a narrow range of concentrations (Wedler and Denman, 1984), whereas further increases in Mn concentration have a negative effect on the enzyme activity (Tholey et al., 1987). GS homogenates from human brain also shows the similar trend of Mn^{2+} dependence of GS activity (Boksha et al., 2000). Decreases in GS activity in the presence of high concentrations of Mn might be mediated by multiple mechanisms. For example, the GS macromolecule is susceptible to oxidative modification after high Mn exposure, resulting in decreased synthetic activity (Levine et al., 1981; Liaw et al., 1993). In addition, the oxidized GS protein undergoes rapid degradation by intracellular proteases leading to decreases in both activity and protein levels.

Glutamine produced in astrocytes via GS is taken up by neighboring glutamatergic or GABAergic neurons as precursors for neurotransmitter synthesis as part

of the glutamate–glutamine cycle (Schousboe et al., 1992). Its formation serves both as a glutamatergic intermediary for glutamate and GABA and also as a by-product of detoxification of ammonia (Cooper and Plum, 1987). In addition to providing glutamine to neurons, other glutamate-derived metabolites, such as the tricarboxylic acid (TCA) cycle precursors lactate, malate and citrate are utilized by neurons for energy production (Sonnewald et al., 1991). Thus, inhibition of GS activity may result in decreased neuronal energy levels, decreased synthesis of glutamine, glutamate and GABA, and inability to detoxify ammonia within the CNS.

Optimal brain function is dependent upon cross talk between multiple cell types. In particular, astrocytes produce trophic factors, regulate neurotransmitter and ion concentrations, and remove toxicants and debris from the extracellular space around the neurons. Therefore, impairment of astrocytic functions by Mn has the potential to indirectly induce and/or exacerbate neuronal dysfunction (Aschner et al., 2002a). For example, in addition to inhibition of GS activity, removal of neurotransmitters such as GABA, glutamate, and DA from the extracellular fluid by astrocytes can be altered after Mn exposure (Lipe et al., 1999; Gwiazda et al., 2002; Erikson and Aschner, 2003). Neurons neighboring affected astrocytes are then potentially made susceptible to excitotoxicity or other downstream dysfunction because of the imbalanced extracellular neurochemistry.

Increasing evidence suggests that astrocytes are involved in early dysfunction in Mn neurotoxicity. In addition to disturbance of GS activity, exposure of astrocytes to Mn also results in other important changes including increased densities of binding sites for

the “peripheral-type” benzodiazepine receptor (PTBR), a class of receptor localized to mitochondria of astrocytes and involved in oxidative metabolism, mitochondria proliferation, and neurosteroid synthesis (Hazell et al., 1999a); increased gene expression and activity of the glycolytic enzyme glyceraldehyde-3-phosphate dehydrogenase (GAPDH), known to be associated with apoptosis (Hazell et al., 1999b); increased expression of NOS2 together with increased uptake of L-arginine, a substrate for NOS2 which can lead to ROS as a consequence of NO production (Hazell and Norenberg, 1998). Potential consequences of these alterations in astrocytes play a key role in Mn-induced neuronal cell death.

It has been reported recently that neurons treated for 5 days with $MnCl_2$ are extremely susceptible to oxidative stress and energy failure as the result of mitochondrial dysfunction (Zwingmann et al., 2003), whereas astrocytes are relatively unaffected after the same treatment. When the cells are co-cultured, Mn-exposed astrocytes fail to provide neurons with substrates for energy and neurotransmitter metabolism, leading to deterioration of neuronal antioxidant capacity (decreased glutathione levels) and energy depletion. It has also been reported in many cases that astrocytes have higher levels of GSH and some other antioxidant defenses than neurons (Tiffany-Castiglioni and Qian, 2001; Hazell, 2002). Several other studies show that up-regulation of intracellular lactate dehydrogenase (LDH) activity (Chen and Liao, 2002), elevation of lactate levels (Hirata et al., 1998) and impairment of oxidative metabolism (Brouillet et al., 1993) are seen in astrocytes after treatment with Mn indicating a switch from oxidative phosphorylation to glycolytic energy production occurrs in these cells. Astrocytes are considered to be

"glycolytic" cells that can survive in an environment toxic to mitochondria, whereas neurons do not have the ability to invoke glycolysis to maintain ATP production (Pauwels et al., 1985; Walz and Mukerji, 1988).

Spranger and colleagues (Spranger et al., 1998) were the first to speculate that activated astrocytes might contribute to Mn-induced parkinsonism through excessive production of NO. They demonstrated that Mn-induced injury to neurons required the presence of astrocytes and was associated with increased astrocytic expression of NOS2. NO can inhibit the activity of certain components of the mitochondrial respiratory chain, including cytochrome *c* oxidase (Bolanos et al., 1997). Furthermore, it has recently been shown that endogenous NO formation in primary neurons triggers a rapid and transient ATP depletion associated with collapse of Ψm across the mitochondrial inner membrane and apoptosis (Almeida and Bolanos, 2001). The mitochondria is a key organelle playing a role in NO-mediated apoptosis because disruption of Ψm dissipates the electrochemical gradient necessary for ATP synthesis (Mitchell, 1961). Moreover, collapse of Ψm is associated with mitochondrial swelling, disruption of the outer mitochondrial membrane, and the release of proapoptotic factors such as cytochrome *c* and apoptosis-inducing factor from the intermembrane space (Liu et al., 1996; Susin et al., 1999).

Studies examining the molecular regulation of NOS2 have begun to elucidate the signaling pathways responsible for activation of this gene in astrocytes. NF-κB, a Rel protein family member, is the principal transcription factor that mediates stress-inducible expression of NOS2 in glial cells (Nishiya et al., 2000; Nomura, 2001). The most well

studied isoform of NF-κB is a heterotrimeric protein composed of p50 and p65 subunits, plus an inhibitory protein, IκBα, that maintains the transcription factor in the cytoplasm in an inactive state. NF-κB is activated by distinct signaling pathways that converge on IκB kinase(IKK), which phosphorylates the NF-κB inhibitory subunit, IκBα, resulting in its dissociation and degradation (Karin et al., 2002). The resulting NF-κB dimer translocates to the nucleus, where it binds cognate DNA sequences and activates transcription of specific target genes such as *nos2* (Grilli and Memo, 1999).

Physiological Function, Cytotoxicity and Synthesis of NO

Physiological Function and Cytotoxicity of NO

NO plays a critical role in a variety of physiologic processes but excessive levels of NO can be cytotoxic. Of importance to normal brain function, NO activates guanylate cyclase (GC) and is thereby involved in various cyclic guanosine monophosphate (cGMP)-regulated signaling pathways, including those that regulate the glycolytic enzyme, GAPDH, in astrocytes. Furthermore, NO has also been implicated to play an important role in a number of other physiological processes in the CNS, i.e. pain perception, synaptic plasticity and learning (Garthwaite et al., 1988; Heales et al., 1997; Heales et al., 1999). However, the reaction between NO and superoxide anion ($O_2^{\cdot -}$) results in the formation of $ONOO^-$, which is cytotoxic (Lipton et al., 1993). Excessive NO and $ONOO^-$ formation have been implicated in the pathogenesis of many neurological disorders (Dawson and Dawson, 1996).

A major target of $ONOO^-$ is mitochondrial MnSOD (MacMillan-Crow et al., 1996). Inactivation of MnSOD by $ONOO^-$ initiates a self-propagating cascade of cell

injury subsequent to failure of scavenging of $O_2^{\cdot -}$ in the mitochondrion, leading to further enhancement of $ONOO^-$ formation. In addition, NO affects mitochondria in three principal ways which all result in energy depletion: reversible inhibition of respiration; irreversible inactivation of mitochondrial enzymes; and induction of mitochondrial PT. Mitochondrial dysfunction is widely thought to be critical to the progression of injury in neurodegenerative diseases including manganism and PD.

The primary function of the mitochondrial electron transport chain (ETC) is ATP synthesis. The ETC located in the inner mitochondrial membrane is comprised of more than 70 polypeptide components which are grouped into four enzyme complexes. Complex I is NADH ubiquinone reductase, complex II is succinate ubiquinone reductase, complex III is ubiquinol cytochrome c reductase and complex IV is cytochrome c oxidase. Transfer of reducing equivalents from NADH or $FADH_2$ to molecular oxygen is coupled with the pumping of protons across the inner mitochondrial membrane and results in the formation of a proton gradient. Dissipation of this proton gradient induces a conformational change in the active site of ATP synthase (complex V) which favors ATP synthesis (Pedersen, 1994). Since NO resembles dioxygen and has an unpaired electron, it binds reversibly to the Fe^{2+} center of cytochrome a_3 and also to the Cu^{2+} center of complex IV so that it can reversibly inhibit complex IV dependent respiration. Furthermore, $ONOO^-$ can also cause irreversible complex II-III-IV damage and complex I damage under the condition of GSH deficiency (Heales et al., 1999).

Mitochondrial PT is caused by certain inner membrane proteins amalgamate and form a nonspecific 2-3nm pore after exposure to oxidizing species. The possible

mechanisms of $ONOO^-$-mediated pore opening include: (1) $ONOO^-$-induced cross-linking of inner membrane protein thiol groups, leading to protein amalgamation and pore formation; (2) $ONOO^-$-induced lipid peroxidation, products of which are potent inducers of PT; and (3) $ONOO^-$-induced mitochondrial respiratory chain dysfunction. Pore opening leads to loss of Ψm (the ability of ATP synthesis) and the ability to sequester Ca^{2+}, both of which may be important factors in necrotic cell death.

However, it also appears that mitochondrial PT is an important early event in programmed cell death (apoptosis). Pore opening leads to the release of mitochondrial cytochrome c, which can be prevented by the anti-apoptic proteins Bcl-2 and Bcl-XL and can be activated by the proapototic protein Bax. Once in the cytoplasm, cytochrome c binds to Apaf1 and procaspase 9, leading to the sequential activation of caspase 9 and caspase 3 (Heales et al., 1999).

NO or $ONOO^-$ can also mediate DNA damage by several possible mechanisms. Production of NO in an oxidative environment can result in formation of nitrogen trioxide (N_2O_3), which can cause DNA-strand breaks. $ONOO^-$ can also oxidize DNA, resulting in DNA-strand breaks. Additionally, $ONOO^-$ can inactivate DNA ligase, further enhancing DNA damage (Wink and Mitchell, 1998). DNA-strand breaks, particularly single-strand breaks, are potent activators of the nuclear enzyme PARP (Szabo and Dawson, 1998). PARP is a nuclear enzyme which facilitates DNA repair and is important in maintaining genomic stability. It is important to know that PARP does not itself repair DNA and that DNA repair occurs in the absence of PARP (Satoh et al., 1994). Upon activation, PARP transfers hundreds to thousands of ADP-ribose moieties

from nicotinamide adenine dinucleotide (NAD) to itself and other nuclear receptor proteins within minutes (Lautier et al., 1993). For every 1 mol of ADP-ribose transferred, 1 mol of NAD is consumed and four ATP are required to regenerate NAD. Over activation of PARP, can therefore, rapidly deplete cellular energy stores (Berger, 1985). Loss of NAD in a setting in which ATP generation is compromised can lead ultimately to energy failure and cell death.

It has been noted that, within the brain, there is a differential susceptibility of various brain cell types to NO/ $ONOO^-$ (Bolanos et al., 1995). Induction of NOS2 in astrocytes leads to marked damage to the ETC. However, despite such damage, cell death does not occur. The apparent resistance of these cells, in this situation, appears to be mediated by a compensatory increase in glycolysis, i.e there was a marked increase in glucose consumption coupled with lactate formation. In contrast to astrocytes, neurons seem to be particular vulnerable to the actions of $ONOO^-$. Such vulnerability may arise from an inability to sustain cellular energy demands by glycolysis and an inferior capacity to handle oxidizing species such as $ONOO^-$ (Almeida et al., 2001). Various lines of evidence are now available to implicate a key role for GSH in dictation cellular susceptibility to $ONOO^-$; the results suggest that astrocytes, but not neurons, up-regulate GSH synthesis as a defense mechanism against excess NO (Gegg et al., 2003). Another study indicates that the concentration of GSH in cultured astrocytes seems to be double that of neurons cultured under identical conditions (Bolanos et al., 1995). Another factor contributing to the relative resistance of astrocytes to $ONOO^-$ exposure may be their greater concentration of α-tocopherol (vitamin E) (Makar et al., 1994). An exception to

the vulnerability of neurons is NOS1 interneurons. NOS1 interneurons are reported to be resistant to the neurotoxic environment they create (NO production) (Koh et al., 1986; Koh and Choi, 1988). Immunohistochemical co-localization experiments confirmed that MnSOD is expressed at higher levels in these neurons than in other neuronal cell types. Antisense knockdown of MnSOD renders NOS1 interneurons susceptible to *N*-methyl-D-aspartate (NMDA) neurotoxicity without influencing the overall susceptibility of other cortical neurons to NMDA neurotoxicity. Knockout of MnSOD through genetic targeting results in exquisite sensitivity of NOS1 neurons to NMDA neurotoxicity (Gonzalez-Zulueta et al., 1998).

Regulation of Nitric Oxide Synthase Expression and Activity

NO is generated by nitric oxide synthase (NOS), of which there are at least three isoforms: neuronal NOS isoform (nNOS, NOS1) being the isoform predominately found in neuronal tissue, inducible NOS isoform (iNOS, NOS2) being the isoform inducible by cytokines and other agents in macrophages, astrocytes and other glial cells, endothelial NOS isoform (eNOS, NOS3) being the isoform first found in vascular endothelial cells. The active form of NOS are composed of two NOS monomers associated with two calmodulin (CaM) subunits (Alderton et al., 2001). All NOS have binding sites for NADPH, FAD, and FMN near the carboxyl terminus (the reductase domain), and binding sites for tetrahydrobiopterin (BH_4) and heme near the amino terminus (the oxygenase domain). The reductase and oxygenase domain are linked by a CaM binding site. NOS catalyzes the conversion of arginine to citrulline and NO (Mayer, 2000) (Figure 1.2).

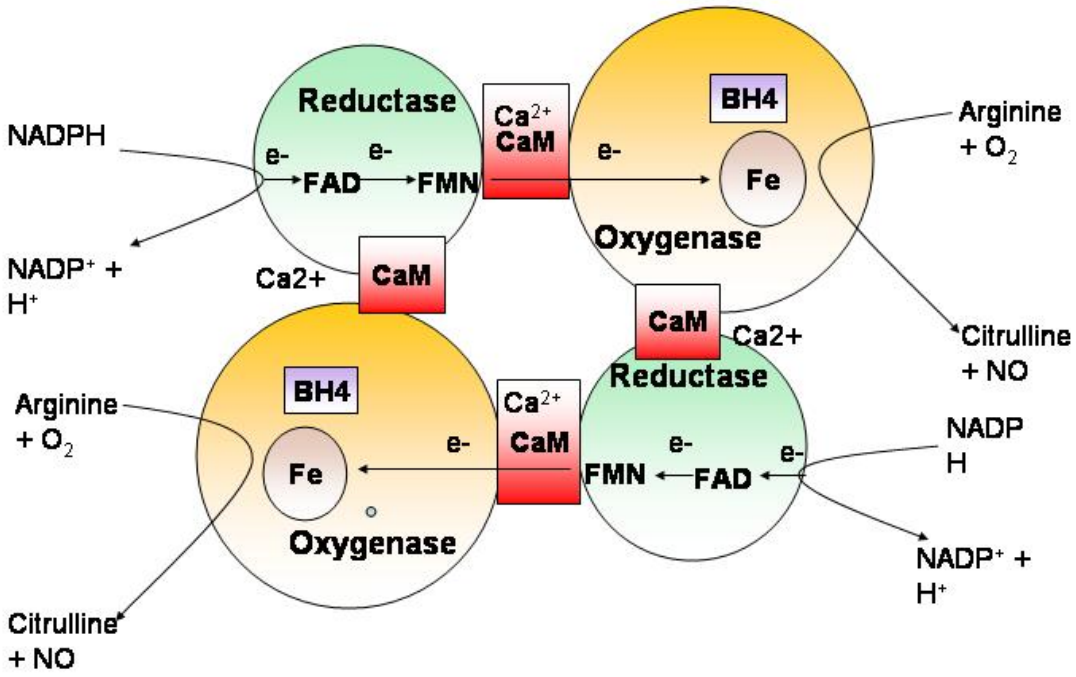

Figure 1.2. Overall Reactions Catalysed and Cofactors of NOS. Figure adapted from (Alderton et al., 2001).

Increased expression of NOS1 mRNA seems to represent a response of neuronal cells to stress or injury induced by physical, chemical and biological agents (Zhang et al., 1994; Lam et al., 1996). NOS1 expression can also be triggered by steroid hormones, estradiol and pregnancy has been demonstrated to induce NOS1 expression (Weiner et al., 1994). Down regulation of NOS1 expression has been documented in rats after lipopolysaccharide (LPS) and interferon gamma (IFN-γ) treatment (Bandyopadhyay et

al., 1997). NOS1 is a Ca^{2+} and calmodulin-dependent enzyme. Its activity is regulated by physiological changes in the intracellular Ca^{2+} concentrations. In addition to this acute mechanism of regulation, another important one is the subcellular localization of NOS1 protein. The N-terminal 220 amino-acids of NOS1 are unique to the neuronal isoform and contain a PDZ domain (PSD-95 discs large/ZO-1 homology domain). PSD-95 (post synaptic density protein 95) targets NOS1 to synaptic sites in brain. The membrane association of NOS1 in neurons is mediated by PDZ domain (Brenman et al., 1996). PSD-95 also binds to the C-terminus of NMDAR through PDZ domains, PSD-95 may contribute to the co-localization and functional coupling of NOS1 to NMDARs (Kornau et al., 1995). Thus, NOS1 may be the enzyme primarily activated during NMDAR-mediated Ca^{2+} influx into neuronal cells. Finally, NOS1 can be phosphorylated at serine and threonine residues by Ca^{2+}/CaM-dependent protein kinase II and protein kinase A, C, and G which reduces the catalytic activity of the enzyme (Nakane et al., 1991; Dinerman et al., 1994).

Like NOS1, NOS3 also requires Ca^{2+} and CaM. Both NOS1 and NOS3 are constitutive, low output, Ca^{2+}-activated enzymes that function in physiological signal transduction. Exercise training and shear stress produced by flowing blood upregulate NOS3 expression; increased NOS3 immunoreactivity has also been reported in cerebral blood vessels during cerebral ischemia (Zhang et al., 1993; Sessa et al., 1994). It has been reported that estrogens can also upregulate the expression of NOS3 mRNA and protein (Weiner et al., 1994). Although an increase in the intracellular concentration of free Ca^{2+} is the most important mechanism for acute changes in enzyme activity, recent

evidence suggests that it can also be activated in a Ca^{2+}–independent way, with tyrosine phosphorylation of NOS3 or an associated regulatory protein (Fleming et al., 1997a; Fleming et al., 1998a). The subcellular targeting of the enzyme to Golgi membranes may be also important for its activity (Sessa et al., 1995).

Expressional regulation of NOS2 is the main mechanism of its activation since once expressed, NOS2 does not seem to be subject to any significant regulation of its enzymatic activity. In uninduced cells, expression of NOS2 is usually very low or undetectable. The first agents to induce its expression are LPS and cytokines, such as interleukin-1 (IL-1), IFN-γ, and tumor necrosis factor-α (TNF-α). The 5'-flanking region of the murine *nos2* gene have been cloned (Lowenstein et al., 1993). The promoter of this gene contains a "TATA box" and numerous consensus sequences for the binding of transcription factors such as NF-κB. The NF-κB inhibitor PDTC blocked the activation of the protein and its binding to the NF-κB-binding site as well as the production of NO in LPS-treated macrophages, indicating that NF-κB activation is essential for transcription of the *nos2* gene (Xie et al., 1994). However, it is noteworthy that signal transduction pathways leading to *nos2* gene induction seem to differ markedly from species to species and even between cells (Kleinert et al., 1996; Linn et al., 1997). In addition to transcriptional regulation, post-transcriptional regulation can also induce NOS2 expression (Weisz et al., 1994).

The Objectives of This Research

This dissertation has three objectives. One objective of this research is to identify the specific vulnerable neurons within the basal ganglia after Mn overexposure which

attribute to the symptoms of manganism and the possible mechanisms of their vulnerability. We hypothesized that the symptoms of manganism were caused by the death of specific neurons in the basal ganglia and the surrounding reactive astrocytes with NO production might be involved in neurodegeneration. In this experiment, 12-week old C57Bl/6J female mice weighing 25 ± 5g given 100mg/kg $MnCl_2$ by gastric gavage for 8 weeks were used as an in vivo model.

The second objective of this research is to elucidate the mechanisms by which astrocyte-derived NO causes loss of neurons after excessive Mn exposure. As some previous studies showed that NF-κB was the principal transcription factor that mediates stress inducible expression of NOS2 in astrocytes (Nishiya et al., 2000).We hypothesized in this study that Mn exposure resulted in astrocyte activation and NF-κB dependent expression of NOS2, which attributed to neuronal injury through the production of NO. The rationale behind this hypothesis was that once the mechanisms of neuronal loss after excessive Mn exposure had been identified, therapeutic intervention would be possible. In order to test the hypothesis, co-cultures of primary astrocytes and differentiated PC12 cells exposed to Mn and cytokines were used as an in vitro model.

Finally, after we demonstrated that Mn exposure resulted in NF-κB dependent expression of NOS2 in activated astrocytes, which attributed to neuronal injury through the production of NO in our co-culture model, we tried to find a practical way to prevent the neurodegeneration. We postulated that activation of NF-κB in this system is regulated by the nuclear receptor PPARγ. To test this hypothesis, co-cultured astrocytes

and differentiated PC12 cells were exposed to Mn and cytokines in the presence of a novel PPARγ agonist, DIM-C-pPhCF$_3$.

CHAPTER II

ASTROCYTE-DERIVED NITRIC OXIDE MODULATES NEURONAL DEGENERATION IN A MOUSE MODEL OF MANGANESE-INDUCED PARKINSONISM

Overview

Chronic exposure to excessive levels of Mn through diet or inhalation results in a neurodegenerative movement disorder called manganism or Mn-induced parkinsonism. A mechanistic basis for Mn-induced neurodegeneration is not well established but involves excitotoxicity and disruption of mitochondrial function within the basal ganglia. The objective of this study was to develop a mouse model of Mn-induced parkinsonism to elucidate cellular and neurochemical targets of Mn in the nigro-striatal system as well as the mechanisms underlying the selective vulnerability of this brain region. Female C57Bl/6J mice were exposed to saline or $MnCl_2$ (100 mg/kg/day) by oral gavage once daily for 8 weeks. At the cessation of treatment animals were evaluated for locomotor activity, catacholamine levels, and histopathological changes in the striatum and SN. Locomotor activity was assessed by open field activity tracking in xyz dimensions using infrared monitoring chambers. DA and its metabolite DOPAC were quantified by high performance liquid chromatography (HPLC). Serial sections from the striatum, GP and SN were analyzed for neuronal viability and expression of TH, NOS1, ENK, ChAT, DYN and glial acidic fibrillary protein (GFAP). Levels of 3-nitrotyrosine protein adducts were also determined by immunohistochemistry. Mn content, as determined by

inductively-coupled plasma-mass spectrometry (ICP-MS), was significantly increased in the striatum after Mn treatment. Striatal DA content decreased in animals exposed to Mn and the DA/DOPAC ratio slightly increased. In open field activity experiments, the total distance traveled was decreased with a trend toward an increase in margin time in the Mn treated group. Mn exposure also caused an increase in fluorojade-positive neurons within the striatum and GP. The NOS1-, ChAT-, and ENK-expressing neurons displayed increased DNA fragmentation upon terminal deoxynucleotidyl transferase-mediated dUTP-biotin nick-end labeling (TUNEL) staining in Mn-treated animals, however, TH-positive neurons and nerve terminals were morphologically unaltered. These regions also displayed an increase in GFAP staining that co-localized with staining for 3-nitrotyrosine protein adduct. Activated GFAP-expressing astrocytes, in the striatum and GP proximal to the microvasculature and to regions where neuronal injury was most evident, co-expressed NOS2. It is concluded from these studies that Mn exposure resulted in depletion of striatal DA levels and degeneration of neurons (NOS1+ and ChAT+ interneurons and ENK+ projection neurons) in the striatum and GP with astrocyte activation, NOS2 expression and overproduction of NO. The location of neuronal injury and astrocyte activation proximal to the microvasculature suggests an involvement of metal transport and/or disrupted BBB function in the mechanism of injury.

Introduction

Mn is an essential nutrient that functions as a co-factor in enzymes involved in the metabolism of proteins, lipids and carbohydrates, such as glycolsyltranserferases,

PEPCK, pyruvate decarboxylase et al., and modulates a variety of other physiological functions (Kemmerer et al., 1931; Keen et al., 2000). However, it is also been recognized that overexposure of Mn causes neurotoxicity resulting in manganism or manganese-induced parkinsonism (Couper, 1837; Kawamura, 1941; Huang et al., 1989; Mergler et al., 1994).

In addition to occupational exposure (such as in the manufacture of dry batteries, steel, aluminum, welding metals and organochemical fungicide) (Keen and Leach, 1988; Keen et al., 2000), individuals receiving TPN (Bertinet et al., 2000) and patients with chronic liver failure are at higher risk of Mn intoxication (Hauser et al., 1994; Krieger et al., 1995). Soy-based infant formulas have levels of Mn up to 200-fold greater than human milk (Lonnerdal, 1994; Krachler and Rossipal, 2000), and the addition of MMT to gasoline in the United States and Canada as an anti-knock agent also increases the risk for excessive exposure to Mn.

Manganism or Mn-induced parkinsonism caused by chronic Mn poisoning, is characterized by psychiatric and motor symptoms. The early phase of manganism is also called “manganese madness” and is characterized by emotional liability, mania, compulsive or violent behavior, hallucinations, disturbance of sleep, and eating and sexual disturbances but few, or subtle, motor effects. A later phase (“established” phase), is dominated by motor symptoms such as bradykinesia, rigidity, and dystonia (prolonged muscle contractions) (Rodier, 1955). A particularly characteristic finding is the so-called “cock walk”, in which patients strut on their toes, with elbows flexed and the spine erect. It is noteworthy that patients can develop the motor deficits of manganism without

having experienced any phase of manganese madness (Huang et al., 1989) and patients with manganism may develop increasing neurological dysfunction long after cessation of exposure (Huang et al., 1993).

Neurochemical changes were observed prior to neuropathological ones (Neff et al., 1969). A severe reduction in DA levels in the caudate nucleus, putamen and SN, a distinct reduction of noradrenaline in hypothalamus and normal 5-HT in these areas was reported in a patient dying with chronic manganism (Bernheimer et al., 1973). A later study showed that after chronic $MnCl_2$ administration in rats, the striatal content of DA, norepinephrine, and homovanillic acid initially increased, then normalized, followed by a decline in catecholamines and their metabolites (Autissier et al., 1982).

The pathologic changes in human manganism are mainly in the GP, especially the medial segment where neuronal loss and astrocytosis occur. A less severe degeneration occurs in the putamen, the caudate nucleus and SNr (Yamada et al., 1986).

Data from nonhuman primates are similar to those obtained from humans with manganism (Calne et al., 1994). However, the type of neuronal loss in the striatum and GP and its role in pathogenesis of manganism has never been identified. So far, rodent studies have yielded variable results (Brenneman et al., 1999; Newland, 1999) and there are only a limited number of mouse models of manganism. It is postulated in this study that specific neuronal subtypes within the striatal-pallidal system are selectively vulnerable to Mn neurotoxicity and that astrocyte-derived NO plays a role in the observed neuronal degeneration. To test this hypothesis, we developed a mouse model of Mn-induced parkinsonism utilizing a gastric gavage dosing regimen to mimic human

dietary exposure to moderate doses of Mn. The findings represent, to our knowledge, the first data on specific subpopulations of neurons vulnerable to Mn in the striatal-pallidal system.

Materials and Methods

Materials

All chemical reagents were obtained from Sigma Chemical Co. (St. Louis, MO). C57Bl/6J mice were obtained from Harlan (Indianapolis, IN). Primary antibodies to TH, ChAT and ENK were from Chemicon (Temecula, CA). Primary antibodies to GFAP and NOS1 were from Santa Cruz Biotechnology (Santa Cruz, CA), primary antibodies to 3-nitrotyrosine were from Upstate (Charlottesville, VA) and primary antibodies to Leumorphin were from Serotec (Oxford, UK). Horseradish peroxidase-conjugated secondary antibodies and diaminobenzidine reagents were part of the Vectastain ABC kit from Vector Labs (Burlingame, CA). Terminal Transferase Recombinants were from Roche Molecular Biochemicals (Indianapolis, IN). AlexaFluor-488-labled dUPT and AlexaFluor-568-labled secondary antibodies were from Molecular Probes (Eugene, OR).

Animal exposure regimen

Twelve week-old female C57Bl/6J mice were housed in microisolator cages (4 animals per cage) and kept on 12 hr light/dark cycles with access to lab chow and water *ad libitum*. Mice received 0.9% normal saline or $MnCl_2$ by gastric gavage at 100 mg/kg (n=19 each group) once daily for 8 weeks.

Locomotor activity

Locomotor activity was determined in each animal at 0, 2, 4, 6 and 8 weeks during the gavage regimen. Activity was assessed in *xyz* planes utilizing infrared beam activity chambers. Computerized integration of the data obtained from the monitors afforded the recording of activity for multiple indices relating to basal ganglia function including total distance traveled, center time or margin time, and horizontal activity et al. (Miller et al., 2001). Treated and control animals were paired in activity monitors during each recording session. Animals were monitored for 20 minutes to 1 hr and the data binned in 1 min increments from 0 - 5 min. Activity data for multiple indices relating to dopaminergic function was analyzed using Microsoft Excel software.

Determination of tissue catacholamine levels and Mn

The content of total striatal DA, DOPAC, GABA, and 5-HT was determined by HPLC using electro-chemical detection as described (Champney et al., 1992). Tissue Mn levels will determined by ICP-MS as described (Melnyk et al., 2003).

Immunohistochemistry and fluorojade staining

All mice were deeply anesthetized intraperitoneally with 2.5% tribromoethanol (0.01ml/g body weight) and perfused intracardially with 4% paraformaldehyde in 0.1 M PBS buffer (pH 7.4). The brains were collected and kept in cold 4% paraformaldehyde overnight and stored in cold PBS buffer. Immunohistochemistry of paraffin embedded, 10 μm coronal serial sections through the SN, STN, GP, and striatum (caudate-putamen) was performed as described (Harlan et al., 2001) with primary antibodies to TH (1:400), GFAP (1:400), and 3-nitrotyrosine (1:200). Sections was developed using horseradish

peroxidase-conjugated secondary antibodies and diaminobenzidine reagents from the Vectastain ABC kit. Fluorojade staining of paraffin-embedded sections was performed as described (Schmued et al., 1997).

Immunofluorescence and TUNEL Staining

Immunofluorescence was performed on fixed, paraffin-embedded, 10 μm coronal serial sections through the caudate-putamen and GP. Sections were first examined for TUNEL-positive cells using Terminal deoxynucleotidyl Transferase (TdT) reagents per the manufacturer's instructions and visualized with AlexaFluor-488-labled dUTP. All slides included a control section lacking primary antibody and TdT to insure specificity of staining. Following TUNEL labeling, sections were incubated with anti-NOS1 (1:200), anti-ChAT (1:50), anti-ENK (1:300), anti-Leumorphin (1:50) antibodies, then with AlexaFluor-568-labeled secondary antibody. Cells were imaged by fluorescence microscopy as described below.

Fluorescence Microscopy

Fluorescence images of fluorojade-stained brain tissue were acquired using a Zeiss Axiovert 200M microscope equipped with a 63X 1.4 N/A oil immersion objective and Hamamatsu ORCA-ER cooled charge-coupled device camera. Samples were excited using a Sutter DG-4 xenon source at 490 nm (Ex) and 515 nm (Em) for TUNEL staining and 555 nm (Ex)/590 nm (Em) for antibody staining. Co-localization of GFAP and NOS2 staining was performed using 3-D deconvolution imaging by acquiring images every 0.5 microns across a 12 micron z-series and applying a no-neighbor algorythm with Slide Book software (v. 4.1, Intelligent Imaging Innovations, Inc, Denver, CO).

The deconvolved images were extrapolated into a single, composite 2-D image to illustrate morphological details not evident in any single optical plane.

Statistics

Differences between two groups were analyzed using a two-tailed *t*-test at $p<0.05$.

Results

Increased Mn Levels in Striatum after Mn Exposure

As shown in Figure 2.1*A*, there were no evident body weight changes before and after Mn exposure in either control or Mn-treated mice. However, there was significant ($p<0.05$) increase in Mn levels in striatum of Mn treated mice in comparison with control mice (Figure 2.1*B*). Mn levels were also elevated in the SN ($p<0.09$).

Decreased Locomotor Activity after Mn Exposure

During 8 weeks' treatment, The moter function indices such as total distance traveled in mice exposed to Mn was initially decreased during the first two weeks (probably due to psychotic symptoms), then increased in the following 5 weeks, peeks at about 6 weeks, then was significantly decreased at the end of 8 weeks (Figure 2.2; Figure 2.3*A*). Horizontal activity decreased some but not significantly (Figure 2.3*B*). There were also slight changes in center time (decreased) and/or margin time (increased) (Figure 2.3*C*,*D*), indicative of alterations in anxiety level and novel seeking behavior in Mn-treated animals (Belzung and Griebel, 2001).

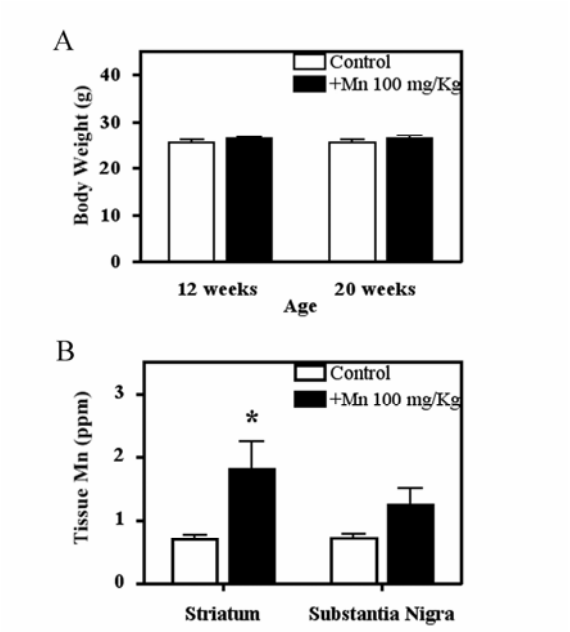

Figure 2.1. Body Weights and Mn Contents in Brain Regions of C57Bl/6J Mice After Mn Exposure. ***A***, Body weights were measured before and after the experiments. ***B***, Tissue Mn levels was determined by inductively coupled plasma-mass spectrometry. Values represent mean ± S.E.M. *$p<0.01$ compared to control striatum. Control striatum: n=12, Mn striatum: n=8; control substantia nigra: n=4, Mn substantia nigra: n=6.

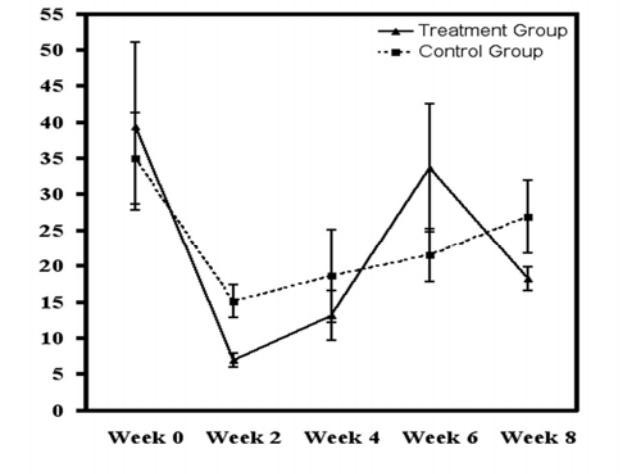

Figure 2.2. Time Course Study of Total Distance Traveled in C57Bl/6J Mice Subchronically Exposed to Mn. Female C57Bl/6J mice were exposed to saline or $MnCl_2$ (100 mg/kg/day) by oral gavage daily for 8 weeks. Mice were paired in recording chambers (control and treated) at week 0, 2, 4, 6, 8 and activity in xyz axes was quantified for 20min. Data from the first 5 min were binned and analyzed for total distance traveled. Values represent mean ± S.E.M. Control: n=6; Mn: n=6.

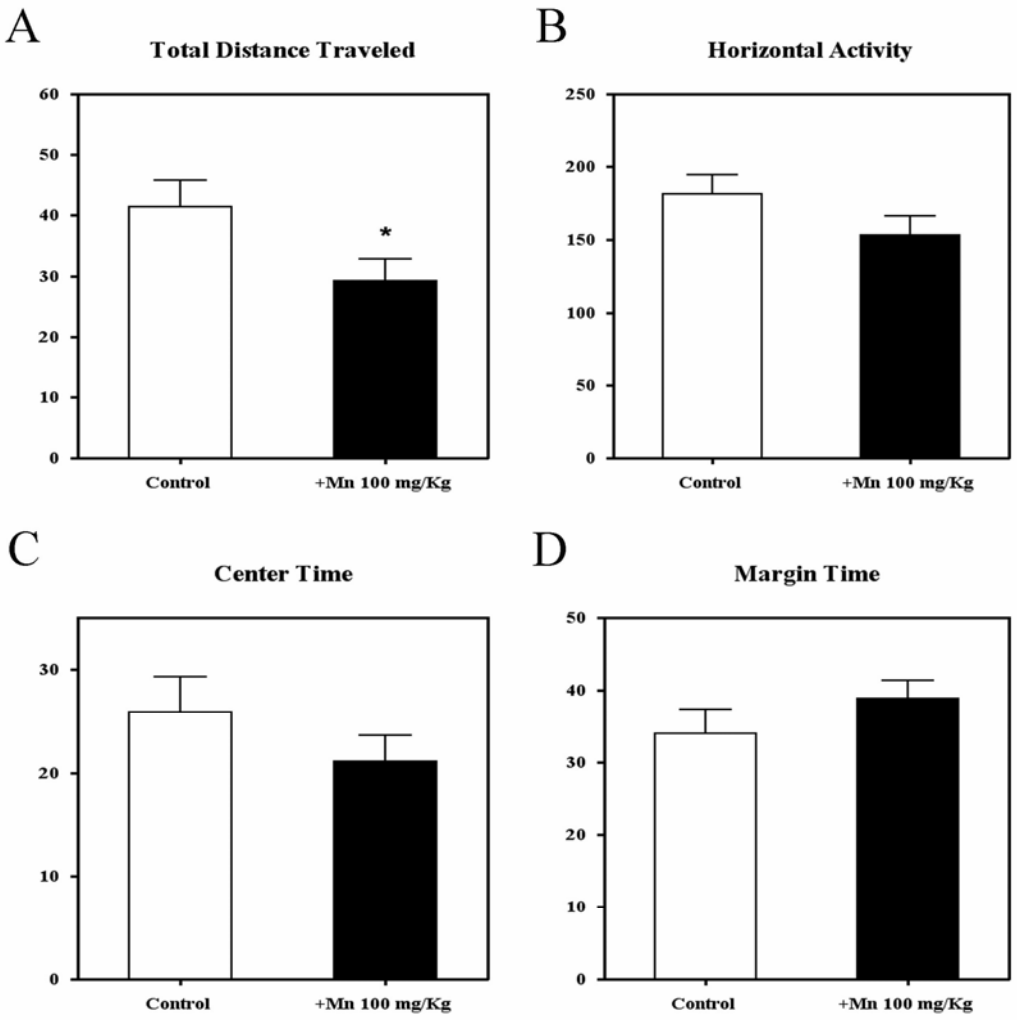

Figure 2.3. Locomotor Activity in C57Bl/6J Mice Subchronically Exposed to Mn. Female C57Bl/6J mice were exposed to saline or $MnCl_2$ (100 mg/kg/day) by oral gavage once daily for 8 weeks. Mice were paired in recording chambers (control and treated) and activity in xyz axes was quantified for 20min. Data from the first 5 min were binned and analyzed for ***A***, total distance traveled; ***B***, horizontal activity; ***C***, center time; ***D***, margin time. Values represent mean ± S.E.M. *$p<0.05$ compared to control. Control: n=19; Mn: n=19.

Decreased DA in the Striatum after Mn Exposure

Measurements of striatal DA (Figure 2.4*A*), DOPAC (Figure 2.4*B*), and GABA (Figure 2.4*D*) contents indicated that there was a decrease of striatal DA in the treated mice while there was no significant change in GABA content. The turnover ratio of DA (DOPAC/DA) (Figure 2.4*C*) was slightly elevated in Mn-treated mice.

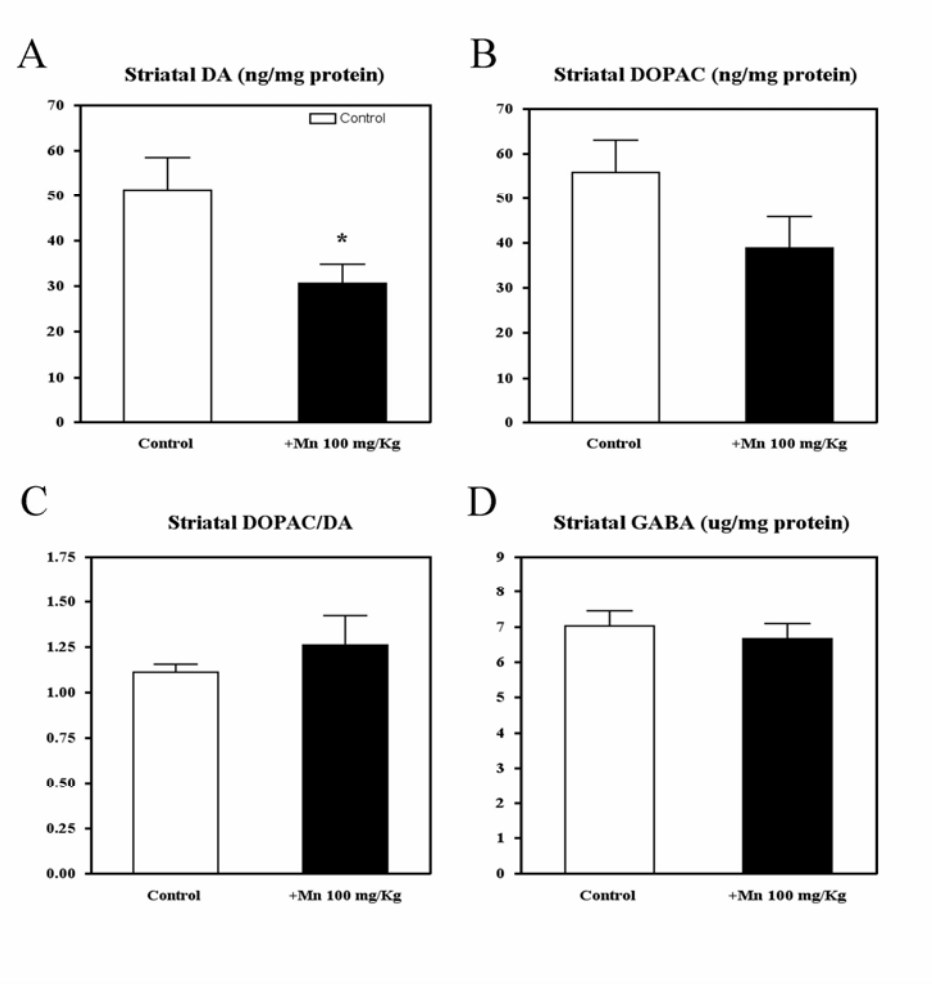

Figure 2.4. Striatal Neurotransmitters in C67Bl/6J Mice Exposed to Mn. Female C57Bl/6J mice were exposed to saline or $MnCl_2$ (100 mg/kg/day) by oral gavage once daily for 8 weeks. At the cessation of treatment animals were evaluated for ***A***, striatal DA; ***B***, DOPAC; ***C***, DOPAC/DA; ***D***, GABA levels by high performance liquid chromatography using electrochemical detection. Values represent mean ± S.E.M. * $p<0.05$ compared to control. Control: n=19; Mn: n=19.

Generalized Nigrostriatal Injury

Generalized neuronal injury in the SN, GP, and striatum was determined by histochemical staining with fluorojade to detect irreversible neurodegeneration. There was significant increase in the number of fluorojade-positive cells in both the striatum (Figure 2.5*A*, *B*) and pallidum, SN (data not shown) in Mn treatment group. Many of the injured cells were appeared to localize to areas proximal to the microvasculature. There was also a marked decrease in the number of darkly staining nissl-positive cell bodies or axons in the striatum (Figure 2.5*C*, *D*) and GP (Figure 2.5*E*, *F*) after Mn exposure.

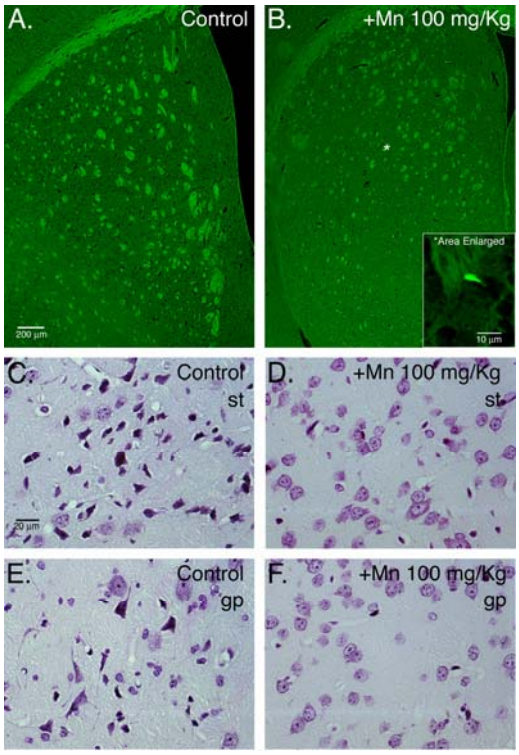

Figure 2.5. Generalized Nigrostriatal Injury in C57Bl/6J Mice Exposed to Mn. Female C57Bl/6J mice were exposed to saline or $MnCl_2$ (100 mg/kg/day) by oral gavage once daily for 8 weeks. At the cessation of treatment animals were evaluated for histopathological changes in the striatum (st) and the globus pallidus (gp). ***A***, ***B***, Fluorojade (***A***, st, control; ***B***, st, +Mn). ***C***-***F***: Cresyl Violet (***C***, st, control; ***D***, st, +Mn; ***E***, gp, control; ***F***, gp, +Mn).

Identification of Vulnerable Neuronal Sub-types

TH-positive neurons in the SN (Figure 2.6*C*, *D*, *E*, *F*) and nerve terminals in the striatum (Figure 2.6*A*, *B*) were morphologically unaltered. Representative images of TUNEL-positive NOS1+ and ChAT+ interneurons and ENK+ projection neurons are shown in Figure 2.7*F*, *I*, *L*. The death of NOS1+ and ChAT+ interneurons can be found in the striatum, GP, and SN. The dying ENK+ projection neurons were mainly located in the GP. DYN+ projection neurons were intact (data not shown). Many of these injured cells were localized near the blood vessels.

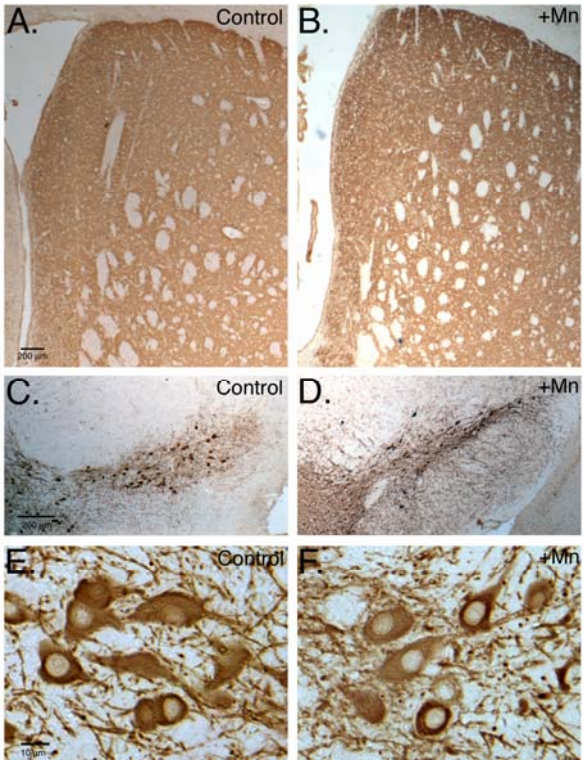

Figure 2.6. Tyrosine Hydroxylase Expression in C57Bl/6J Mice Exposed to Mn. Female C57Bl/6J mice were exposed to saline or $MnCl_2$ (100 mg/kg/day) by oral gavage once daily for 8 weeks. At the cessation of treatment animals were evaluated for expression of TH in the striatum (st) and substantia nigra (sn) by immunohistochemistry. ***A***, st, control; ***B***, st, +Mn. ***C***, sn, control; ***D***, sn, +Mn. ***E***, ***F***, representative images of dopaminergic neurons in sn (***E***, control; ***F***, +Mn).

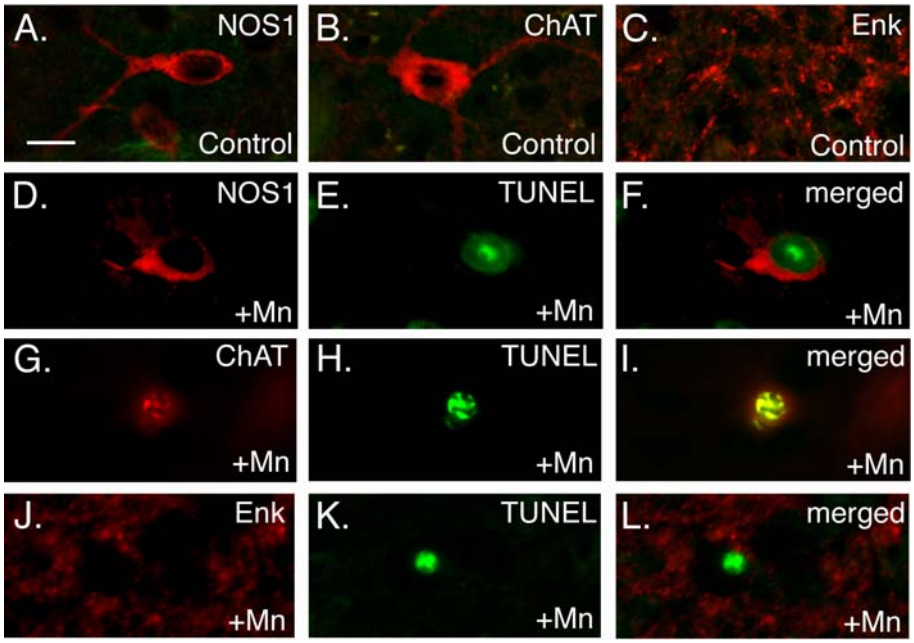

Figure 2.7. Identification of Vulnerable Neuronal Sub-types. Immunofluorescence was performed to detect TUNEL-positive cells using TdT reagents and visualized with AlexaFluor-488-labled dUPT. Following TUNEL labeling, tissue sections were incubated with anti-NOS1, anti-ChAT, anti- ENK, and anti-Leumorphin antibodies and visualized with AlexaFluor-568-labeled secondary antibody. Cells were imaged using a Zeiss 63X oil immersion 1.4 N/A objective and Hamamatsu ORCA-ER camera. *A*, ***B***, ***C***, representative images of NOS1+ interneuron, ChAT+ interneuron and ENK+ projection neuron respectively in saline treated animals. ***D***-***F***, representative TUNEL-positive NOS1+ interneuron in the striatum after Mn treatment. ***D***, NOS1+ interneuron; ***E***, TUNEL-positive nucleus; ***F***, merged image of TUNEL-positive nucleus of NOS1+ interneuron. ***G-I,*** representative TUNEL-positive ChAT+ interneuron in the striatum after Mn treatment. ***G***, ChAT+ interneuron; H, TUNEL-positive nucleus; ***I***, merged image of TUNEL-positive nucleus of ChAT+ interneuron. ***J***-***L***: representative TUNEL-positive ENK+ projection neuron in the striatum after Mn treatment. ***J***, ENK+ projection neuron; ***K***, TUNEL-positive nucleus; ***L***, merged image of TUNEL-positive nucleus of ENK+ projection neuron. Scale bar = 10 μm.

Astrocyte Activation and Nitric Oxide Production

Activation of astrocytes was examined in the GP and striatum using antibodies to GFAP (Figure 2.8*A*, *B*, *C*, *D*; Figure 2.9*A*, *E*) and NOS2 (Figure 2.9*B, F*), respectively. Production of NO/peroxynitrite was determined using a primary antibody directed against 3-nitrotyrosine-modified proteins (Figure 2.8*G*, *H*). There were increased reactive astrocytes (Figure 2.8*A*, *B*) and 3-nitrotyrosine protein adducts ($ONOO^-$

formation) in the striatum and GP after Mn exposure (Figure 2.8*G*, *H*). Further evidence showed that GFAP-positive astrocytes were the only cells that expressed NOS2 (Figure 2.9*H*). NOS2-expressing astrocytes were nearly always located proximal to blood vessels in both the striatum and GP. In contrast to the high levels of astrocytosis observed, no apparent microgliosis occurred in these Mn-treated mice, based upon immunohistochemcial staining with Mac-1/cd11b (data not shown).

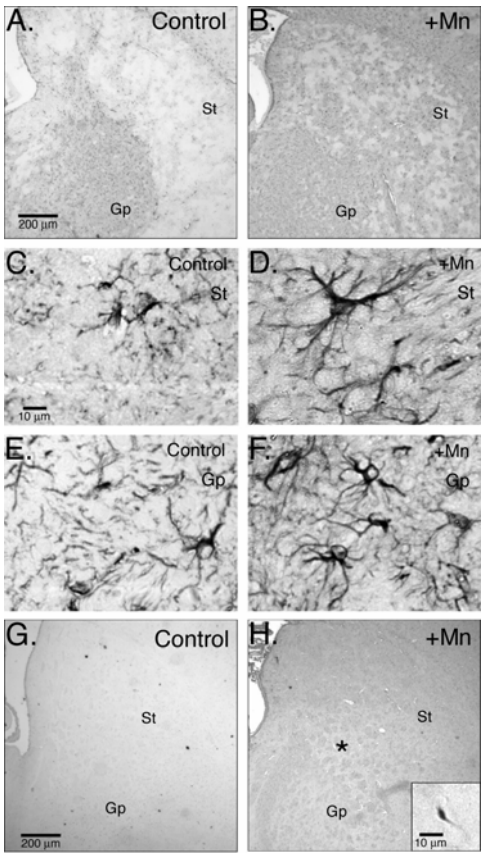

Figure 2.8. Astrocyte Activation and Peroxynitrite Formation in C57Bl/6J Mice Exposed to Mn. Control and Mn-treated mice were evaluated for expression of glial fibrillary acidic protein (GFAP) and 3-nitrotyrosine protein adducts by immunohistochemistry. Relative intensities for GFAP and 3-nitrotyrosine were determined by digital imaging. ***A***, ***B***, st and gp, GFAP (10X). ***A***, control; ***B***, +Mn. ***C***, ***D***, st, GFAP (60X). ***C***, control; ***D***, +Mn. ***E***, ***F***, gp, GFAP (60X). ***E***, control; ***F***, +Mn. ***G***, ***H***, st, 3-nitrotyrosine (10X). ***G***, control; ***H***, +Mn.

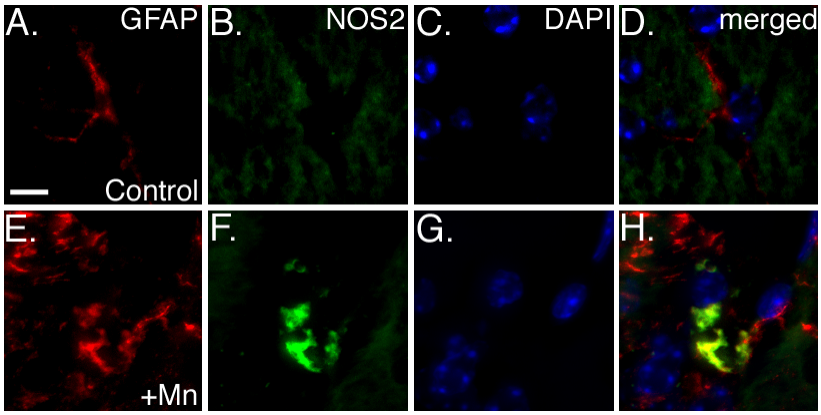

Figure 2.9. Co-localize GFAP and NOS2 in the Striatum of C57Bl/6J Mice Exposed to Mn. Control and Mn-treated mice were evaluated for co-localization of GFAP and NOS2 by immunofluorescence. Images were acquired using a Zeiss 63X PlanApochromat oil objective by 3-D deconvolution imaging. Spatial bar represents 10 microns. ***A***, control GFAP; ***B***, control NOS2; ***C***, control DAPI; ***D***, control merged image of GFAP, NOS2 and DAPI. ***E***, control GFAP; ***F***, control NOS2; ***G***, control DAPI; ***H***, control merged image of GFAP, NOS2 and DAPI.

Discussion

Lesions of the basal ganglia in humans lead to various types of motor disturbances that range from hypokinesia (e.g., PD) to hyperkinesia (e.g., hemiballismus and chorea) and psychotic disorders, such as schizophrenia. The striatum is the major recipient structure of the basal ganglia; the GPi and SNr are the two major output structures of the basal ganglia. These brain regions are severely affected in manganism but precise cellular mechanisms underlying the known pathological effects of Mn have remained elusive. The present studies provide insight into both the vulnerable neuronal subtypes in the striatal-pallidal system as well as the role of astrocyte-derived NO in the pathological changes observed.

The regional distribution of Mn after overexposure in rodents varies, (Takeda et al., 1994), but in our model there were significant ($p<0.05$) increases of Mn levels in striatum of Mn treated mice compared to controls, consistent with reports in exposed

humans and macaque monkeys (Eriksson et al., 1992; Nagatomo et al., 1999). Mn levels increased ($p<0.09$) in SN, but variability within the relatively small sample size ($n=4$ in Mn-treated group) reduced the power of this observation. Additionally, the small overall size of this brain region in the mouse contributes to the difficulty of acquiring an anatomically precise section of tissue for analytical determination of metal content (Figure 2.1*B*). Elevated brain Mn in exposed mice correlated with hypoactivity (decrease in total distance traveled) as well as development of anxiety and novelty seeking (increased center time or decreased margin time) (Figure 2.3). Moreover, these changes in behavioral indices were associated with a drop in striatal DA of approximately 50% (Figure 2.4). This degree of diminution in catecholamine content represents an early established phase of manifestation and indicates the effectiveness of utility of these behavior measures in assessing locomotor dysfunction following Mn overexposure.

A study in rats after chronic $MnCl_2$ administration showed that, the striatal content of dopamine, norepinephrine, and homovanillic acid initially increased, then normalized, followed by a decline in catecholamines and their metabolites (Autissier et al., 1982), which may explain the motor activity changes (from overactive to hypoactive) occurred in our preliminary time couse study (Figure 2.2).

The striatum receives excitatory cortical inputs and dopaminergic inputs from SNc, and projects to GPi and SNr through direct and indirect inhibitory pathways. DA input from SNc can differentially affect striatal projection neurons based on the DA receptor subtypes (Gerfen et al., 1990). DYN+/SP+ projection neurons of the direct pathway express D1 receptor and their activity can be enhanced by DA; whereas indirect

pathway ENK+ projection neurons express D2 receptor and are inhibited by DA (Gerfen and Young, 1988). Activation of the direct pathway results in reduction of inhibitory basal ganglia output, therefore, disinhibition of thalamocortical neurons and facilitation of movement. By contrast, activation of indirect pathway leads to increased basal ganglia output and suppression of movement (Wichmann and DeLong, 1996). In this mice model of early established phase of Mn-induced parkinsonism, the neuropathology showed that ENK+ projection neurons of indirect pathway and ChAT+ interneurons were preferentially lost (Figure 2.7), as reported in early Huntington's disease (Growdon et al., 1977; Reiner et al., 1988; Sun et al., 2002). ChAT+ interneurons can inhibit DYN+ projection neurons of the direct pathway and excite ENK+ projection neurons (Gauchy et al., 1991; Dimova et al., 1993). Consequently, the loss of ChAT+ and ENK+ neurons reduces the inhibition of neurons in the Gpe, causing excessive discharge of these neurons and inhibition of STN neurons. The resulting functional inactivation of STN neurons in turn causes reduction of the basal ganglia output and less inhibition of the thalamus, which could explain the overactive symptoms during Mn exposure (Figure 2.2).

The symptoms of early established phase of Mn induced parkinsonism observed in our study may be either caused by the loss of NOS1+ interneurons or the malfunction of the neurons in the direct pathway (DYN+ projection neurons) without morphological degeneration. The role of NOS1+ interneurons in motor control is not quite clear yet, but evidence suggested that they had an influence on DA related responses of the DYN+ projection neurons (Saka et al., 2002). Interestingly, it has been reported that striatal

somtostatin (another neuropeptide carried by NOS1+ neurons) is reduced in parkinsonism and increased in Huntington's chorea (Bolam et al., 2000).

NOS1+ interneurons are reported to be resistant to the neurotoxic environment they create (NO production). Immunohistochemical co-localization experiments confirmed that MnSOD is expressed at higher levels in NOS1+ neurons than in other neuronal cell types. Knockout of MnSOD through genetic targeting results in increased sensitivity of NOS1+ neurons to NMDA neurotoxicity (Gonzalez-Zulueta et al., 1998). The death of NOS1+ neurons in this study (Figure 2.7) may be due to malfunction of MnSOD and excessive excitotoxicity during Mn exposure although there was no direct evidence. It has been reported that Mn neurotoxicity may be due to an indirect excitotoxic event caused by increased extracellular glutamate levels (Brouillet et al., 1993). Since Mn is concurrently released with glutamate from glutamatergic neuron terminals (Takeda et al., 2002), the hyperactivity of corticostriatal neurons observed in the course of Mn intoxication may partially contribute to the elevated extracellular glutamate levels (Centonze et al., 2001). Glutamate excitotoxicity is associated with increased influx of Na^+ and Ca^{2+} ions, which causes cell swelling and eventually cell lysis. In addition, Ca^{2+} overload leads to stimulation of numerous Ca^{2+}–activated enzymes that degrade cellular structual proteins and produce ROS. ROS inhibits EAA transporter function of excess extracellular glutamate removal, thus producing increased NMDAR stimulation, further production of ROS and greater inhibition of EAA transport. This feed-forward NMDAR- and Ca^{2+} mediated cycle will eventually lead to cell death. Furthermore, elevated extracellular glutamate inhibits the uptake of cystine, a

precursor of GSH, thus decreases intracellular GSH levels and antioxidant function (Choi, 1992; Sonnewald et al., 2002).

The location and morphology of dying cells identified by Fluojade staining (Figure 2.5) suggest that endothelial cells of the striatal microvasculature may be an important target of dysfunction in Mn neurotoxicity, with subsequent disruption of the BBB. This may explain why much of the noted neuronal injury and astrocytosis occurred proximal to vessels. It was postulated earlier by Spranger and colleagues (Spranger et al., 1998) that activated astrocytes might contribute to Mn-induced parkinsonism through excessive production of NO in studies that showed that Mn-induced injury to neurons required the presence of astrocytes and was associated with increased astrocytic expression of NOS2. In our study, the observed relative increased intensities for GFAP and 3-nitrotyrosine (Figure 2.8) as well as co-localization of GFAP and NOS2 after Mn exposure (Figure 2.9) indicated that astrocytosis and atrocyte-derived NO may be involved in the neurodegeneration. Further evidence showed that NOS2-expressing astrocytes were nearly always located proximal to blood vessels in both the striatum and GP, suggesting that the death or dysfunction of endothelial cells comprising the BBB might trigger astrocytosis and NOS2 expression in astrocytes which in turn predisposes to neuronal injury in these areas after Mn exposure.

Collectively, the data from these studies demonstrate that subchronic exposure of mice to moderate levels of Mn by intragastric gavage recapitulates both locomotor and neurochemical features of manganism. Moreover, it appears that astrocytosis and subsequent overproduction of NO are involved in neuronal injury and that this injury

occurs in specific neuronal subtypes within the striatum and GP. Dysfunction of the BBB is suggested by the proximal location of injured neurons and activated astrocytes to blood vessels. It is suggested that this dietary exposure regimen represents a good model with which to study early pathological changes within the basal ganglia that are relevant to human manganism.

CHAPTER III

NF-κB-DEPENDENT PRODUCTION OF NITRIC OXIDE BY ASTROCYTES MEDIATES APOPTOSIS IN DIFFERENTIATED PC12 CELLS FOLLOWING EXPOSURE TO MANGANESE AND CYTOKINES *

Overview

Neuronal injury in manganism is accompanied by activation of astrocyte within the basal ganglia that is thought to increase production of inflammatory mediators such as NO. The present studies postulated that astrocyte-derived NO mediates neuronal apoptosis induced by Mn and pro-inflammatory cytokines. PC12 cells differentiated with nerve growth factor (NGF) were co-cultured with primary astrocytes and exposed to Mn and TNF-α plus IFN-γ. Mn enhanced cytokine-induced expression of NOS2 and production of NO in astrocytes that correlated with apoptosis in co-cultured PC12 cells, as determined by caspase activity, TUNEL, and nuclear morphology. Apoptosis in PC12 cells required the presence of astrocytes and was blocked by overexpression of a phosphorylation-deficient mutant of IκBα (S32/36A) in astrocytes which prevented induction of NOS2. Pharmacologic inhibition of NOS2 with (±)-2-amino-5,6-dihydro-6-

* Reprinted with permission from NF-κB-dependent Production of Nitric Oxide by Astrocytes Mediates Apoptosis in Differentiated PC12 Cells Following Exposure to Manganese and Cytokines by Xuhong Liu, Julie A. Buffington, Ronald B. Tjalkens, Molecular Brain Research, accepted. Copyright 2005 by Elsevier.

methyl-4H-1,3-thiazine (AMT) significantly reduced apoptosis of PC12 cells and the addition of low concentrations of the NO donor, S-nitroso-*N*-acetyl penacillamine (SNAP) to PC12 cells cultured without astrocytes was sufficient to recover the apoptotic phenotype following exposure to Mn and TNF-α/IFN-γ. It is concluded that Mn-and cytokine-dependent apoptosis in PC12 cells requires astrocyte-derived NO and NF-κB-dependent expression of NOS2.

Introduction

Mn is an essential element for numerous enzymes important to metabolic homeostasis in the CNS, including GS (Wedler and Toms, 1986), MnSOD (Stallings et al., 1991), and PEPCK (Bentle and Lardy, 1976). It is also involved in cell-matrix interactions that regulate neurite outgrowth through binding to β1 integrin receptor (Walowitz and Roth, 1999; Ivins et al., 2000; Poinat et al., 2002). However, excessive exposure to Mn through dietary or industrial sources produces neurotoxicity resulting in a degenerative brain disorder (manganism, Mn-induced parkinsonism) characterized by psychiatric symptoms and extrapyramidal neurological deficits (Pal et al., 1999; Albin, 2000). Pathologic changes in human manganism present as neuronal loss and astrocytosis within the basal ganglia, principally the GPi and SNr (Yamada et al., 1986). Injury to the striatum and an accompanying loss of striatal DA levels are also observed that contribute to the motor deficits of the disorder (Daniels and Abarca, 1991; Huang et al., 2003). However, the role of astrocyte in the pathophysiology of manganism remains poorly understood.

Several lines of evidence implicate astrocytes as an early target of Mn. Astrocytes are the principal repository for Mn in the CNS, demonstrated by studies showing that GS, for which Mn is a required cofactor, is located predominantly in this cell type (Martinez-Hernandez et al., 1977). Astrocytes also possess a high affinity uptake system for Mn (Aschner et al., 1992). A selective decrease in immunoreactivity for GFAP and S100β occurs in rats exposed to Mn that precedes any apparent neuronal injury (Henriksson and Tjalve, 2000). Additionally, it was recently observed that an early upregulation of the PTBR occured in adult rats exposed subacutely to Mn that was associated with astrocytosis in the GP (Hazell et al., 2003).

Astrocytes activated during stress and injury produce a number of inflammatory mediators that are injurious to neurons, including IL-1β, TNF-α, IFN-γ, and NO, which are elevated in several disorders of the basal ganglia (Hirsch et al., 1998; Langston et al., 1999). Although it has been reported that Mn potentiates the effects of pro-inflammatory cytokines on expression of NOS2 and production of NO in astrocytes that promotes injury to co-cultured neurons (Spranger et al., 1998), the specific signaling pathways underlying the observed induction of NOS2 have not been identified. NF-κB, a Rel protein family member, is the principal transcription factor that mediates inducible expression of NOS2 in response to LPS and pro-inflammatory cytokines (Xie and Nathan, 1993; Xie et al., 1994). NF-κB is activated by distinct signaling pathways that converge on IKK, which phosphorolates the NF-κB inhibitory subunit, IκBα, resulting in its dissociation and degradation by the 26S proteosome (Karin et al., 2002). Recent studies from our laboratory demonstrated that inhibition of NF-κB through

overexpression of a dominant-negative mutant of IκBα completely blocks the enhancement of Mn on LPS-induced expression of NOS2 in C6 glioma cells (Barhoumi et al., 2004). It was therefore postulated in the present studies that potentiation of cytokine-induced NOS2 expression in astrocytes by Mn is NF-κB dependent and that astrocyte-derived NO causes neuronal injury resulting in apoptosis.

Materials and Methods

Materials

PC12 cells were obtained from the American Type Culture Collection (Manassas, Virginia, Catalog number CRL-1721). C57B1/6 mice were obtained from The Jackson Laboratory (Bar Harbor, ME). Cell culture media, fetal bovine serum, antibiotics, and laminin were purchased from Sigma-Aldrich (St. Louis, MO). Co-culture 6-well companion plates and inserts were from BD Biosiences (Bedford, MA). Polyvinylpyrolidine membranes (Hybond-N), enhanced chemiluminescence (ECL) reagents were purchased from Amersham Biosciences (Piscataway, NJ). Polyclonal antibodies against mouse NOS2 and horseradish peroxidase-conjugated anti-rabbit IgG were obtained from BD Pharmingen (San Diego, CA). Monoclonal antibody to β-actin was obtained from Sigma (St. Louis, MO). Prolong Antifade kit, cell permeant pan-caspase substrate rhodamine 110 *bis*-(L-aspartic acid amide), Hoechst 3342, 4-amino-5-methylamino-2', 7'-difluorofluorescein diacetate (DAF-FM diacetate), and SNAP were purchased from Molecular Probes (Eugene, Oregon). AMT was purchased from Calbiochem (La Jolla, CA). Terminal Transferase Recombinants and Complete™

protease inhibitor cocktails were from Roche Molecular Biochemicals (Indianapolis, IN).

Cell Culture

PC12 cells were maintained in Dulbecco's modified Eagle's medium/Ham's F12 50/50 mix (DMEM/F12) supplemented with 10% heat-inactivated fetal bovine serum (FBS), 50 units/ml penicillin, 50 ng/ml streptomycin, and 100 ng/ml neomycin (PSN) in a humidified atmosphere at 37 °C, 5% CO_2. Primary astrocytes were isolated from the cortex of day 1 postnatal C57B1/6 mice essentially as described (Aschner et al., 1992), except that the number of extractions was reduced by half to accommodate the lower yield of cortical tissue from mice as compared to rats. Astrocyte cultures were maintained at 37 °C, 5% CO_2 in Minimal Essential Medium (MEM) supplemented with Earle's salts, 10% FBS, and PSN, and grown 18 days to maturity prior to experiments. In our laboratory, this method routinely yields cultures consisting of 95-98% astrocytes, based upon immunofluorescence staining for GFAP.

Astrocyte-neuron Co-culture

Confluent PC12 cells were detached with 0.5 mM EDTA and subcultured onto laminin-coated (5 μg/ml) 22 mm round glass coverslips in 6-well plates at 3×10^5/well, then differentiated with NGF (50 ng/ml) for 5 days prior to experiments. Astrocytes were detached with 0.25% Trypsin/0.5mM EDTA and plated on permeable cell culture inserts (0.45 μm pore size) at 2×10^4/well in DMEM/F12 medium containing 10% FBS and PSN 3 days before co-culture with PC12 cells. Upon treatment, PC12 cells and astrocytes were washed with phosphate-buffered saline (PBS, pH 7.4), the culture

medium was changed to DMEM/F12 containing 10% FBS without phenol red or PSN. PC12 cells were treated singly or in co-culture with astrocytes for 1 – 3 days with physiologic saline, 50μM $MnCl_2$, TNF-α (10 μg/ml)/IFN-γ (1 ng/ml), or 50μM $MnCl_2$ + TNF-α/IFN-γ. Astrocytes were removed at the conclusion of treatment and PC12 cells were examined for indices of apoptosis as described below.

Determination of Steady-state Nitric Oxide Production

Steady-state production of NO in live astrocytes was measured by wide-field fluorescence microscopy using the fluorescent indicator DAF-FM diacetate (Kojima et al., 1998), prepared as a 5 mM stock solution in DMSO and diluted in culture medium to a final concentration of 5 μM. The fluorescence intensity of DAF-FM diacetate was determined kinetically by collecting images at 490 nm excitation/520 nm emission at 15 sec intervals for 20 min (see below for microscopy) to permit reaction of NO with DAF-FM diacetate to reach equilibrium. Intensity data were then analyzed by calculating a normalized fluorescence value for each image as dF/F_0, where F represents the background-subtracted fluorescence of a given cell at time *t* divided by the background-subtracted fluorescence of the same cell at time zero (F_0).

Determination of NOS2 mRNA and Protein

Steady state-levels of NOS2 mRNA were determined by real-time PCR using a Prism 7700 instrument and Syber Green reagents (PerkinElmer Life and Analytical Sciences, Inc., Boston, MA) and normalized to β-actin mRNA. The following primers from the mouse NOS2 and β-actin coding sequences were used: (*NOS2*) 5' - TCA CGC TTG GGT CTT GTT C - 3' (forward), 5 ' - CAG GTC ACT TTG GTA GGA TTT G - 3'

(reverse); (*β-actin*) 5' - GCT GTG CTA TGT TGC TCT AG - 3' (forward), ' - CGC TCG TTG CCA ATA GTG - 3' (reverse). RNA was isolated using the RNAeasy kit (Qiagen, Valencia, CA). NOS2 protein levels were determined in astrocytes by immunoblotting. Both mRNA and protein were measured after 24 hrs exposure to Mn and/or TNF-α/IFN-γ in DMEM/F12 culture medium containing 10% fetal bovine serum without phenol red or antibiotics. Total protein was harvested in RIPA buffer (50 mM HEPES, pH 7.4, 500 mM NaCl, 1.5 mM $MnCl_2$, 1 mM EGTA, 10% glycerol, 1% Triton X-100) containing 0.2 mM sodium orthovanadate and Complete™ protease inhibitor cocktail. Cells isolates were then incubated on ice for 1 h and debris pelleted by centrifugation at 10,000 × g for 10 min at 4°C to yield a supernatant designated as total cellular protein. 50 μg of total protein was resolved by 10% SDS-PAGE and transferred to polyvinylpyrolidine membranes. Primary polyclonal antibody for NOS2 was used at 1:500 dilution. Blots were visualized by ECL with a horseradish peroxidase-conjugated secondary antibody at 1:1000 dilution. Blots were stripped and reprobed with a monoclonal antibody to β-actin at 1:1000 dilution to control for the amount of protein loaded.

Expression of Mutant-IκBα

A phosphorylation-deficient mutant of IκBα, IκBα-(S32,36A)-HA, was overexpressed in primary astrocytes using an adenoviral vector (provided by Dr. David Brenner, Columbia University), delivered for 24 hrs at 2×106 viral particles per ml of culture medium, with a multiplicity of infection (MOI) of 1×103 virions per cell. Parallel control experiments utilized the same adenoviral construct lacking the insert. Following

incubation with the mutant IκBα construct for 24 hrs, astrocytes were washed with PBS to remove viral particles and cultured in fresh medium for 24 hrs prior to gene expression studies or co-culture with PC12 cells. Expression of the mutant construct in infected astrocytes was confirmed by immunoblotting for the hemaglutinen epitope.

Caspase Acitvation and Fluorescence Imaging

Activation of caspases was detected using the cell permeant pan-caspase substrate rhodamine 110 *bis*-(L-aspartic acid amide). Cleavage of the aspartate amide by active caspases results in a highly fluorescent product that is readily visualized by fluorescence microscopy. Cellular and nuclear morphology were examined by differential interference contrast (DIC) imaging and staining with Hoechst 3342, respectively. Following 24 hrs co-culture in the presence of Mn and/or TNF-α/IFN-γ, astrocytes were removed and PC12 cells loaded with 10μM rhodamine 110 *bis*-(L-aspartic acid amide) and 10 μM Hoechst 3342 for 20 min at 37 °C in incubation medium (phenol red-free DMEM/F12 plus 2 mM L-glutamine and 25 mM HEPES, pH 7.4). Following incubation, cells were placed into fresh incubation medium and examined by wide field fluorescence microscopy for activation of caspases. Nomarski differential interference contrast images were acquired sequentially with images of rhodamine 110 *bis*-(L-aspartic acid amide) and Hoechst 3342 fluorescence at 490 nm excitation /520 nm emission and 380 nm excitation/400 nm emission, respectively, on an Olympus IX-70 microscope equipped with an ORCA-ER cooled, interline charge-coupled device camera (Hamamatsu Photonics, Hamamatsu City, Japan). The mean fluorescence intensity per cell was calculated using Simple PCI software (Compix, Cranberry Township, PA).

TUNEL and Determination of Nuclear Apoptotic Phenotype

PC12 cells were co-cultured and treated as described above and fixed with 4% paraformaldehyde. Fixed cells were permeabilized with 0.1% Triton X-100 and incubated in equilibration buffer (1X Tris EDTA, pH7.4, 5X terminal transferase buffer, 25mM $CoCl_2$) and TUNEL reaction buffer (1X Tris EDTA, pH7.4, 5X terminal transferase buffer, 25mM $CoCl_2$, 1 mM Alexafluor 488 dUTP, 1mM dATP) for 30 min at 37 °C, then soaked in 1X SSC (150mM NaCl, 15mM sodium citrate) for 15 min to stop the reaction. Hoechst 3342 (0.5 μM) was added to the final 10 min of the wash. Cover slips were mounted onto slides using Prolong Antifade reagent mounting medium. TUNEL-positive nuclei were detected by fluorescence imaging at 490 nm excitation/520 nm emission as described above using a 10X PlanApochromat air objective and quantified by counting a minimum of 800 – 1000 cells per treatment group from at least 3 independent experiments. Images of nuclear morphology were collected at 380 nm excitation/400 nm emission using a 60X 1.45 N/A PlanAprochromat oil immersion objective.

Statistical Analysis

Differences between two treatments were analyzed using a two-tailed *t*-test at $p<0.05$, while differences between multiple treatments were evaluated by one-way ANOVA followed by Tukey's test for multiple comparisons using a significance value of $p<0.05$.

Results

Mn and Cytokine-induced NOS2 Expression and NO Production in Primary Astrocytes Requires Activation of NF-κB

The capacity of Mn to potentiate cytokine-induced expression of NOS2 and production of NO was examined in primary murine cortical astrocytes exposed to TFN-α and IFN-γ (Figure 3.1). Only modest increases in NOS2 mRNA (Figure 3.1*A*) and protein (Figure 3.1*B*) were observed following 24 hrs exposure to either 50 μM $MnCl_2$ or 10 pg/ml TNF-α + 1 ng/ml IFN-γ individually. However, combined exposure to Mn and TFN-α/IFN-γ resulted in large increases in steady-state levels of mRNA and protein. This induction was abrogated by blocking activation of NF-κB through adenovirus-mediated overexpression of a phosphorylation-deficient mutant of IκBα (mtIκBα, IκBα-S32/36A). This genetic approach was selected to inhibit NF-κB without affecting other pathways, otherwise the use of less specific pharmacologic inhibitors, such as TPCK (N-tosyl-L-phenylalanine chloromethyl ketone), will broadly inhibit cellular proteases (Papaccio et al., 2005). Expression mtIκBα completely prevented induction of NOS2 mRNA in cells exposed to either Mn or TNF-α/IFN-γ individually but only partially inhibited induction of NOS2 mRNA in cells exposed to both Mn and TFN-α/IFN-γ. Levels of NOS2 message and protein in cells infected with a control adenoviral vector and exposed to Mn and TFN-α/IFN-γ were similar to uninfected wildtype controls. Similarly, cytokine-induced production of NO in astrocytes was dramatically potentiated by Mn (Figure 3.1*C*), as determined by live-cell digital fluorescence microscopy within

single astrocytes using the fluorescent NO indicator DAF-FM diacetate. Production of NO was attenuated by expression of mtIκBα but not by the control vector.

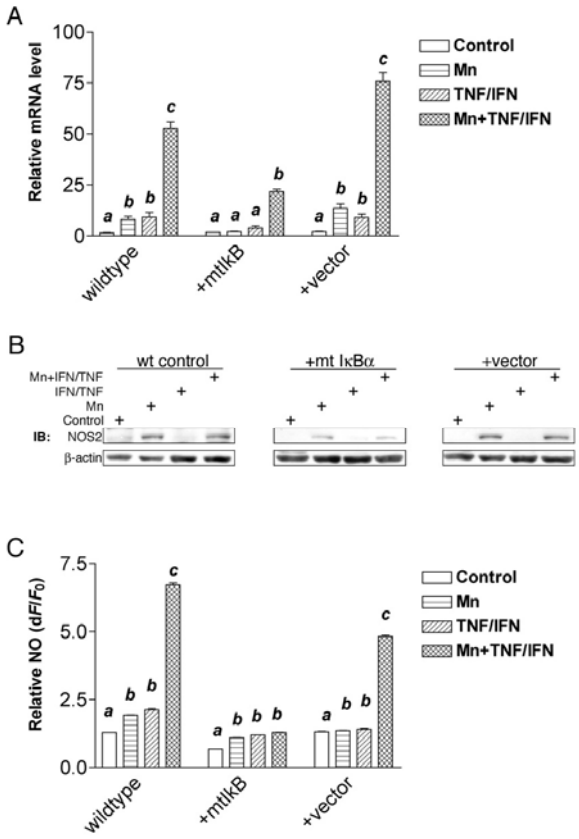

Figure 3.1. Mn and Cytokine-induced NO Production and Expression of NOS2 in Primary Murine Astrocytes Requires Activation of NF-κB. Primary astrocytes were exposed for 24 hrs to saline control, 50μM $MnCl_2$, 10 pg/ml TNF-α + 1 ng/ml IFN-γ, or 50μM $MnCl_2$ + 10pg/ml TNF-α + 1ng/ml IFN-γ. Levels of NOS2 mRNA ***A***, protein ***B***, and NO ***C*** were determined in the absence or presence of a dominant-negative mutant of IκBα (IκBα-S32/36A) or control vector. NOS2 mRNA was determined by semi-quantitative real-time PCR and was normalized to β-actin. NOS2 immunoblots were stripped and re-probed with anti-β-actin primary antibody to control for protein loading. Steady-state production of NO was determined by live cell fluorescence imaging. Data represent the mean ± S.E.M. for triplicate determinations from three independent experiments. Differing letters denote significant difference from other treatment groups (p>0.05).

Caspase Activation in Co-cultured PC12 Cells Exposed to Mn and Cytokines Requires Functional NF-κB in Astrocytes

To examine the effect of Mn- and cytokine-activated astrocytes on co-cultured neurons, PC12 cells differentiated to a neuronal phenotype with NGF were exposed to Mn and TFN-α/IFN-γ in co-culture with astrocytes grown on permeable inserts that permit diffusion of small molecules but not cell-cell contact (Figure 3.2). Following 24 hrs exposure to Mn and TFN-α/IFN-γ, astrocytes were removed and caspase activity was examined in live PC12 cells by fluorescence microscopy using the cell permeant *pan*-caspase substrate, rhodamine 110 *bis*-(L-aspartic acid amide). No differences were observed in either cell morphology or caspase activation in co-cultured neurons exposed to saline control or 50 μM $MnCl_2$ (Figure 3.2*A*, *B*). Neurites and axons were evident in these treatment groups and no loss of dendritic arborization occurred. Quantitation of caspase activity by fluorescence cytometry (Figure 3.2*C* and inset) in adherent populations of co-cultured PC12 cells revealed no differences in rhodamine 110 fluorescence between control and Mn-treated cells. PC12 cells co-cultured with astrocytes in the presence of TNF-α/IFN-γ displayed a similar lack of change in either cell morphology or caspase activity (Figure 3.2*D*), but the addition of both Mn and TNF-α/IFN-γ resulted in widespread activation of caspases and a loss of differentiated neuronal morphology (Figure 3.2*E*, *F*). Quantitation of rhodamine 110 fluorescence (Figure 3.2*F*) revealed a significant increase in the number of neurons with activated intracellular caspases. Overexpression of mtIκBα in astrocytes 24 hrs prior to incubation

with neurons completely blocked Mn- and cytokine-induced activation of caspases in co-cultured PC12 cells and prevented loss of differentiated morphology (Figure 3.2*G*). Caspase activity was still increased upon exposure to Mn and TNF-α/IFN-γ in PC12 cells co-incubated with astrocytes expressing control vector and differentiated morphology was lost (Figure 3.2*H*, *I*).

NF-κB-dependent NOS2 Expression in Astrocyte Mediates DNA Fragmentation and Nuclear Condensation in Co-cultured PC12 cells Exposed to Mn and Cytokines

To determine if the observed increases in caspase activity in co-cultured PC12 cells resulted in apoptosis, cells were assessed for DNA fragmentation by TUNEL and for nuclear morphology by Hoechst 3322 at 1 – 3 days following exposure to Mn and TNF-α/IFN-γ in the presence of astrocytes (Figure 3.3). The number of TUNEL-positive cells was increased over control in co-cultured PC12 cells exposed to Mn and TNF-α/IFN-γ as early as 24 hrs after exposure, peaking at 72 hrs at approximately 12% of cells (Figure 3.3*A*). Exposure to Mn or TNF-α/IFN-γ individually did not result in a significant increase in TUNEL-positive cells (data not shown). The observed increase in TUNEL staining was completely prevented by overexpression of mtIκBα in astrocytes prior to incubation with PC12 cells, but not by control vector (Figure 3.3*B*). Similarly, overexpression of mtIκBα in astrocytes prevented nuclear fragmentation in co-cultured PC12 cells exposed to Mn and TNF-α/IFN-γ, as determined by live-cell fluorescence microscopic analysis of Hoechst-stained cells (Figure 3.3*C*).

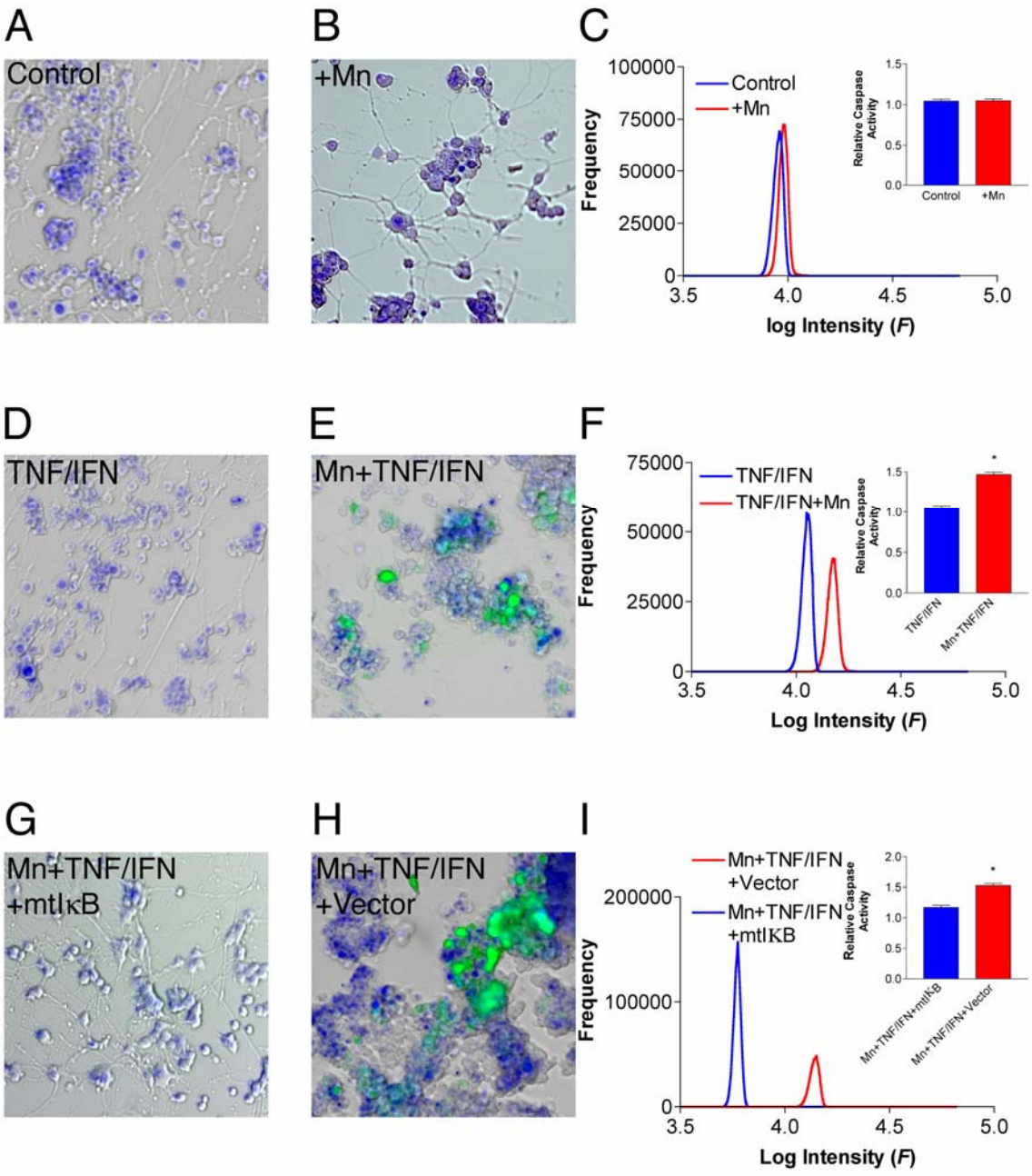

Figure 3.2. Caspase Activation in Co-cultured PC12 cells Exposed to Mn and Cytokines Requires Functional NF-κB in Astrocytes. Caspase activity in co-cultured PC12 cells was assessed by imaging the fluorescence of rhodamine 110 (bis-L-aspartic acid) following exposure to ***A***, saline control, ***B***, 50μM $MnCl_2$, ***D***, 10 pg/ml TNF-α + 1 ng/ml IFN-γ, and ***E***, 50μM $MnCl_2$ + 10pg/ml TNF-α + 1ng/ml IFN-γ. ***C***,***F***,Quantitation of caspase activity by fluorescence cytometry. ***G-I***, Caspase activity in co-cultured neurons exposed to 50μM $MnCl_2$ + 10pg/ml TNF-α + 1ng/ml IFN-γ in the presence of astrocytes expressing mutant IκBα ***G***, or control vector ***H***. * Denotes significant difference from paired treatment (p<0.05).

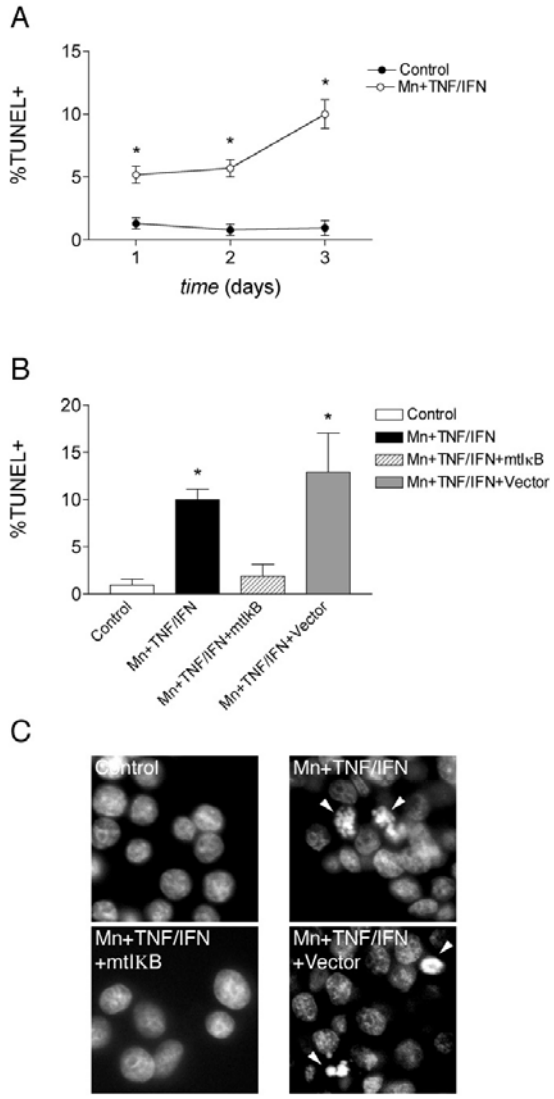

Figure 3.3. NF-κB-dependent NOS2 Expression in Astrocyte Mediates DNA Fragmentation and Nuclear Condensation in Co-cultured PC12 Cells Exposed to Mn and Cytokines. ***A***, Quantitation of TUNEL-positive neurons following 1 – 3 days exposure in co-culture to saline control or 50μM $MnCl_2$ + TNF-α (10pg/ml) + IFN-γ (1ng/ml). ***B***, Quantitation of TUNEL-positive neurons following 3 days exposure in co-culture to Mn and TNF-α/IFN-γ in the presence of astrocytes expressing mutant IκBα or control vector. ***C***, Morphology of Hoechst-stained nuclei in neurons following 3 days exposure in co-culture to Mn and TNF-α/IFN-γ in the presence of astrocytes expressing mutant IκBα or control vector. Field = 40 μm. *Denotes significant difference from control ($p<0.05$).

Inhibition of NOS2 Enzyme Activity Prevents Astrocyte-mediated Neuronal Apoptosis Following Exposure to Mn and Cytokines

The role of NOS2 in astrocyte-mediated neuronal apoptosis was examined by exposing co-cultured astrocytes and PC12 cells to Mn and TNF-α/IFN-γ in the presence of AMT, a highly selective inhibitor of NOS2 enzyme activity (k_i=4.2 nM for the murine isoform) (Nakane et al., 1995). Following 24 hrs exposure to Mn and TNF-α/IFN-γ, caspase activation in co-cultured neurons was completely blocked by 25 nM AMT (Figure 3.4*A*). AMT also decreased, but did not completely prevent, TUNEL-positive cells in co-cultured PC12 cells exposed to Mn and TNF-α/IFN-γ for 3 days in the presence of astrocytes (Figure 3.4*B*) and prevented nuclear condensation and fragmentation in co-cultured neurons (Figure 3.4*C*).

Exogenous NO is Required to Induce Neuronal Apoptosis by Mn and Cytokines in the Absence of Astrocytes

The requirement for astroglial-derived NO in neuronal apoptosis was assessed by exposing PC12 cells to Mn and TNF-α/IFN-γ in the absence of astrocytes and determining the relative changes in caspase activity and apoptosis (Figure 3.5). PC12 cells exposed to both Mn and TNF-α/IFN-γ for 24 hrs in the absence of astrocytes displayed no measurable change in caspase activity, as determined by analysis of rhodamine 110 fluorescence intensity (Figure 3.5*A*). However, combined exposure to Mn and TNF-α/IFN-γ in the presence of the NO donor, 10 μM SNAP, resulted in caspase activation (Figure 3.5*B*), increased TUNEL staining (Figure 3.5*C*), and apoptotic fragmentation of nuclei (Figure 3.5*D*) in PC12 cells. Exposure to 10 μM

SNAP alone did not elicit any apoptotic changes in PC12 cells (Figure 3.5*B-D*), nor did exposure to Mn or TNF-α/IFN-γ individually (data not shown).

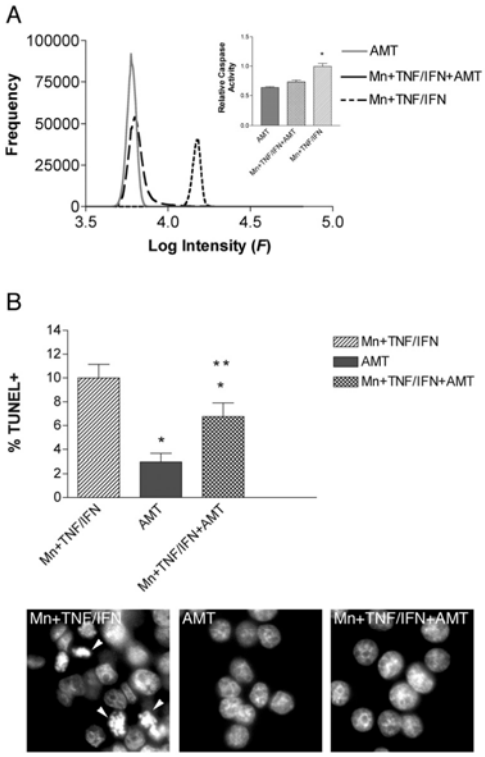

Figure 3.4. Inhibition of NOS2 Enzyme Activity Prevents Astrocyte-mediated Neuronal Apoptosis Following Exposure to Mn and Cytokines. Caspase activity and apoptosis was examined in co-cultured PC12 cells exposed to Mn and TNF-α/IFN-γ for 3 days in the absence or presence of the NOS2 inhibitor AMT. ***A***, Relative caspase activity in co-cultured PC12 cells exposed to 50μM $MnCl_2$ + 10pg/ml TNF-α + 1ng/ml IFN-γ in the absence or presence of 25 nM AMT. ***B***, Percent TUNEL-positive cells after the same treatment as in ***A***. ***C***, Representative Hoechst images of nuclear morphology from ***B***. *Denotes significant difference from Mn + TNF-α/IFN-γ treatment group ($p<0.05$). **Denotes significant difference from 25 nM AMT alone ($p<0.01$).

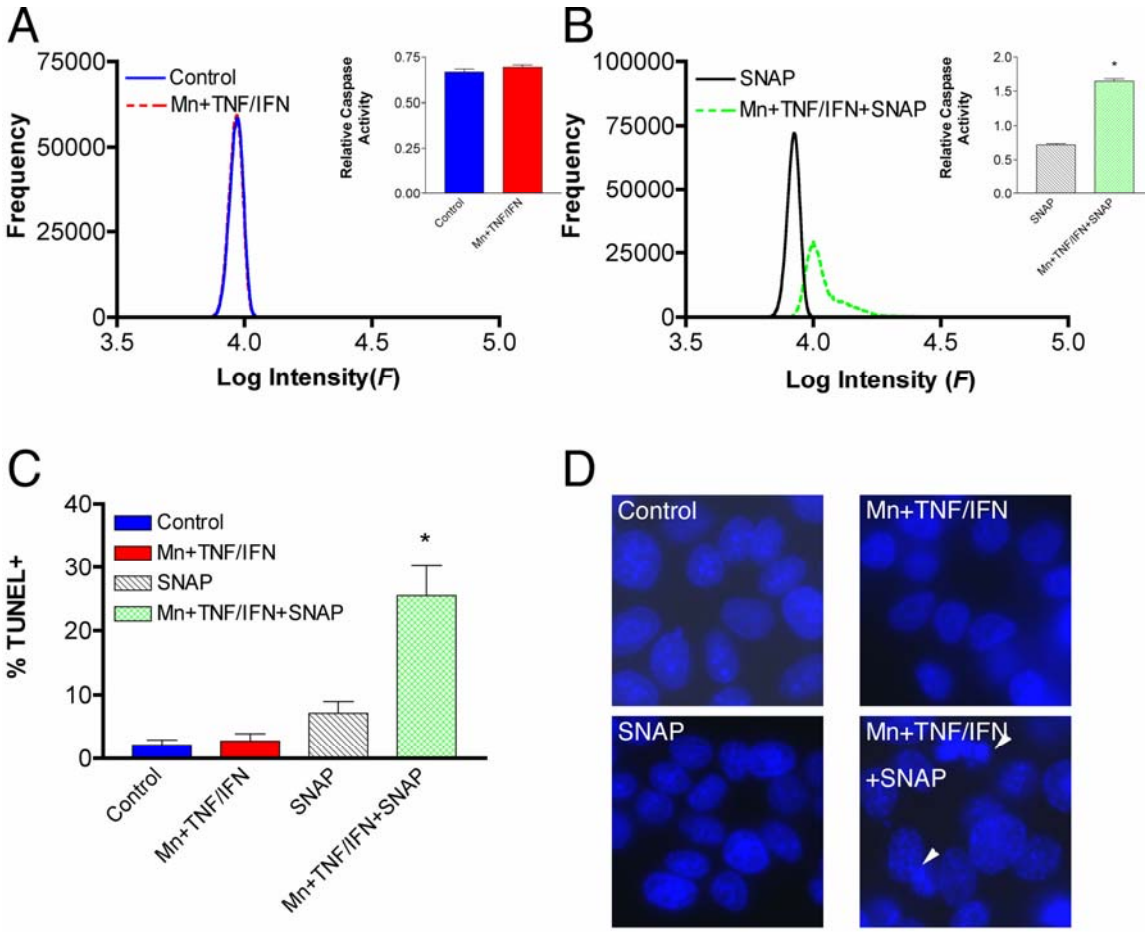

Figure 3.5. Exogenous NO is Required to Induce Neuronal Apoptosis by Mn and Cytokines in the Absence of Astrocytes. Caspase activation was determined in PC12 cells exposed to 50μM $MnCl_2$ + 10pg/ml TNF-α + 1ng/ml IFN-γ for 24 hrs in the absence ***A*** or presence ***B*** of the NO donor, 10 μM SNAP. Percent TUNEL-positive cells ***C*** and nuclear morphology ***D*** in PC12 cells exposed to saline control, 50μM $MnCl_2$ + 10pg/ml TNF-α + 1ng/ml IFN-γ, 10 μM SNAP, or 50μM $MnCl_2$ + 10pg/ml TNF-α + 1ng/ml IFN-γ + 10 μM SNAP for 24 hrs. Field = 40 μm. *Denotes significant difference from AMT group (p<0.05).

Discussion

Astrocytes protect neurons from toxic and ischemic injury by increasing metabolic activity and production of growth and trophic factors. Activation of astrocytes by microglial-derived cytokines such as IL-1β, TNF-α, and IFN-γ promotes adaptive

changes designed to maintain ionic homeostasis within the CNS and to preserve the essential function of the BBB (Liberto et al., 2004). However, more severe injury promotes anisomorphic activation of astrocytes that can exacerbate neuronal dysfunction through enhanced production of inflammatory mediators such as NO, TNF-α, arachidonic acid metabolites, and ROS, resulting in formation of a limiting astrogliotic scar around the site of injury (Liberto et al., 2004). It is therefore of interest to understand the mechanism of action of compounds that diminish the trophic capacity and adaptive responses of activated astrocytes, leading to an activated phenotype that promotes neuronal injury. Mn in excess may function as such a compound by interfering with critical metabolic and trophic functions of astrocytes; Mn decreases uptake of glutamate (Hazell and Norenberg, 1997) and expression of the glutamate transporters GLAST and GLT-1 (Erikson and Aschner, 2002) in cultured astrocytes, disrupts mitochondrial calcium buffering (Gunter and Pfeiffer, 1990), and promotes cytokine-mediated expression of NOS2 (Spranger et al., 1998; Barhoumi et al., 2004).

The present studies demonstrate that Mn dramatically potentiates induction of NOS2 and production of NO in cultured astrocytes exposed to modest concentrations of the inflammatory cytokines TNF-α and IFN-γ. NF-κB is a central regulator of NOS2 transcriptional activation (Xie et al., 1994) and, accordingly, overexpression of a dominant-negative 'super repressor' of NF-κB blocked the expression of NOS2 in astrocytes exposed to Mn or cytokines singly but did not completely block the potentiating effect of combined exposure (Figure 3.1). This phenomenon could be explained through other transcription factors that activate the promoter of NOS2 in

addition to NF-κB, such as Elk-1 and AP-1 (Xie and Nathan, 1993). Elk-1 is activated via the ERK pathway, which is potently stimulated by Mn (Walowitz and Roth, 1999; Ivins et al., 2000), and activation of AP-1 is promoted by ROS, which are increased in glial cells by Mn through disruption of mitochondrial calcium (Barhoumi et al., 2004). However, analysis of steady-state production of NO in astrocytes by real-time imaging revealed that inhibition of NF-κB decreased Mn- and cytokine-induced NO to levels only slightly above control (Figure 3.1*C*). This is consistent with other studies describing NF-κB as the principal transcription factor involved in inflammatory activation of NOS2 (Xie and Nathan, 1993; Xie et al., 1994). Although NOS2 protein levels did not appear to be strongly potentiated by combined exposure to Mn and TNFα/IFN-γ, compared to individual exposure (Figure 3.1*B*), steady-state production of NO was greatly enhanced (Figure 3.1*C*). This observation could be explained in part by the availability of co-factors, such as, BH_4 which are required for synthesis of NO, and have been shown to be coordinately upregulated with NOS2 (Linscheid et al., 2003).

The potentiation of cytokine-induced NOS2 expression in astrocytes by Mn elicits apoptotic changes in co-cultured PC12 cells. Only combined exposure to Mn and TNF-α/IFN-γ was sufficient to increase activation of caspases, fragmentation of DNA, and nuclear condensation in co-cultured PC12 cells (Figure 3.2 and Figure 3.3). Individual exposure to these compounds did not elicit any apoptotic changes in co-cultured neurons. Overexpression of mtIκBα in astrocytes prevented all indices of apoptosis in co-cultured neurons for up to three days following combined exposure to Mn and TNF-α/IFN-γ, indicating that NF-κB-dependent gene expression in astrocytes is

required for neuronal apoptosis in this system. Pharmacologic inhibition of NOS2 with 25 nM AMT blocked activation of caspases in co-cultured neurons (Figure 3.4*A*) but did not completely prevent Mn- and cytokine-induced apoptosis (Figure 3.4*B*). These data suggest that NO is responsible for most, but not all, of the observed apoptotic changes in co-cultured neurons. This observation is not surprising, considering that numerous other inflammatory mediators are regulated by NF-κB, including prostaglandin E2 and cytokines such as IL-1β, that likely contribute to astrocyte-mediated injury.

In the absence of astrocytes, combined exposure to Mn and TNF-α/IFN-γ fails to induce apoptosis in co-cultured neurons. However, the apoptotic phenotype was recovered in PC12 cells exposed to Mn and TNF-α/IFN-γ in the absence of astrocytes by the addition of low concentrations of the NO donor SNAP (Figure 3.5), indicating that astrocyte-derived NO is both necessary and sufficient to induce apoptosis in co-cultured neurons. Although the expression of NOS2 has been reported in undifferentiated PC12 cells (Chung et al., 1999), the primary involvement of astrocyte-specific NOS2 in Mn- and cytokine-dependent apoptosis is demonstrated by the requirement for NF-κB-dependent gene expression in astrocytes (Figure 3.2 and Figure 3.3), as well as the effectiveness of NOS2 inhibition in preventing neuronal apoptosis (Figure 3.). Moreover, apoptosis in the absence of astrocytes is only recovered through the addition of NO (Figure 3.5), precluding the involvement of neuronally-derived NO in the observed apoptotic changes. It has been previously reported that NO donors can induce apoptosis in undifferentiated PC12 cells at relatively high concentrations (~100 μM) (Yuyama et al., 2003), but in the present studies no significant degree of caspase

activation was detected in differentiated PC12 cells at the low concentrations of SNAP utilized (10 μM; Figure 3.5).

Collectively, these data demonstrate that Mn potentiates cytokine-induced expression of NOS2 in astrocytes by an NF-κB-dependent mechanism and that subsequent overproduction of NO results in apoptosis of co-cultured neurons. This is, to our knowledge, the first report of a specific transcription factor in astrocytes that has been shown to mediate NO-dependent neuronal apoptosis following exposure to Mn. Related studies from our laboratory in C6 glioma cells indicated that the upstream signaling events by which Mn exerts this effect on NF-κB-dependent expression of NOS2 appear to involve both direct stimulatory effects on cytokine-mediated stimulation of IκBα phosphorylation as well as enhancement of mitochondrial-derived ROS (Barhoumi et al., 2004). Unraveling these complex and convergent signaling events in primary astrocytes will provide additional insight into the role of astrocyte-derived NO in the neurotoxicity of Mn.

CHAPTER IV

1,1-BIS(3'-INDOLYL)-1-(P-TRIFLUOROMETHYLPHENYL) ETHANE INHIBITS ASTROCYTE-MEDIATED NEURONAL APOPTOSIS AFTER MN EXPOSURE

Overview

Astrocytosis is thought to play an important role in neuronal injury induced by excessive Mn exposure which results in a clinical movement disorder, termed manganism that shares certain neurogical features with PD. Previous studies demonstrated that astrocyte-derived NO mediates apoptosis in differentiated PC12 cells after exposure to Mn and pro-inflammatory cytokines by a mechanism requiring activation of NF-κB. In this study, we postulated that activation of NF-κB in this system is regulated by the orphan nuclear receptor PPARγ. To test this hypothesis, co-cultured astrocytes and PC12 cells differentiated with NGF were exposed to Mn and TNFα plus IFN-γ in the presence of novel pharmacologic ligands of PPARγ, DIM-C-pPhCF$_3$. Apoptosis of co-cultured neuronal cells was dramatically attenuated by DIM-C-pPhCF$_3$, whereas the addition of PPARγ antagonist GW9622 resulted in an increase in neuronal cell death. Apoptosis in co-cultured neuronal cells was correlated with PPARγ-dependent NOS2 expression in astrocytes. It is concluded from this study that PPARγ is involved in the regulation of NOS2 expression in astrocytes and that agonists of PPARγ may represent a potential therapeutic modality for Mn neurotoxicity.

Introduction

Our previous data demonstrated that Mn potentiated cytokine-induced expression of NOS2 in astrocytes by an NF-κB-dependent mechanism and that subsequent overproduction of NO resulted in apoptosis of co-cultured PC12 cells. Presumably, treatments that inhibit the NF-κB-dependent NOS2 expression in astrocytes may be effective at diminishing the severity of Mn neurotoxicity.

Recent studies suggest that multiple coactivators play a critical role in NF-κB-dependent transcription: the p65 component of NF-κB binds to the coactivator CBP (cyclic AMP response element binding protein [CREB]-binding protein) and its structural homolog p300 (Gerritsen et al., 1997); p50 interacts with steroid receptor-coactivator-1 (SRC-1) or nuclear receptor coactivator-1 (NCoA-1) from the p160 family (Na et al., 1998). SRC-1/NCoA-1 also interacts with CBP through two helical domains that contain the core LXXLL consensus sequence (Torchia et al., 1997). The co-activator complex used by p50-p65 closely resembles that used by PPARγ (Sheppard et al., 1999), a member of the nuclear hormone receptor superfamily that activates target gene transcription in a ligand-dependent manner. CBP and p300 are recruited to PPARγ through bridging factors that include SRC-1, although CBP and p300 also contain an N-terminal LXXLL domain that can interact directly with PPARγ (Schulman et al., 1998). The SRC-1 class of co-activators interacts with nuclear receptors through a conserved region with the consensus sequence LXXLL (Torchia et al., 1997). Liganded PPARγ has been shown to inhibit transcription of genes induced by IFN-γ and/or LPS, including the *nos2* gene. This inhibition is considered transrepression because it does not appear to

involve direct binding to the *nos2* promoter but may be achieved partially through antagonizing the activities of NF-κB (Li et al., 2000). It has been suggested that competition for limiting amounts of general coactivators CBP/p300 and SRC-1 represents a mechanism for transrepression of NF-κB by PPARγ (Kamei et al., 1996; Li et al., 2000). Mutations that cause significantly weakened interactions between PPARγ and the SRC-1/CBP coactivators result in coordinate loss of transrepression activities, which suggest that PPARγ-dependent transrepression of the *nos2* promoter involves the targeting of CBP–SRC-1 coactivator complexes (Li et al., 2000). PPARγ positively regulates gene expression by binding to response elements in target genes as a heterodimer with retinoid X receptors (RXRs) (Kliewer et al., 1992). When either the PPARγ or RXR components of the heterodimer are bound by agonists, the respective ligand binding domains (LBDs) undergo a conformational change and recruit coactivators (Torchia et al., 1997) which may inhibit p50-p65 induced *nos2* gene transcription.

These studies support the potential of PPARγ agonists in the treatment of NF-κB dependent inflammatory diseases. Currently, thiazolidinediones (TZDs), including rosiglitazone, ciglitazone, and pioglitazone, a class of synthetic PPARγ agonists are currently being used in the treatment of type-II diabetes and are also found effective in inhibiting the onset and duration of EAE, an animal model of multiple sclerosis (MS) (Feinstein et al., 2002). The expression of PPARγ in astrocytes makes these cells potential targets for the anti-inflammatory actions of TZDs (Cristiano et al., 2001). Another study also demonstrated that TZDs inhibited the production of NO and pro-

inflammatory cytokines and chemokines from stimulated mouse astrocytes (Storer et al., 2005).

In this study we evaluate a new class of PPARγ agonist, DIM-C-pPhCF$_3$, as a potential treatment of Mn neurotoxicity. Diindolylmethane (DIM) is a metabolite of indole-3-carbinol, a phytochemical that contributes to the anticarcinogenic activity of cruciferous vegetables (Murillo and Mehta, 2001). DIM-C-pPhCF$_3$ is one of the DIMs containing substituted phenyl groups at the methylene carbon (C-substituted DIMs) which has been reported to induce PPARγ dependent transactivation and PPARγ-coactivator interactions in MCF-7 cells (Qin et al., 2004). So far, this is the first study to apply this chemical in the treatment of Mn neurotoxicity.

Materials and Methods

Materials

PC12 cells were obtained from the American Type Culture Collection (Manassas, Virginia, Catalog number CRL-1721). C57B1/6 mice were obtained from The Jackson Laboratory (Bar Harbor, ME). Cell culture media, fetal bovine serum, antibiotics, and laminin were purchased from Sigma-Aldrich (St. Louis, MO). Co-culture 6-well companion plates and inserts were from BD Biosciences (Bedford, MA). Polyvinylpyrolidine membranes (Hybond-N), ECL reagents were purchased from Amersham Biosciences (Piscataway, NJ). Polyclonal antibodies against mouse NOS2 and horseradish peroxidase-conjugated anti-rabbit IgG were obtained from BD Pharmingen (San Diego, CA). Monoclonal antibody to β-actin was obtained from Sigma (St. Louis, MO). Monoclonal antibody to PPARγ was obtained from Santa Cruz

Biotechnology (Santa Cruz, CA). Prolong Antifade kit, cell permeant pan-caspase substrate rhodamine 110 *bis*-(L-aspartic acid amide), Hoechst 3342 were purchased from Molecular Probes (Eugene, Oregon). Terminal Transferase Recombinants and Complete™ protease inhibitor cocktails were from Roche Molecular Biochemicals (Indianapolis, IN). DIM-C-pPhCF_3 and GW9622 were provided by Dr. Stephen Safe (Texas A&M University).

Cell Culture

PC12 cells were maintained in Dulbecco's modified Eagle's medium/Ham's F12 50/50 mix (DMEM/F12) supplemented with 10% heat-inactivated fetal bovine serum (FBS), 50 units/ml penicillin, 50 ng/ml streptomycin, and 100 ng/ml neomycin (PSN) in a humidified atmosphere at 37 °C, 5% CO_2. Primary astrocytes were isolated from the cortex of day 1 postnatal C57B1/6 mice essentially as described (Aschner et al., 1992), except that the number of extractions was reduced by half to accommodate the lower yield of cortical tissue from mice as compared to rats. Astrocyte cultures were maintained at 37 °C, 5% CO_2 in Minimal Essential Medium (MEM) supplemented with Earle's salts, 10% FBS, and PSN, and grown 18 days to maturity prior to experiments. In our laboratory, this method routinely yields cultures consisting of 95-98% astrocytes, based upon immunofluorescence staining for GFAP.

Astrocyte-neuron Co-culture

Confluent PC12 cells were detached with 0.5 mM EDTA and subcultured onto laminin-coated (5 μg/ml) 22 mm round glass coverslips in 6-well plates at 3×10^5/well, then differentiated with NGF (50 ng/ml) for 5 days prior to experiments. Astrocytes

were detached with 0.25% Trypsin/0.5mM EDTA and plated on permeable cell culture inserts (0.45 μm pore size) at 2×10^4/well in DMEM/F12 medium containing 10% FBS and PSN 3 days before co-culture with PC12 cells. Upon treatment, PC12 cells and astrocytes were washed with phosphate-buffered saline (PBS, pH 7.4), the culture medium was changed to DMEM/F12 containing 10% FBS without phenol red or PSN. PC12 cells were treated in co-culture with astrocytes for 1–3 days with physiologic saline, 50μM $MnCl_2$, TNF-α (10 μg/ml)/IFN-γ (1 ng/ml), or 50μM $MnCl_2$ + TNF-α/IFN-γ. Astrocytes were removed at the conclusion of treatment and neuronal cells were examined for indices of apoptosis as described below.

Western Blot Analysis

NOS2 protein level was determined in astrocytes after 24 hrs exposure to Mn and TNF-α/IFN-γ with 1μM DIM-C-pPhCF$_3$ or 10μM GW9622 in DMEM/F12 culture medium containing 10% fetal bovine serum without phenol red or antibiotics. PPARγ expression was detected in untreated NGF differentiated PC12 cells and primary astrocytes. Total protein was harvested in RIPA buffer (50 mM HEPES, pH 7.4, 500 mM NaCl, 1.5 mM $MnCl_2$, 1 mM EGTA, 10% glycerol, 1% Triton X-100) containing 0.2 mM sodium orthovanadate and Complete™ protease inhibitor cocktail. Cells isolates were then incubated on ice for 1 h and debris pelleted by centrifugation at 10,000 × g for 10 min at 4°C to yield a supernatant designated as total cellular protein. 50 μg of total protein was resolved by 10% SDS-PAGE and transferred to polyvinylpyrolidine membranes. Primary polyclonal antibody for NOS2 was used at 1:500 dilution. Primary monoclonal antibody to PPARγ was used at 1:1000 dilution. Blots were visualized by

ECL with a horseradish peroxidase-conjugated secondary antibody at 1:1000 dilution. Blots were stripped and reprobed with a monoclonal antibody to β-actin at 1:1000 dilution to control for the amount of protein loaded.

Caspase Acitvation and Fluorescence Imaging

Activation of caspases was detected using the cell permeant pan-caspase substrate rhodamine 110 *bis*-(L-aspartic acid amide). Cleavage of the aspartate amide by active caspases results in a highly fluorescent product that is readily visualized by fluorescence microscopy. Cellular and nuclear morphology were examined by DIC imaging and staining with Hoechst 3342, respectively. Following 24 hrs co-culture in the presence of Mn and/or TNF-α/IFN-γ, astrocytes were removed and PC12 cells loaded with 10μM rhodamine 110 *bis*-(L-aspartic acid amide) and 10 μM Hoechst 3342 for 20 min at 37 °C in incubation medium (phenol red-free DMEM/F12 plus 2 mM L-glutamine and 25 mM HEPES, pH 7.4). Following incubation, cells were placed into fresh incubation medium and examined by wide field fluorescence microscopy for activation of caspases. Images of rhodamine 110 *bis*-(L-aspartic acid amide) and Hoechst 3342 fluorescence were acquired sequentially at 490 nm excitation /520 nm emission and 380 nm excitation/400 nm emission, respectively, with Nomarski differential interference contrast images using a Zeiss Axiovert 200M microscope equipped with an ORCA-ER cooled, interline charge-coupled device camera (Hamamatsu Photonics, Hamamatsu City, Japan). Acquisition and analysis of images was performed using Slidebook software (v. 4.1, Intelligent Imaging Innovations,

Denver, CO). Fluorescence intensities were quantified as the mean intensity per cell and population means were then compared using the statistical methods described below.

TUNEL and Determination of Nuclear Condensation

PC12 cells were co-cultured and treated as described above and fixed with 4% paraformaldehyde. Fixed cells were permeabilized with 0.1% Triton X-100 and incubated in equilibration buffer (1X Tris EDTA, pH7.4, 5X terminal transferase buffer, 25mM $CoCl_2$) and TUNEL reaction buffer (1X Tris EDTA, pH7.4, 5X terminal transferase buffer, 25mM $CoCl_2$, 1 mM Alexafluor 488 dUTP, 1mM dATP) for 30 min at 37 °C, then soaked in 1X SSC (150mM NaCl,15mM sodium citrate) for 15 min to stop the reaction. Hoechst 3342 (0.5 μM) was added to the final 10 min of the wash. Cover slips were mounted onto slides using Prolong Antifade reagent mounting medium. TUNEL-positive nuclei were detected by fluorescence imaging at 490 nm excitation/520 nm emission as described above using a 10X PlanApochromat air objective and quantified by counting a minimum of 800 – 1000 cells per treatment group from at least 3 independent experiments. Images of nuclear morphology were collected at 380 nm excitation/400 nm emission using a 60X 1.45 N/A PlanAprochromat oil immersion objective.

Statistical Analysis

Differences between two treatments were analyzed using a two-tailed *t*-test at $p<0.05$, while differences between multiple treatments were evaluated by one-way ANOVA followed by Tukey's test for multiple comparisons using a significance value

of $p<0.05$. Analyses were performed using Prism software (Graphpad Software, Inc, v4.0a).

Results

PPARγ-dependent Neuronal Death in Neuron-astrocyte Co-culture System

Our caspase study showed that co-cultured NGF differentiated PC12 cells underwent apoptosis in the presence of 50 μM $MnCl_2$ + 10 pg/ml TNF-α and 1 ng/ml IFNγ within 24hrs and 1 μM PPARγ agonist DIM-C-pPhCF$_3$ efficiently inhibited it, however, 10μM PPARγ antagonist GW9622 did not exacerbate it (Figure 4.1*A*). Our further experiments of nuclear staining for propidium iodide showed that GW9622 induced necrosis in stead of apoptosis in co-cultured PC12 cells after Mn and cytokines exposure (Figure 4.1*B*, *C*). Quantitation of TUNEL-positive co-cultured differentiated PC12 cells after 3 days exposure to 50μM $MnCl_2$ + 10 pg/ml TNF-α + 1ng/ml IFNγ in the presence of 1 μM DIM-C-pPhCF$_3$ or 10μM GW9622 showed that DIM-C-pPhCF$_3$ protected PC12 cells from apoptotic cell death and GW9622 exacerbated it (Figure 4.2).

PPARγ Expression in Differentiated PC12 Cells and Primary Astrocytes

Both PC12 cells differentiated with NGF (50 ng/ml) for 5 days and primary astrocytes expressed PPARγ as shown by western blot (Figure 4.3). Expression of PPARγ was greater in differentiated PC12 cells than in primary astrocytes.

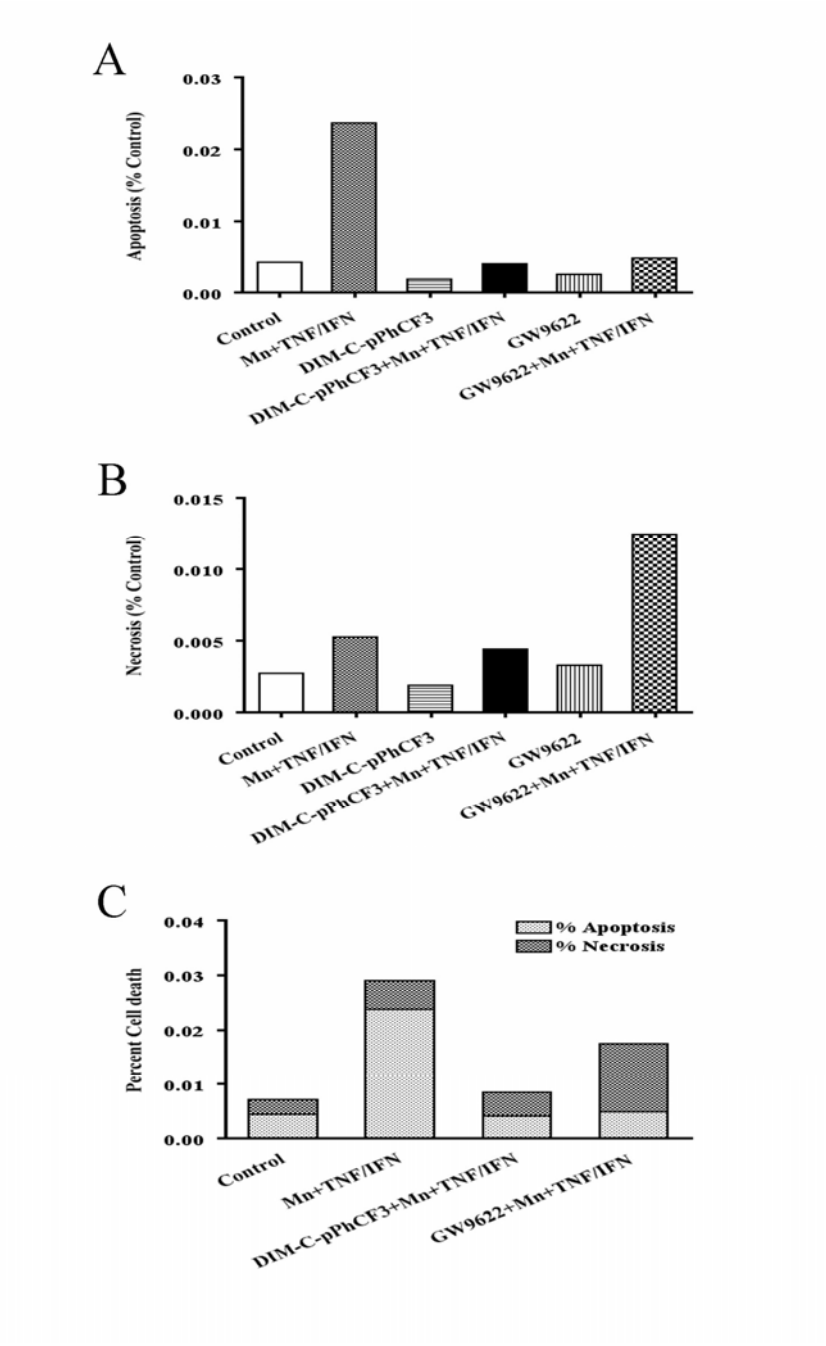

Figure 4.1. Caspase Activity in Differentiated PC12 cells Co-cultured with Astrocytes in the Absence or Presence of PPARγ Ligands. Differentiated PC12 cells were co-cultured with astrocytes and treated with 50 μM MnCl2 and TNFα/IFNγ in the absence or presence of DIM-C-pPhCF3 (1 μM) or GW9622 (10 μM) for 24hrs and examined for the extent of apoptosis and necrosis by live-cell fluorescence imaging ***C***. Apoptosis was quantified as the number of caspase-positive cells relative to control ***A***; necrosis was quantified by the number of cells with positive nuclear staining for propidium iodide relative to control ***B***.

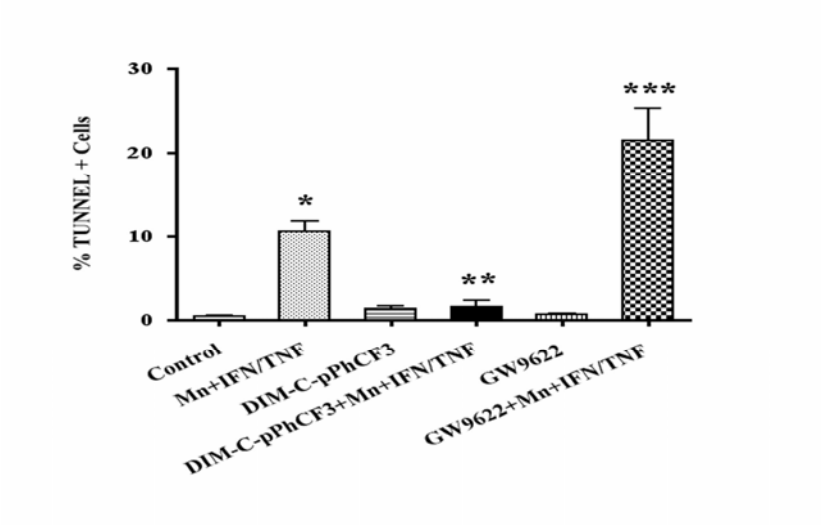

Figure 4.2. Quantitation of TUNEL-positive Co-cultured PC12 Cells After 3 Days Exposure to Mn and TNF-α/IFN-γ in the Presence of PPARγ Agonist or PPARγ Antagonist. NGF differentiated PC12 cells were co-cultured with primary astrocytes and treated with saline control, 50μM $MnCl_2$ + 10pg/ml TNF-α + 1ng/ml IFNγ, 1μM PPARγ agonist DIM-C-pPhCF$_3$, 10μM PPARγ antagonist GW9622, 50μM $MnCl_2$ + 10pg/ml TNF-α + 1ng/ml IFNγ with 1μM DIM-C-pPhCF$_3$ or 10μM GW9622 for 3 days. DNA fragmentation and nuclear condensation of co-cultured PC12 cells were determined by TUNEL and Hoechst 3342 staining. TUNEL-positive nuclei were detected by fluorescence imaging and quantified by counting a minimum of 800-1000 cells per treatment group from at least 3 independent experiments. *p<0.001, compared with control; **p<0.01, compared with Mn + IFN/TNF; ***p<0.001, compared with Mn + IFN/TNF.

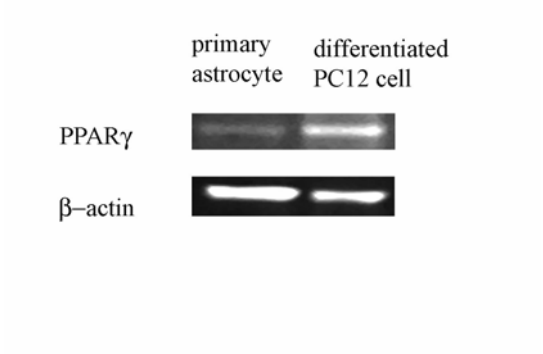

Figure 4.3. PPARγ Expression in NGF Differentiated PC12 Cells and Primary Astrocytes. PC12 cells were differentiated with NGF (50 ng/ml) for 5 days, primary astrocytes were maintained in Minimal Essential Medium (MEM) supplemented with Earle's salts, 10% FBS, and PSN, and grown 18 days to maturity prior to experiments. 50 μg of total protein was loaded on a 7.5% polyacrylamide gel and transferred to polyvinylpyrolidine membranes. Primary monoclonal antibody to PPARγ was used at 1:1000 dilution. Blots were stripped and reprobed with a monoclonal antibody to β-actin at 1:1000 dilution to control for the amount of protein loaded. The data are representatives for three independent experiments.

PPARγ-dependent NOS2 Expression

Exposure to 50μM $MnCl_2$ + 10pg/ml TNF-α + 1ng/ml IFNγ for 24 hrs resulted in NOS2 expression in primary murine cortical astrocytes. This induction was abrogated by 1μM DIM-C-pPhCF$_3$ and enhanced by 10μM GW9622, as indicated by the immunoblot studies in Figure 4.4.

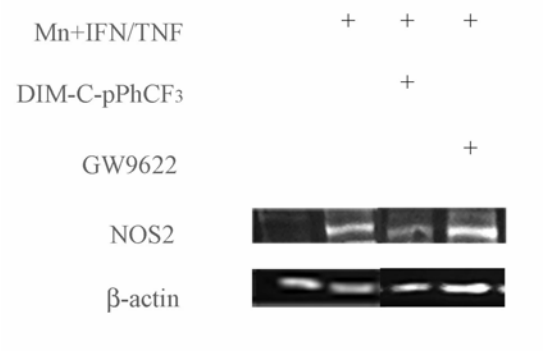

Figure 4.4. PPARγ-dependent NOS2 Expression. Primary astrocytes were exposed for 24 hrs to saline control, 50μM $MnCl_2$ + 10pg/ml TNF-α + 1ng/ml IFNγ, 50μM $MnCl_2$ + 10pg/ml TNF-α + 1ng/ml IFNγ with 1μM DIM-C-pPhCF$_3$ or 10μM GW9622. 50 μg of total protein was loaded on a 7.5% polyacrylamide gel and transferred to polyvinylpyrolidine membranes. Primary polyclonal antibody for NOS2 was used at 1:500 dilution. Blots were stripped and reprobed with a monoclonal antibody to β-actin at 1:1000 dilution to control for the amount of protein loaded. The data are representatives for three independent experiments.

Effects of PPARγ Agonist on Apoptosis of Neurons in Neuronal Culture

NGF differentiated PC12 cells did not undergo apoptosis in the presence of 50μM $MnCl_2$ + 10pg/ml TNF-α + 1ng/ml IFNγ or 10 μM NO donor SNAP alone for 1 day. However, with the combination of 10 μM SNAP and 50μM $MnCl_2$ + 10pg/ml TNF-α + 1ng/ml IFNγ, the caspase activity and TUNEL-positive cells significantly increased (Figure 4.5). Quantitation of relative caspase activity and TUNEL-positive cells after 1 day exposure to 10 μM SNAP + 50 μM $MnCl_2$ + 10 pg/ml TNF-α + 1

ng/ml IFNγ in the presence of 1μM DIM-C-pPhCF$_3$ showed that DIM-C-pPhCF$_3$ did not protect PC12 cells from apoptosis (Figure 4.5*A*, *B*). Also, the PPARγ antagonist, GW9622, did not enhance SNAP-and Mn-induced apoptosis in differentiated PC12 neuronal cells in the absence of astrocytes (Figure 4.5*A*).

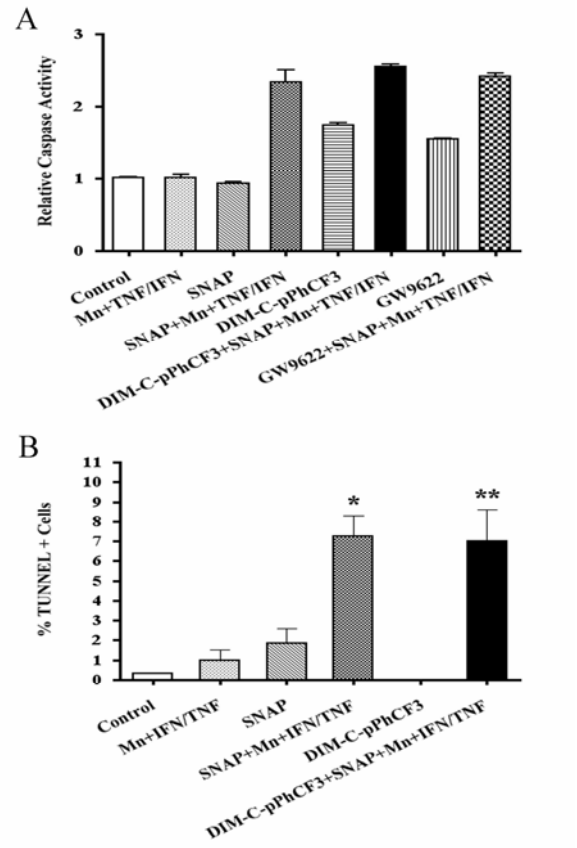

Figure 4.5. **Quantitation of Relative Caspase Activity and TUNEL-positive PC12 Cells After 1 Day Treatment.** NGF differentiated PC12 cells were treated with saline control, 50 μM $MnCl_2$ + 10 pg/ml TNF-α + 1ng/ml IFNγ, 10 μM SNAP, 10 μM SNAP + 50μM $MnCl_2$ + 10 pg/ml TNF-α + 1ng/ml IFNγ, 1μM DIM-C-pPhCF3, 50 μM $MnCl_2$ + 10pg/ml TNF-α + 1ng/ml IFNγ + 10 μM SNAP with 1μM DIM-C-pPhCF3 for 1 day. Caspase activity was detected using the cell permeant pan-caspase substrate rhodamine 110 bis-(L-aspartic acid amide) ***A***, DNA fragmentation and nuclear condensation of PC12 cells were determined by TUNEL and Hoechst 3342 staining ***B***. Caspase activation and TUNEL-positive nuclei were detected by fluorescence imaging and quantified by counting a minimum of 800-1000 cells per treatment group from at least 3 independent experiments. *$p<0.001$, compared with control; **$p<0.01$, compared with control.

Discussion

Our previous data showed that astrocytes mediated the apoptosis of PC12 cells through NF-κB-dependent NOS2 expression and subsequent NO production after exposed to Mn and pro-inflammatory cytokines and the number of TUNEL-positive co-cultured PC12 cells was increased over control as early as 24hrs after exposure, peaking at 72hrs. In the present studies, DIM-C-pPhCF$_3$, a novel pharmacologic agonist of PPARγ, protected differentiated PC12 cells from astrocyte-induced apoptosis following exposure to Mn and TNFα/IFNγ (Figure 4.1 and Figure 4.2). Although PC12 cells also express PPARγ (Figure 4.3), this effect appeared to be specific to astrocytes, because no protection against apoptosis was conferred by DIM-C-pPhCF$_3$ in PC12 cells upon exposure to Mn, TNFα/IFNγ, and the NO donor SNAP in the absence of astrocytes (Figure 4.5). Moreover, the PPARγ antagonist, GW9622, did not exacerbate the extent of apoptosis in PC12 cells in the absence of astrocytes (Figure 4.5*A*). Thus, it is likely that the PPAR**γ**-dependent increase in TUNEL-positive co-cultured PC12 cells after Mn and cytokines exposure (as shown in Figure 4.2) is caused by PPAR**γ**-dependent NOS2 expression (Figure 4.4) and subsequent NO production (data not shown) in astrocytes rather than by the PPAR**γ** dependent survival mechanisms in PC12 cells.

The PPAR**γ** dependent expression of NOS2 in astrocytes (Figure 4.4) parallels the death of PC12 cells (Figure 4.2), supporting the role of NO in apoptosis of PC12 cells after exposure to Mn and cytokines. Our previous data showed that NOS2 expression in primary astrocytes after Mn and TNF-α/IFN-γ exposure was NF-κB dependent. The competition for the limiting amounts of general co-activators CBP/p300

and SRC-1 required for the activation of both NF-κB and PPARγ dependent transcription has been suggested to be a mechanism for transrepression of NF-κB by PPARγ (Kamei et al., 1996; Li et al., 2000). Upon activation by agonists, PPARγ will recruit additional co-activator proteins (Torchia et al., 1997) that may inhibit p50-p65 induced *nos2* gene transcription. PPARγ antagonists, on the other hand, will block the binding of co-activators with PPARγ, thus indirectly potentiating p50-p65 induced NOS2 expression.

Research on the possible role of PPARγ in neuronal survival has not been fully considered yet. It has been previously reported that PC12 cells have no detectable PPARγ by western blot (Jung et al., 2003) and phosphorylation-dephosphorylation mechanisms could play a role in the NGF-induced PPARγ transcriptional activity. As 15-deoxy-PGJ2 (PPARγ agonist, a naturally occurring ligand of PPARγ) did not induce PPARγ expression during neurite extension, activation of p38 MAP kinase in conjunction with AP-1 signal pathway was shown to be important in the promoting activity of 15-deoxy-PGJ2 on the differentiation of PC12 cells (Jung et al., 2003).

However, another recent study detected a 60kDa PPARγ band in PC12 cells (Fuenzalida et al., 2005). NGF has been shown to increase the transcriptional activity of PPARγ dependent on tyrosine kinase (TrkA) activation in PC12 cells (Fuenzalida et al., 2005). TrkA activation induces a rapid release and catabolism of arachidonic acid through the lipoxygenase pathway (Fink and Guroff, 1990), which is required for neurite outgrowth (Nakashima et al., 2003) and several eicosanoids, products of lipoxygenase action, are supposed to be PPARγ ligands (Nagy et al., 1998). These results suggest that

PPARγ might function as a novel target of the TrkA-mediated neuronal cell survival and differentiating pathway (Fuenzalida et al., 2005).

The divergence of PPARγ expression in PC12 cells might be due to different experimental conditions, particularly the culture conditions, or to different sources or batches of PPARγ antibodies (Fuenzalida et al., 2005). Our data showed that PC12 cells differentiated with NGF for 5 days displayed a more intensive expression of PPARγ than primary astrocytes (Figure 4.3), however, PPARγ agonist DIM-C-pPhCF_3 did not protect PC12 cells themselves from apoptosis after NO, Mn and cytokines exposure (Figure 4.5). The reason for that is not known yet. One possibility is that PPARγ function (expression or activation) is not involved in the neurite extension in PC12 cells. As evidence for this, another synthetic PPARγ agonist troglitazone did not have promoting activity in the NGF-induced neurite extension (Satoh et al., 1999) and the PPARγ antagonist bisphenol A diglycidyl did not inhibit the promoting ability of 15-deoxy-PGJ2 on the NGF-induced neurite extension (Jung et al., 2003). Another possibility is that Mn and cytokines treatment inhibit PPARγ expression in PC12 cells. As one of the study showed that IFNγ treatment of adipocytes resulted in decreased PPARγ expression which was mediated by inhibition of PPARγ synthesis and increased degradation (Floyd and Stephens, 2002). Further experiments are needed to verify these hypotheses.

In summary, NOS2 expression in astrocytes is a major cause of cell death in co-cultured PC12 cells after exposure to Mn and cytokines. The PPARγ agonist DIM-C-pPhCF_3 effectively suppresses induction of NOS2 in astrocytes may represent a potential

new therapeutic approach for limiting inflammatory injury caused by excessive production of NO in astrocytes.

CHAPTER V

CONCLUSIONS AND FUTURE RESEARCH WORK

General Conclusions

The studies presented in this work demonstrate the establishment of a mouse model of manganism (Mn-induced parkinsonism) that recapitulates the early established stages of this clinical disorder, including alterations in locomotor activity and neurochemistry. Our study first reported the death of NOS1+ and ChAT+ interneurons and ENK+ projection neurons in the striatum and GP of mice subchronic exposed to Mn, suggesting the important role of interneurons in control of movement activity and the indirect dopaminergic pathway disrupted in this stage of the disease. This model implicates activation of astrocytes, with subsequent expression of NOS2 and production of NO, in the death of striatal-pallidal neurons. The regional distribution of injury proximal to the brain microvasculature also suggests that disruption of BBB function may be an important early event in the progression of injury following exposure to Mn.

Our in vitro model of NGF differentiated PC12 cells co-cultured with primary astrocytes demonstrated that NOS2 expression and NO production in astrocytes correlated with the apoptosis of PC12 cells, as pharmacologic inhibition of NOS2 with AMT significantly reduced apoptosis of PC12 cells and the addition of low concentrations of the NO donor SNAP to PC12 cells cultured without astrocytes was sufficient to recover the apoptotic phenotype following exposure to Mn and TNF-α/IFN-γ. Apoptosis in PC12 cells required the presence of astrocytes and was blocked by

overexpression of a phosphorylation-deficient mutant of IκBα (S32/36A) which prevented induction of NOS2 in astrocytes. It is therefore concluded that Mn- and cytokine-induced apoptosis in PC12 cells requires astrocyte-derived NO as well as NF-κB-dependent expression of NOS2 in astrocytes.

The next step of this research is try to find a practical way to prevent neurodegeneration caused by astrocytosis and NO production after Mn exposure. To this end, a new class of PPARγ agonist, DIM-C-pPhCF$_3$ was used in the primary astrocyte and NGF differentiated PC12 cell co-culture system. DIM-C-pPhCF$_3$ inhibited apoptosis of co-cultured PC12 cells and the NOS2 expression in the primary astrocytes after exposure to Mn and TNF-α/IFN-γ. Although both differentiated PC12 cell and primary astrocyte express PPARγ, DIM-C-pPhCF$_3$ did not protect PC12 cells not co-cultured with astrocytes from apoptosis after Mn, TNF-α/IFN-γ and NO exposure.

Thus, significant overall conclusions are:

1. Mn induces selective loss of striatal-pallidal neurons through a mechanism involving astrocytosis and astrocyte-derived NO, implicating astrocytes as an important early target of Mn.

2. Mn strongly potentiates cytokine-induced expression of NOS2 and production of NO in cultured astrocytes by signaling mechanisms that converge on the NF-κB pathway.

3. Mn-induced production of NO in astrocytes is sufficient to induce neuronal apoptosis *in vitro* and requires NF-κB-dependent expression of NOS2.

4. PPARγ is an important regulator of NOS2 in astrocytes and can be pharmacologically modulated to mitigate NF-κB-dependent production of NO following exposure to Mn and pro-inflammatory cytokines.

5. The PPARγ agonist, DIM-C-pPhCF$_3$ may represent a new potential therapeutic intervention for limiting astrocyte-derived inflammatory mediators in manganism and related degenerative movement disorders of the basal ganglia.

Future Research Work

Our research raises the question of how Mn is transported across the BBB as we observed that the endothelial cells of blood vessels in the basal ganglia were disrupted after oral Mn overexposure. Astrocytes are implicated to have different characters in different brain regions (Gahring et al., 2004), it is reasonable to ask if BBB formed by astrocytes and endothelial cells of blood vessels differs in its sensitivity to Mn overexposure in different regions of brain which could account for the special vulnerability of the basal ganglia? Co-culture of primary endothelial cells and astrocytes from different brain regions may be helpful in answering these questions.

Another unsolved issue related to Mn is the capacity of neurons and astrocytes in accumulating this metal. Tholey et al. have done research in chick primary neuron and astrocyte cultures and conclude that Mn concentration in neurons is almost 3 times more than in astrocytes (Tholey et al., 1988a; Tholey et al., 1988b). However, Wedler and Denman did another study in ovine brain and show that 80% of brain Mn is associated with GS (Wedler and Denman, 1984). According to previous research which showed that GS was mainly located in astrocytes (Martinez-Hernandez et al., 1977), it's

reasonable to postulate that almost 80% brain Mn is located in astrocytes. Subsequent studies show that astrocytes possess a high affinity transport system for Mn and can accumulate more than 50-fold greater concentration of Mn than the culture medium while neurons can not (Aschner et al., 1992). The question of which cell type accumulates more Mn is still hard to answer based on the evidence mentioned above. First, the character of avian neurons and astrocytes may be different from those of mammals; second, the number of astrocytes are much more than the number of neurons in CNS; third, although Mn concentration in neurons is higher than that in astrocytes (Tholey et al., 1988a), the intracellular water volume is higher in astocytes than in neurons. So which cell type can accumulate more Mn still needs further investigation.

Although it has long been considered that the level of astrocytic Mn could regulate GS activity (Wedler et al., 1994). Some studies showed that Mn has a complex effect on GS activity. In a narrow range of concentration (1–10 μM) in the presence of 5mM Mg^{2+}, Mn activates GS (Wedler and Denman, 1984), whereas further increases in Mn concentration have a negative effect on the enzyme activity, reaching a maximum inhibition at approximately 20 μM (Tholey et al., 1987). Boksha reported that in homogenates from human brain, the Mn^{2+} dependence of GS activity shows a maximum at ~0.6-1.0mM and a drastic decrease at higher Mn^{2+} concentrations (Boksha et al., 2000). However, all these studies are carried out in the test tube, the GS activity measurement in vivo after Mn exposure has never been reported, and thus the physiological and pathological relevance of GS activity and Mn^{2+} concentrations in astrocytes or in certain area of brain is not known. Research on this subject will be very

helpful to answer the question of whether and how Mn is involved in excitotoxity. Also, the kinetic changes of MnSOD activity level after Mn exposure in vivo especially in NOS1+ interneurons have never been carefully carried out. As MnSOD has been reported to be the main reason for the NOS1+ interneurons relative resistance to NO and other pathological conditions (Gonzalez-Zulueta et al., 1998), research related to Mn and MnSOD will be very promising in understanding why NOS1+ interneurons are the most vulnerable type of neurons after Mn overexposure and may be helpful in developing potential preventive and therapeutic method of manganism.

Several studies suggest that signal transduction pathways leading to *nos2* gene induction after cytokines exposure seem to differ markedly from species to species and even between cells (Kleinert et al., 1996; Linn et al., 1997). Another recent study in human primary astrocytes show that different cytokines or different combination of cytokines exposure result in different signal transduction pathways leading to NOS2 expression (Jana et al., 2005). So far, nobody has done the research work in human striatal astrocytes to verify the NF-κB dependent NOS2 expression after Mn overexposure, and further the effectiveness of PPARγ agonist in preventing NO induced striatal neurodegeneration.

Some interesting questions related to NOS1+ interneurons based on our study are: 1) why are NOS1 interneurons the most vulnerable populations of neurons after Mn overexposure while they are relatively spared in most other neurodegenerative diseases such as Huntington's and Alzheimer's disease (Ferrante et al., 1985; Hyman et al., 1992); and 2) what's the function of NOS1+ interneurons in regulating DA

concentration in the striatum and their potential role in coordinating motor activity. To answer these questions a time course study of neurochemistry, behavior and neuropathology after Mn overexposure is necessary and also an in vitro primary striatal neuron and astrocyte co-culture experiments will be helpful to understand the mechanisms of Mn neurotoxicity.

It is also necessary to identify the effects of Mn on neurotransmitter, especially DA, metabolism, uptake, and efflux, given that Mn can both increase or decrease levels of striatal DA depending on its exposure time and dose (Autissier et al., 1982), representing up or down-regulation in the function of certain neurons that have succumbed to the effect of Mn. It should also be pointed out that other neurotransmitters such as GABA and glutamate are co-localized to the same brain areas and therefore may play active roles in Mn-induced neurotoxicity.

In addition, it is still interesting to further investigate whether the toxicity of Mn is secondary to disturbances in Fe metabolism. Both Mn and Fe share similarities in their chemistry and biochemistry, so it is reasonable to postulate that the mechanisms underlying Mn distribution are dependent on Fe homeostasis (Aschner 2000).

REFERENCES

Aisen P, Aasa R, Redfield AG (1969) The chromium, manganese, and cobalt complexes of transferrin. J Biol Chem 244:4628-4633.

Albin RL (2000) Basal ganglia neurotoxins. Neurol Clin 18:665-680.

Alderton WK, Cooper CE, Knowles RG (2001) Nitric oxide synthases: structure, function and inhibition. Biochem J 357:593-615.

Alexander GE, Crutcher MD (1990) Functional architecture of basal ganglia circuits: neural substrates of parallel processing. Trends Neurosci 13:266-271.

Ali SF, Duhart HM, Newport GD, Lipe GW, Slikker W, Jr. (1995) Manganese-induced reactive oxygen species: comparison between Mn+2 and Mn+3. Neurodegeneration 4:329-334.

Almeida A, Bolanos JP (2001) A transient inhibition of mitochondrial ATP synthesis by nitric oxide synthase activation triggered apoptosis in primary cortical neurons. J Neurochem 77:676-690.

Almeida A, Almeida J, Bolanos JP, Moncada S (2001) Different responses of astrocytes and neurons to nitric oxide: the role of glycolytically generated ATP in astrocyte protection. Proc Natl Acad Sci U S A 98:15294-15299.

Archibald FS, Tyree C (1987) Manganese poisoning and the attack of trivalent manganese upon catecholamines. Arch Biochem Biophys 256:638-650.

Aschner M, Aschner JL (1990) Manganese transport across the blood-brain barrier: relationship to iron homeostasis. Brain Res Bull 24:857-860.

Aschner M, Aschner JL (1991) Manganese neurotoxicity: cellular effects and blood-brain barrier transport. Neurosci Biobehav Rev 15:333-340.

Aschner M, Gannon M, Kimelberg HK (1992) Manganese uptake and efflux in cultured rat astrocytes. J Neurochem 58:730-735.

Aschner M, Vrana KE, Zheng W (1999) Manganese uptake and distribution in the central nervous system (CNS). Neurotoxicology 20:173-180.

Aschner M, Mutkus L, Allen JW (2001) Aspartate and glutamate transport in acutely and chronically ethanol exposed neonatal rat primary astrocyte cultures. Neurotoxicology 22:601-605.

Aschner M, Sonnewald U, Tan KH (2002a) Astrocyte modulation of neurotoxic injury. Brain Pathol 12:475-481.

Aschner M, Shanker G, Erikson K, Yang J, Mutkus LA (2002b) The uptake of manganese in brain endothelial cultures. Neurotoxicology 23:165-168.

Autissier N, Rochette L, Dumas P, Beley A, Loireau A, Bralet J (1982) Dopamine and norepinephrine turnover in various regions of the rat brain after chronic manganese chloride administration. Toxicology 24:175-182.

Ballatori N, Miles E, Clarkson TW (1987) Homeostatic control of manganese excretion in the neonatal rat. Am J Physiol 252:R842-847.

Bandyopadhyay A, Chakder S, Rattan S (1997) Regulation of inducible and neuronal nitric oxide synthase gene expression by interferon-gamma and VIP. Am J Physiol 272:C1790-1797.

Barhoumi R, Faske J, Liu X, Tjalkens RB (2004) Manganese potentiates lipopolysaccharide-induced expression of NOS2 in C6 glioma cells through mitochondrial-dependent activation of nuclear factor kappaB. Brain Res Mol Brain Res 122:167-179.

Beal MF (1992) Does impairment of energy metabolism result in excitotoxic neuronal death in neurodegenerative illnesses? Ann Neurol 31:119-130.

Bell JG, Keen CL, Lonnerdal B (1989) Higher retention of manganese in suckling than in adult rats is not due to maturational differences in manganese uptake by rat small intestine. J Toxicol Environ Health 26:387-398.

Belzung C, Griebel G (2001) Measuring normal and pathological anxiety-like behaviour in mice: a review. Behav Brain Res 125:141-149.

Bentle LA, Lardy HA (1976) Interaction of anions and divalent metal ions with phosphoenolpyruvate carboxykinase. J Biol Chem 251:2916-2921.

Berg D, Gerlach M, Youdim MB, Double KL, Zecca L, Riederer P, Becker G (2001) Brain iron pathways and their relevance to Parkinson's disease. J Neurochem 79:225-236.

Berger NA (1985) Poly(ADP-ribose) in the cellular response to DNA damage. Radiat Res 101:4-15.

Bernheimer H, Birkmayer W, Hornykiewicz O, Jellinger K, Seitelberger F (1973) Brain dopamine and the syndromes of Parkinson and Huntington. Clinical, morphological and neurochemical correlations. J Neurol Sci 20:415-455.

Bertinet DB, Tinivella M, Balzola FA, de Francesco A, Davini O, Rizzo L, Massarenti P, Leonardi MA, Balzola F (2000) Brain manganese deposition and blood levels in patients undergoing home parenteral nutrition. JPEN J Parenter Enteral Nutr 24:223-227.

Beuter A, Mergler D, de Geoffroy A, Carriere L, Belanger S, Varghese L, Sreekumar J, Gauthier S (1994) Diadochokinesimetry: a study of patients with Parkinson's disease and manganese exposed workers. Neurotoxicology 15:655-664.

Bikashvili TZ, Shukakidze AA, Kiknadze GI (2001) Changes in the ultrastructure of the rat cerebral cortex after oral doses of manganese chloride. Neurosci Behav Physiol 31:385-389.

Bogousslavsky J, Fisher M (1998) Textbook of Neurology. Boston: Butterworth-Heinemann.

Boksha IS, Tereshkina EB, Burbaeva GS (2000) Glutamine synthetase and glutamine synthetase-like protein from human brain: purification and comparative characterization. J Neurochem 75:2574-2582.

Bolam JP, Hanley JJ, Booth PA, Bevan MD (2000) Synaptic organisation of the basal ganglia. J Anat 196 (Pt 4):527-542.

Bolanos JP, Heales SJ, Land JM, Clark JB (1995) Effect of peroxynitrite on the mitochondrial respiratory chain: differential susceptibility of neurones and astrocytes in primary culture. J Neurochem 64:1965-1972.

Bolanos JP, Almeida A, Stewart V, Peuchen S, Land JM, Clark JB, Heales SJ (1997) Nitric oxide-mediated mitochondrial damage in the brain: mechanisms and implications for neurodegenerative diseases. J Neurochem 68:2227-2240.

Bonilla E (1980) L-tyrosine hydroxylase activity in the rat brain after chronic oral administration of manganese chloride. Neurobehav Toxicol 2:37-41.

Brenman JE, Chao DS, Gee SH, McGee AW, Craven SE, Santillano DR, Wu Z, Huang F, Xia H, Peters MF, Froehner SC, Bredt DS (1996) Interaction of nitric oxide synthase with the postsynaptic density protein PSD-95 and alpha1-syntrophin mediated by PDZ domains. Cell 84:757-767.

Brenneman KA, Cattley RC, Ali SF, Dorman DC (1999) Manganese-induced developmental neurotoxicity in the CD rat: is oxidative damage a mechanism of action? Neurotoxicology 20:477-487.

Brenneman KA, Wong BA, Buccellato MA, Costa ER, Gross EA, Dorman DC (2000) Direct olfactory transport of inhaled manganese ((54)MnCl(2)) to the rat brain:

toxicokinetic investigations in a unilateral nasal occlusion model. Toxicol Appl Pharmacol 169:238-248.

Britton AA, Cotzias GC (1966) Dependence of manganese turnover on intake. Am J Physiol 211:203-206.

Brouillet EP, Shinobu L, McGarvey U, Hochberg F, Beal MF (1993) Manganese injection into the rat striatum produces excitotoxic lesions by impairing energy metabolism. Exp Neurol 120:89-94.

Burdo JR, Martin J, Menzies SL, Dolan KG, Romano MA, Fletcher RJ, Garrick MD, Garrick LM, Connor JR (1999) Cellular distribution of iron in the brain of the Belgrade rat. Neuroscience 93:1189-1196.

Calabrese V, Scapagnini G, Giuffrida Stella AM, Bates TE, Clark JB (2001) Mitochondrial involvement in brain function and dysfunction: relevance to aging, neurodegenerative disorders and longevity. Neurochem Res 26:739-764.

Calabresi P, Ammassari-Teule M, Gubellini P, Sancesario G, Morello M, Centonze D, Marfia GA, Saulle E, Passino E, Picconi B, Bernardi G (2001) A synaptic mechanism underlying the behavioral abnormalities induced by manganese intoxication. Neurobiol Dis 8:419-432.

Calne DB, Snow BJ (1993) PET imaging in Parkinsonism. Adv Neurol 60:484-487.

Calne DB, Chu NS, Huang CC, Lu CS, Olanow W (1994) Manganism and idiopathic parkinsonism: similarities and differences. Neurology 44:1583-1586.

Carlsson M, Carlsson A (1990) Interactions between glutamatergic and monoaminergic systems within the basal ganglia--implications for schizophrenia and Parkinson's disease. Trends Neurosci 13:272-276.

Castro SL, Zigmond MJ (2001) Stress-induced increase in extracellular dopamine in striatum: role of glutamatergic action via N-methyl-D-aspartate receptors in substantia nigra. Brain Res 901:47-54.

Centonze D, Gubellini P, Bernardi G, Calabresi P (2001) Impaired excitatory transmission in the striatum of rats chronically intoxicated with manganese. Exp Neurol 172:469-476.

Champney TH, Hanneman WH, Nichols MA (1992) gamma-Aminobutyric acid, catecholamine and indoleamine determinations from the same brain region by high-performance liquid chromatography with electrochemical detection. J Chromatogr 579:334-339.

Chen CJ, Liao SL (2002) Oxidative stress involves in astrocytic alterations induced by manganese. Exp Neurol 175:216-225.

Chen JY, Tsao GC, Zhao Q, Zheng W (2001) Differential cytotoxicity of Mn(II) and Mn(III): special reference to mitochondrial [Fe-S] containing enzymes. Toxicol Appl Pharmacol 175:160-168.

Choi DW (1992) Excitotoxic cell death. J Neurobiol 23:1261-1276.

Chua AC, Morgan EH (1997) Manganese metabolism is impaired in the Belgrade laboratory rat. J Comp Physiol [B] 167:361-369.

Chung KC, Park JH, Kim CH, Ahn YS (1999) Tumor necrosis factor-alpha and phorbol 12-myristate 13-acetate differentially modulate cytotoxic effect of nitric oxide generated by serum deprivation in neuronal PC12 cells. J Neurochem 72:1482-1488.

Cicchetti F, Beach TG, Parent A (1998) Chemical phenotype of calretinin interneurons in the human striatum. Synapse 30:284-297.

Clayton CA, Pellizzari ED, Whitmore RW, Perritt RL, Quackenboss JJ (1999) National Human Exposure Assessment Survey (NHEXAS): distributions and associations of lead, arsenic and volatile organic compounds in EPA region 5. J Expo Anal Environ Epidemiol 9:381-392.

Connor JR, Menzies SL, St Martin SM, Mufson EJ (1990) Cellular distribution of transferrin, ferritin, and iron in normal and aged human brains. J Neurosci Res 27:595-611.

Contant C, Umbriaco D, Garcia S, Watkins KC, Descarries L (1996) Ultrastructural characterization of the acetylcholine innervation in adult rat neostriatum. Neuroscience 71:937-947.

Cook DG, Fahn S, Brait KA (1974) Chronic manganese intoxication. Arch Neurol 30:59-64.

Cooper AJ, Plum F (1987) Biochemistry and physiology of brain ammonia. Physiol Rev 67:440-519.

Cotzias GC, Horiuchi K, Fuenzalida S, Mena I (1968) Chronic manganese poisoning. Clearance of tissue manganese concentrations with persistance of the neurological picture. Neurology 18:376-382.

Couper J (1837) On the effects of black oxide of manganese when inhaled into the lungs. Brit Ann Med Pharmacol 1:41-42.

Cowan RL, Wilson CJ, Emson PC, Heizmann CW (1990) Parvalbumin-containing GABAergic interneurons in the rat neostriatum. J Comp Neurol 302:197-205.

Cristiano L, Bernardo A, Ceru MP (2001) Peroxisome proliferator-activated receptors (PPARs) and peroxisomes in rat cortical and cerebellar astrocytes. J Neurocytol 30:671-683.

Crossgrove JS, Yokel RA (2004) Manganese distribution across the blood-brain barrier III. The divalent metal transporter-1 is not the major mechanism mediating brain manganese uptake. Neurotoxicology 25:451-460.

Crossgrove JS, Allen DD, Bukaveckas BL, Rhineheimer SS, Yokel RA (2003) Manganese distribution across the blood-brain barrier. I. Evidence for carrier-mediated influx of managanese citrate as well as manganese and manganese transferrin. Neurotoxicology 24:3-13.

Crowley JD, Traynor DA, Weatherburn DC (2000) Enzymes and proteins containing manganese: an overview. Met Ions Biol Syst 37:209-278.

Danbolt NC (2001) Glutamate uptake. Prog Neurobiol 65:1-105.

Daniels AJ, Abarca J (1991) Effect of intranigral Mn2+ on striatal and nigral synthesis and levels of dopamine and cofactor. Neurotoxicol Teratol 13:483-487.

Dastur DK MD, Raghavendran KV (1968) Distribution and fate of 54Mn in the monkey: studies of different parts of the central nervous system and other organs. J Clin Invest 50:9-20.

Davidsson L, Cederblad A, Lonnerdal B, Sandstrom B (1991) The effect of individual dietary components on manganese absorption in humans. Am J Clin Nutr 54:1065-1070.

Davidsson L, Cederblad A, Hagebo E, Lonnerdal B, Sandstrom B (1988) Intrinsic and extrinsic labeling for studies of manganese absorption in humans. J Nutr 118:1517-1521.

Davidsson L, Lonnerdal B, Sandstrom B, Kunz C, Keen CL (1989) Identification of transferrin as the major plasma carrier protein for manganese introduced orally or intravenously or after in vitro addition in the rat. J Nutr 119:1461-1464.

Davis CD, Zech L, Greger JL (1993) Manganese metabolism in rats: an improved methodology for assessing gut endogenous losses. Proc Soc Exp Biol Med 202:103-108.

Dawson VL, Dawson TM (1996) Nitric oxide neurotoxicity. J Chem Neuroanat 10:179-190.

DeLong MR (2000) The basal ganglia. In: Principles of Neural Science, 4th Edition (Kandel ER, Schwartz JH, Jessell TM, eds), p 856. New York: McGraw-Hill, Health Professions Division, c2000.

Derouiche A, Frotscher M (1991) Astroglial processes around identified glutamatergic synapses contain glutamine synthetase: evidence for transmitter degradation. Brain Res 552:346-350.

Desjardins C, Parent A (1992) Distribution of somatostatin immunoreactivity in the forebrain of the squirrel monkey: basal ganglia and amygdala. Neuroscience 47:115-133.

Desole MS, Sciola L, Delogu MR, Sircana S, Migheli R (1996) Manganese and 1-methyl-4-(2'-ethylpheny1)-1,2,3,6-tetrahydropyridine induce apoptosis in PC12 cells. Neurosci Lett 209:193-196.

Desole MS, Miele M, Esposito G, Migheli R, Fresu L, De Natale G, Miele E (1994) Dopaminergic system activity and cellular defense mechanisms in the striatum and striatal synaptosomes of the rat subchronically exposed to manganese. Arch Toxicol 68:566-570.

Desole MS, Esposito G, Migheli R, Sircana S, Delogu MR, Fresu L, Miele M, de Natale G, Miele E (1997) Glutathione deficiency potentiates manganese toxicity in rat striatum and brainstem and in PC12 cells. Pharmacol Res 36:285-292.

DiFiglia M, Pasik P, Pasik T (1976) A Golgi study of neuronal types in the neostriatum of monkeys. Brain Res 114:245-256.

Dimova R, Vuillet J, Nieoullon A, Kerkerian-Le Goff L (1993) Ultrastructural features of the choline acetyltransferase-containing neurons and relationships with nigral dopaminergic and cortical afferent pathways in the rat striatum. Neuroscience 53:1059-1071.

Dinerman JL, Steiner JP, Dawson TM, Dawson V, Snyder SH (1994) Cyclic nucleotide dependent phosphorylation of neuronal nitric oxide synthase inhibits catalytic activity. Neuropharmacology 33:1245-1251.

Donaldson J, LaBella FS, Gesser D (1981) Enhanced autoxidation of dopamine as a possible basis of manganese neurotoxicity. Neurotoxicology 2:53-64.

Donaldson J, McGregor D, LaBella F (1982) Manganese neurotoxicity: a model for free radical mediated neurodegeneration? Can J Physiol Pharmacol 60:1398-1405.

Dorman DC, Struve MF, James RA, Marshall MW, Parkinson CU, Wong BA (2001) Influence of particle solubility on the delivery of inhaled manganese to the rat brain: manganese sulfate and manganese tetroxide pharmacokinetics following repeated (14-day) exposure. Toxicol Appl Pharmacol 170:79-87.

Dorman DC, Brenneman KA, McElveen AM, Lynch SE, Roberts KC, Wong BA (2002) Olfactory transport: a direct route of delivery of inhaled manganese phosphate to the rat brain. J Toxicol Environ Health A 65:1493-1511.

Eckenstein F, Sofroniew MV (1983) Identification of central cholinergic neurons containing both choline acetyltransferase and acetylcholinesterase and of central neurons containing only acetylcholinesterase. J Neurosci 3:2286-2291.

Erikson K, Aschner M (2002) Manganese causes differential regulation of glutamate transporter (GLAST) taurine transporter and metallothionein in cultured rat astrocytes. Neurotoxicology 23:595-602.

Erikson KM, Aschner M (2003) Manganese neurotoxicity and glutamate-GABA interaction. Neurochem Int 43:475-480.

Erikson KM, Shihabi ZK, Aschner JL, Aschner M (2002) Manganese accumulates in iron-deficient rat brain regions in a heterogeneous fashion and is associated with neurochemical alterations. Biol Trace Elem Res 87:143-156.

Eriksson H, Heilbronn E (1983) Changes in the redox state of neuroblastoma cells after manganese exposure. Arch Toxicol 54:53-59.

Eriksson H, Tedroff J, Thuomas KA, Aquilonius SM, Hartvig P, Fasth KJ, Bjurling P, Langstrom B, Hedstrom KG, Heilbronn E (1992) Manganese induced brain lesions in Macaca fascicularis as revealed by positron emission tomography and magnetic resonance imaging. Arch Toxicol 66:403-407.

Farcich EA, Morgan EH (1992) Diminished iron acquisition by cells and tissues of Belgrade laboratory rats. Am J Physiol 262:R220-224.

Farde L, Eriksson L, Blomquist G, Halldin C (1989) Kinetic analysis of central [11C]raclopride binding to D2-dopamine receptors studied by PET--a comparison to the equilibrium analysis. J Cereb Blood Flow Metab 9:696-708.

Feinstein DL, Galea E, Gavrilyuk V, Brosnan CF, Whitacre CC, Dumitrescu-Ozimek L, Landreth GE, Pershadsingh HA, Weinberg G, Heneka MT (2002) Peroxisome proliferator-activated receptor-gamma agonists prevent experimental autoimmune encephalomyelitis. Ann Neurol 51:694-702.

Ferrante RJ, Kowall NW, Beal MF, Richardson EP, Jr., Bird ED, Martin JB (1985) Selective sparing of a class of striatal neurons in Huntington's disease. Science 230:561-563.

Ferre S, Fredholm BB, Morelli M, Popoli P, Fuxe K (1997) Adenosine-dopamine receptor-receptor interactions as an integrative mechanism in the basal ganglia. Trends Neurosci 20:482-487.

Fink DW, Jr., Guroff G (1990) Nerve growth factor stimulation of arachidonic acid release from PC12 cells: independence from phosphoinositide turnover. J Neurochem 55:1716-1726.

FitzGerald MJT, Folan-Curran J (2002) Clinical neuroanatomy and related neuroscience, 4th Edition. Edinburgh: W.B. Saunders.

Fleming I, Bauersachs J, Busse R (1997a) Calcium-dependent and calcium-independent activation of the endothelial NO synthase. J Vasc Res 34:165-174.

Fleming I, Bauersachs J, Fisslthaler B, Busse R (1998a) Ca2+-independent activation of the endothelial nitric oxide synthase in response to tyrosine phosphatase inhibitors and fluid shear stress. Circ Res 82:686-695.

Fleming MD, Romano MA, Su MA, Garrick LM, Garrick MD, Andrews NC (1998b) Nramp2 is mutated in the anemic Belgrade (b) rat: evidence of a role for Nramp2 in endosomal iron transport. Proc Natl Acad Sci U S A 95:1148-1153.

Fleming MD, Trenor CC, 3rd, Su MA, Foernzler D, Beier DR, Dietrich WF, Andrews NC (1997b) Microcytic anaemia mice have a mutation in Nramp2, a candidate iron transporter gene. Nat Genet 16:383-386.

Floyd ZE, Stephens JM (2002) Interferon-gamma-mediated activation and ubiquitin-proteasome-dependent degradation of PPARgamma in adipocytes. J Biol Chem 277:4062-4068.

Foradori AC, Bertinchamps A, Gulibon JM, Cotzias GC (1967) The discrimination between magnesium and manganese by serum proteins. J Gen Physiol 50:2255-2266.

Fuenzalida KM, Aguilera MC, Piderit DG, Ramos PC, Contador D, Quinones V, Rigotti A, Bronfman FC, Bronfman M (2005) Peroxisome proliferator-activated receptor gamma is a novel target of the nerve growth factor signaling pathway in PC12 cells. J Biol Chem 280:9604-9609.

Gahring LC, Persiyanov K, Rogers SW (2004) Neuronal and astrocyte expression of nicotinic receptor subunit beta4 in the adult mouse brain. J Comp Neurol 468:322-333.

Gailit J, Ruoslahti E (1988) Regulation of the fibronectin receptor affinity by divalent cations. J Biol Chem 263:12927-12932.

Galvani P, Fumagalli P, Santagostino A (1995) Vulnerability of mitochondrial complex I in PC12 cells exposed to manganese. Eur J Pharmacol 293:377-383.

Garcia-Aranda JA, Wapnir RA, Lifshitz F (1983) In vivo intestinal absorption of manganese in the rat. J Nutr 113:2601-2607.

Garthwaite J, Charles SL, Chess-Williams R (1988) Endothelium-derived relaxing factor release on activation of NMDA receptors suggests role as intercellular messenger in the brain. Nature 336:385-388.

Gauchy C, Desban M, Krebs MO, Glowinski J, Kemel ML (1991) Role of dynorphin-containing neurons in the presynaptic inhibitory control of the acetylcholine-evoked release of dopamine in the striosomes and the matrix of the cat caudate nucleus. Neuroscience 41:449-458.

Gavin CE, Gunter KK, Gunter TE (1990) Manganese and calcium efflux kinetics in brain mitochondria. Relevance to manganese toxicity. Biochem J 266:329-334.

Gavin CE, Gunter KK, Gunter TE (1992) Mn2+ sequestration by mitochondria and inhibition of oxidative phosphorylation. Toxicol Appl Pharmacol 115:1-5.

Gavin CE, Gunter KK, Gunter TE (1999) Manganese and calcium transport in mitochondria: implications for manganese toxicity. Neurotoxicology 20:445-453.

Gegg ME, Beltran B, Salas-Pino S, Bolanos JP, Clark JB, Moncada S, Heales SJ (2003) Differential effect of nitric oxide on glutathione metabolism and mitochondrial function in astrocytes and neurones: implications for neuroprotection/neurodegeneration? J Neurochem 86:228-237.

Gerfen CR (1991) Substance P (neurokinin-1) receptor mRNA is selectively expressed in cholinergic neurons in the striatum and basal forebrain. Brain Res 556:165-170.

Gerfen CR, Young WS, 3rd (1988) Distribution of striatonigral and striatopallidal peptidergic neurons in both patch and matrix compartments: an in situ hybridization histochemistry and fluorescent retrograde tracing study. Brain Res 460:161-167.

Gerfen CR, Engber TM, Mahan LC, Susel Z, Chase TN, Monsma FJ, Jr., Sibley DR (1990) D1 and D2 dopamine receptor-regulated gene expression of striatonigral and striatopallidal neurons. Science 250:1429-1432.

Gerritsen ME, Williams AJ, Neish AS, Moore S, Shi Y, Collins T (1997) CREB-binding protein/p300 are transcriptional coactivators of p65. Proc Natl Acad Sci U S A 94:2927-2932.

Gonzalez-Zulueta M, Ensz LM, Mukhina G, Lebovitz RM, Zwacka RM, Engelhardt JF, Oberley LW, Dawson VL, Dawson TM (1998) Manganese superoxide dismutase protects nNOS neurons from NMDA and nitric oxide-mediated neurotoxicity. J Neurosci 18:2040-2055.

Graham DG (1984) Catecholamine toxicity: a proposal for the molecular pathogenesis of manganese neurotoxicity and Parkinson's disease. Neurotoxicology 5:83-95.

Graveland GA, DiFiglia M (1985) The frequency and distribution of medium-sized neurons with indented nuclei in the primate and rodent neostriatum. Brain Res 327:307-311.

Graybiel AM, Ragsdale CW, Jr. (1978) Histochemically distinct compartments in the striatum of human, monkeys, and cat demonstrated by acetylthiocholinesterase staining. Proc Natl Acad Sci U S A 75:5723-5726.

Graybiel AM, Aosaki T, Flaherty AW, Kimura M (1994) The basal ganglia and adaptive motor control. Science 265:1826-1831.

Grilli M, Memo M (1999) Nuclear factor-kappaB/Rel proteins: a point of convergence of signalling pathways relevant in neuronal function and dysfunction. Biochem Pharmacol 57:1-7.

Growdon JH, Cohen EL, Wurtman RJ (1977) Huntington's disease: clinical and chemical effects of choline administration. Ann Neurol 1:418-422.

Gunshin H, Mackenzie B, Berger UV, Gunshin Y, Romero MF, Boron WF, Nussberger S, Gollan JL, Hediger MA (1997) Cloning and characterization of a mammalian proton-coupled metal-ion transporter. Nature 388:482-488.

Gunter TE, Pfeiffer DR (1990) Mechanisms by which mitochondria transport calcium. Am J Physiol 258:C755-786.

Gwiazda RH, Lee D, Sheridan J, Smith DR (2002) Low cumulative manganese exposure affects striatal GABA but not dopamine. Neurotoxicology 23:69-76.

HaMai D, Campbell A, Bondy SC (2001) Modulation of oxidative events by multivalent manganese complexes in brain tissue. Free Radic Biol Med 31:763-768.

Harlan RE, Webber DS, Garcia MM (2001) Involvement of nitric oxide in morphine-induced c-Fos expression in the rat striatum. Brain Res Bull 54:207-212.

Harris WR, Chen Y (1994) Electron paramagnetic resonance and difference ultraviolet studies of Mn2+ binding to serum transferrin. J Inorg Biochem 54:1-19.

Hauser RA, Zesiewicz TA, Rosemurgy AS, Martinez C, Olanow CW (1994) Manganese intoxication and chronic liver failure. Ann Neurol 36:871-875.

Hazell AS (2002) Astrocytes and manganese neurotoxicity. Neurochem Int 41:271-277.

Hazell AS, Norenberg MD (1997) Manganese decreases glutamate uptake in cultured astrocytes. Neurochem Res 22:1443-1447.

Hazell AS, Norenberg MD (1998) Ammonia and manganese increase arginine uptake in cultured astrocytes. Neurochem Res 23:869-873.

Hazell AS, Desjardins P, Butterworth RF (1999a) Chronic exposure of rat primary astrocyte cultures to manganese results in increased binding sites for the 'peripheral-type' benzodiazepine receptor ligand 3H-PK 11195. Neurosci Lett 271:5-8.

Hazell AS, Desjardins P, Butterworth RF (1999b) Increased expression of glyceraldehyde-3-phosphate dehydrogenase in cultured astrocytes following exposure to manganese. Neurochem Int 35:11-17.

Hazell AS, Normandin L, Nguyen B, Kennedy G (2003) Upregulation of 'peripheral-type' benzodiazepine receptors in the globus pallidus in a sub-acute rat model of manganese neurotoxicity. Neurosci Lett 349:13-16.

Heales SJ, Bolanos JP, Stewart VC, Brookes PS, Land JM, Clark JB (1999) Nitric oxide, mitochondria and neurological disease. Biochim Biophys Acta 1410:215-228.

Heales SJ, Barker JE, Stewart VC, Brand MP, Hargreaves IP, Foppa P, Land JM, Clark JB, Bolanos JP (1997) Nitric oxide, energy metabolism and neurological disease. Biochem Soc Trans 25:939-943.

Hemler ME (1990) VLA proteins in the integrin family: structures, functions, and their role on leukocytes. Annu Rev Immunol 8:365-400.

Henriksson J, Tjalve H (2000) Manganese taken up into the CNS via the olfactory pathway in rats affects astrocytes. Toxicol Sci 55:392-398.

Henry B, Brotchie JM (1996) Potential of opioid antagonists in the treatment of levodopa-induced dyskinesias in Parkinson's disease. Drugs Aging 9:149-158.

Hirata Y (2002) Manganese-induced apoptosis in PC12 cells. Neurotoxicol Teratol 24:639-653.

Hirata Y, Adachi K, Kiuchi K (1998) Activation of JNK pathway and induction of apoptosis by manganese in PC12 cells. J Neurochem 71:1607-1615.

Hirsch EC, Hunot S, Damier P, Faucheux B (1998) Glial cells and inflammation in Parkinson's disease: a role in neurodegeneration? Ann Neurol 44:S115-120.

Holt DJ, Hersh LB, Saper CB (1996) Cholinergic innervation in the human striatum: a three-compartment model. Neuroscience 74:67-87.

Huang CC, Weng YH, Lu CS, Chu NS, Yen TC (2003) Dopamine transporter binding in chronic manganese intoxication. J Neurol 250:1335-1339.

Huang CC, Lu CS, Chu NS, Hochberg F, Lilienfeld D, Olanow W, Calne DB (1993) Progression after chronic manganese exposure. Neurology 43:1479-1483.

Huang CC, Chu NS, Lu CS, Wang JD, Tsai JL, Tzeng JL, Wolters EC, Calne DB (1989) Chronic manganese intoxication. Arch Neurol 46:1104-1106.

Hughes AJ, Ben-Shlomo Y, Daniel SE, Lees AJ (2001) What features improve the accuracy of clinical diagnosis in Parkinson's disease: a clinicopathologic study. 1992. Neurology 57:S34-38.

Humphries MJ (1996) Integrin activation: the link between ligand binding and signal transduction. Curr Opin Cell Biol 8:632-640.

Hyman BT, Marzloff K, Wenniger JJ, Dawson TM, Bredt DS, Snyder SH (1992) Relative sparing of nitric oxide synthase-containing neurons in the hippocampal formation in Alzheimer's disease. Ann Neurol 32:818-820.

Ivins JK, Yurchenco PD, Lander AD (2000) Regulation of neurite outgrowth by integrin activation. J Neurosci 20:6551-6560.

Jana M, Anderson JA, Saha RN, Liu X, Pahan K (2005) Regulation of inducible nitric oxide synthase in proinflammatory cytokine-stimulated human primary astrocytes. Free Radic Biol Med 38:655-664.

Jung KM, Park KS, Oh JH, Jung SY, Yang KH, Song YS, Son DJ, Park YH, Yun YP, Lee MK, Oh KW, Hong JT (2003) Activation of p38 mitogen-activated protein kinase and activator protein-1 during the promotion of neurite extension of PC-12 cells by 15-deoxy-delta12,14-prostaglandin J2. Mol Pharmacol 63:607-616.

Kaiser J (2003) Manganese: a high-octane dispute. Science 300:926-928.

Kamei Y, Xu L, Heinzel T, Torchia J, Kurokawa R, Gloss B, Lin SC, Heyman RA, Rose DW, Glass CK, Rosenfeld MG (1996) A CBP integrator complex mediates transcriptional activation and AP-1 inhibition by nuclear receptors. Cell 85:403-414.

Kannurpatti SS, Joshi PG, Joshi NB (2000) Calcium sequestering ability of mitochondria modulates influx of calcium through glutamate receptor channel. Neurochem Res 25:1527-1536.

Karin M, Cao Y, Greten FR, Li ZW (2002) NF-kappaB in cancer: from innocent bystander to major culprit. Nat Rev Cancer 2:301-310.

Kawamura R, Ikuta, H., Fukuzumi, S., Yamadaa,R., Tsubaki, S., Kodama, T., Kurata, S. (1941) Intoxication by manganese in well water. Kitasato Arch Exp Med 18:145-169.

Keen CL, Leach RM (1988) Manganese. In: Handbook on Toxicity of Inorganic Compounds (Seiler HG, Sigel H, eds), pp 405-415. New York: Marcel Dekker.

Keen CL, Bell JG, Lonnerdal B (1986) The effect of age on manganese uptake and retention from milk and infant formulas in rats. J Nutr 116:395-402.

Keen CL, Ensunsa JL, Clegg MS (2000) Manganese metabolism in animals and humans including the toxicity of manganese. Met Ions Biol Syst 37:89-121.

Keen CL, Ensunsa JL, Watson MH, Baly DL, Donovan SM, Monaco MH, Clegg MS (1999) Nutritional aspects of manganese from experimental studies. Neurotoxicology 20:213-223.

Kemmerer AR, Elvehjem CA, Hart EB (1931) Studies on the relation of manganese to the nutrition of the mouse. J Biol Chem 92:623-630.

Kish SJ, Shannak K, Hornykiewicz O (1988) Uneven pattern of dopamine loss in the striatum of patients with idiopathic Parkinson's disease. Pathophysiologic and clinical implications. N Engl J Med 318:876-880.

Kitazawa M, Wagner JR, Kirby ML, Anantharam V, Kanthasamy AG (2002) Oxidative stress and mitochondrial-mediated apoptosis in dopaminergic cells exposed to methylcyclopentadienyl manganese tricarbonyl. J Pharmacol Exp Ther 302:26-35.

Kleinert H, Euchenhofer C, Ihrig-Biedert I, Forstermann U (1996) Glucocorticoids inhibit the induction of nitric oxide synthase II by down-regulating cytokine-

induced activity of transcription factor nuclear factor-kappa B. Mol Pharmacol 49:15-21.

Kliewer SA, Umesono K, Noonan DJ, Heyman RA, Evans RM (1992) Convergence of 9-cis retinoic acid and peroxisome proliferator signalling pathways through heterodimer formation of their receptors. Nature 358:771-774.

Koh JY, Choi DW (1988) Cultured striatal neurons containing NADPH-diaphorase or acetylcholinesterase are selectively resistant to injury by NMDA receptor agonists. Brain Res 446:374-378.

Koh JY, Peters S, Choi DW (1986) Neurons containing NADPH-diaphorase are selectively resistant to quinolinate toxicity. Science 234:73-76.

Kojima H, Nakatsubo N, Kikuchi K, Kawahara S, Kirino Y, Nagoshi H, Hirata Y, Nagano T (1998) Detection and imaging of nitric oxide with novel fluorescent indicators: diaminofluoresceins. Anal Chem 70:2446-2453.

Kondo K, Hashimoto H, Kitanaka J, Sawada M, Suzumura A, Marunouchi T, Baba A (1995) Expression of glutamate transporters in cultured glial cells. Neurosci Lett 188:140-142.

Kono Y, Takahashi MA, Asada K (1976) Oxidation of manganous pyrophosphate by superoxide radicals and illuminated spinach chloroplasts. Arch Biochem Biophys 174:454-462.

Kornau HC, Schenker LT, Kennedy MB, Seeburg PH (1995) Domain interaction between NMDA receptor subunits and the postsynaptic density protein PSD-95. Science 269:1737-1740.

Krachler M, Rossipal E (2000) Concentrations of trace elements in extensively hydrolysed infant formulae and their estimated daily intakes. Ann Nutr Metab 44:68-74.

Krieger D, Krieger S, Jansen O, Gass P, Theilmann L, Lichtnecker H (1995) Manganese and chronic hepatic encephalopathy. Lancet 346:270-274.

Ky SQ, Deng HS, Xie PY, Hu W (1992) A report of two cases of chronic serious manganese poisoning treated with sodium para-aminosalicylic acid. Br J Ind Med 49:66-69.

Lai JC, Minski MJ, Chan AW, Leung TK, Lim L (1999) Manganese mineral interactions in brain. Neurotoxicology 20:433-444.

Lam HH, Hanley DF, Trapp BD, Saito S, Raja S, Dawson TM, Yamaguchi H (1996) Induction of spinal cord neuronal nitric oxide synthase (NOS) after formalin injection in the rat hind paw. Neurosci Lett 210:201-204.

Langston JW, Forno LS, Tetrud J, Reeves AG, Kaplan JA, Karluk D (1999) Evidence of active nerve cell degeneration in the substantia nigra of humans years after 1-methyl-4-phenyl-1,2,3,6-tetrahydropyridine exposure. Ann Neurol 46:598-605.

Lautier D, Lagueux J, Thibodeau J, Menard L, Poirier GG (1993) Molecular and biochemical features of poly (ADP-ribose) metabolism. Mol Cell Biochem 122:171-193.

Leblondel G, Allain P (1999) Manganese transport by Caco-2 cells. Biol Trace Elem Res 67:13-28.

Lein P, Gallagher PJ, Amodeo J, Howie H, Roth JA (2000) Manganese induces neurite outgrowth in PC12 cells via upregulation of alpha(v) integrins. Brain Res 885:220-230.

Levine RL, Oliver CN, Fulks RM, Stadtman ER (1981) Turnover of bacterial glutamine synthetase: oxidative inactivation precedes proteolysis. Proc Natl Acad Sci U S A 78:2120-2124.

Levine WG (1970) Heavy metal antagonists. In: The Pharmacological Basis of Therapeutics, 4th Edition (Goodman LS, Gilman A, eds), p 950. New York: MacMillan Co.

Li M, Pascual G, Glass CK (2000) Peroxisome proliferator-activated receptor gamma-dependent repression of the inducible nitric oxide synthase gene. Mol Cell Biol 20:4699-4707.

Liaw SH, Villafranca JJ, Eisenberg D (1993) A model for oxidative modification of glutamine synthetase, based on crystal structures of mutant H269N and the oxidized enzyme. Biochemistry 32:7999-8003.

Liberto CM, Albrecht PJ, Herx LM, Yong VW, Levison SW (2004) Pro-regenerative properties of cytokine-activated astrocytes. J Neurochem 89:1092-1100.

Liccione JJ, Maines MD (1988) Selective vulnerability of glutathione metabolism and cellular defense mechanisms in rat striatum to manganese. J Pharmacol Exp Ther 247:156-161.

Liccione JJ, Maines MD (1989) Manganese-mediated increase in the rat brain mitochondrial cytochrome P-450 and drug metabolism activity: susceptibility of the striatum. J Pharmacol Exp Ther 248:222-228.

Linn SC, Morelli PJ, Edry I, Cottongim SE, Szabo C, Salzman AL (1997) Transcriptional regulation of human inducible nitric oxide synthase gene in an intestinal epithelial cell line. Am J Physiol 272:G1499-1508.

Linscheid P, Keller U, Blau N, Schaer DJ, Muller B (2003) Diminished production of nitric oxide synthase cofactor tetrahydrobiopterin by rosiglitazone in adipocytes. Biochem Pharmacol 65:593-598.

Lioy PJ (1983) Air pollution emission profiles of toxic and trace elements from energy related sources: status and needs. Neurotoxicology 4:103-112.

Lipe GW, Duhart H, Newport GD, Slikker W, Jr., Ali SF (1999) Effect of manganese on the concentration of amino acids in different regions of the rat brain. J Environ Sci Health B 34:119-132.

Lipton SA, Choi YB, Pan ZH, Lei SZ, Chen HS, Sucher NJ, Loscalzo J, Singel DJ, Stamler JS (1993) A redox-based mechanism for the neuroprotective and neurodestructive effects of nitric oxide and related nitroso-compounds. Nature 364:626-632.

Liu X, Kim CN, Yang J, Jemmerson R, Wang X (1996) Induction of apoptotic program in cell-free extracts: requirement for dATP and cytochrome c. Cell 86:147-157.

Lonnerdal B (1994) Nutritional aspects of soy formula. Acta Paediatr Suppl 402:105-108.

Loranger S, Zayed J (1997) Environmental contamination and human exposure assessment to manganese in the St-Lawrence River ecozone (Quebec, Canada) using an environmental fate/exposure model: GEOTOX. SAR QSAR Environ Res 6:105-119.

Lowenstein CJ, Alley EW, Raval P, Snowman AM, Snyder SH, Russell SW, Murphy WJ (1993) Macrophage nitric oxide synthase gene: two upstream regions mediate induction by interferon gamma and lipopolysaccharide. Proc Natl Acad Sci U S A 90:9730-9734.

Lu CS, Huang CC, Chu NS, Calne DB (1994) Levodopa failure in chronic manganism. Neurology 44:1600-1602.

Lucaciu CM, Dragu C, Copaescu L, Morariu VV (1997) Manganese transport through human erythrocyte membranes. An EPR study. Biochim Biophys Acta 1328:90-98.

Lucchini R, Albini E, Placidi D, Gasparotti R, Pigozzi MG, Montani G, Alessio L (2000) Brain magnetic resonance imaging and manganese exposure. Neurotoxicology 21:769-775.

MacMillan-Crow LA, Crow JP, Kerby JD, Beckman JS, Thompson JA (1996) Nitration and inactivation of manganese superoxide dismutase in chronic rejection of human renal allografts. Proc Natl Acad Sci U S A 93:11853-11858.

Makar TK, Nedergaard M, Preuss A, Gelbard AS, Perumal AS, Cooper AJ (1994) Vitamin E, ascorbate, glutathione, glutathione disulfide, and enzymes of glutathione metabolism in cultures of chick astrocytes and neurons: evidence that astrocytes play an important role in antioxidative processes in the brain. J Neurochem 62:45-53.

Malecki EA (2001a) Limited role of transferrin in manganese transport to the brain. J Nutr 131:1584-1585.

Malecki EA (2001b) Manganese toxicity is associated with mitochondrial dysfunction and DNA fragmentation in rat primary striatal neurons. Brain Res Bull 55:225-228.

Malecki EA, Devenyi AG, Beard JL, Connor JR (1999) Existing and emerging mechanisms for transport of iron and manganese to the brain. J Neurosci Res 56:113-122.

Malecki EA, Radzanowski GM, Radzanowski TJ, Gallaher DD, Greger JL (1996) Biliary manganese excretion in conscious rats is affected by acute and chronic manganese intake but not by dietary fat. J Nutr 126:489-498.

Maneuf YP, Mitchell IJ, Crossman AR, Woodruff GN, Brotchie JM (1995) Functional implications of kappa opioid receptor-mediated modulation of glutamate transmission in the output regions of the basal ganglia in rodent and primate models of Parkinson's disease. Brain Res 683:102-108.

Mansour A, Fox CA, Meng F, Akil H, Watson SJ (1994a) Kappa 1 receptor mRNA distribution in the rat CNS: comparison to kappa receptor binding and prodynorphin mRNA. Mol Cell Neurosci 5:124-144.

Mansour A, Fox CA, Burke S, Meng F, Thompson RC, Akil H, Watson SJ (1994b) Mu, delta, and kappa opioid receptor mRNA expression in the rat CNS: an in situ hybridization study. J Comp Neurol 350:412-438.

Martin WR, Palmer MR, Patlak CS, Calne DB (1989) Nigrostriatal function in humans studied with positron emission tomography. Ann Neurol 26:535-542.

Martinez-Hernandez A, Bell KP, Norenberg MD (1977) Glutamine synthetase: glial localization in brain. Science 195:1356-1358.

Mayer B, ed (2000) Nitric Oxide. New York: Springer-Verlag Berlin Heidelberg.

Maynard LS, Cotzias GC (1955) The partition of manganese among organs and intracellular organelles of the rat. J Biol Chem 214:489-495.

McGinty JF (1999) Regulation of neurotransmitter interactions in the ventral striatum. Ann N Y Acad Sci 877:129-139.

Melnyk LJ, Morgan JN, Fernando R, Pellizzari ED, Akinbo O (2003) Determination of metals in composite diet samples by inductively coupled plasma-mass spectrometry. J AOAC Int 86:439-447.

Mena I, Court J, Fuenzalida S, Papavasiliou PS, Cotzias GC (1970) Modification of chronic manganese poisoning. Treatment with L-dopa or 5-OH tryptophane. N Engl J Med 282:5-10.

Mergler D, Huel G, Bowler R, Iregren A, Belanger S, Baldwin M, Tardif R, Smargiassi A, Martin L (1994) Nervous system dysfunction among workers with long-term exposure to manganese. Environ Res 64:151-180.

Miele M, Serra PA, Esposito G, Delogu MR, Migheli R, Rocchitta G, Desole MS (2000) Glutamate and catabolites of high-energy phosphates in the striatum and brainstem of young and aged rats subchronically exposed to manganese. Aging (Milano) 12:393-397.

Miller DK, Nation JR, Bratton GR (2001) The effects of perinatal exposure to lead on the discriminative stimulus properties of cocaine and related drugs in rats. Psychopharmacology (Berl) 158:165-174.

Mitchell P (1961) Coupling of phosphorylation to electron and hydrogen transfer by a chemi-osmotic type of mechanism. Nature 191:144-148.

Montes S, Alcaraz-Zubeldia M, Muriel P, Rios C (2001) Striatal manganese accumulation induces changes in dopamine metabolism in the cirrhotic rat. Brain Res 891:123-129.

Moos T (1996) Immunohistochemical localization of intraneuronal transferrin receptor immunoreactivity in the adult mouse central nervous system. J Comp Neurol 375:675-692.

Moos T, Trinder D, Morgan EH (2002) Effect of iron status on DMT1 expression in duodenal enterocytes from beta2-microglobulin knockout mice. Am J Physiol Gastrointest Liver Physiol 283:G687-694.

Mulder AH, Wardeh G, Hogenboom F, Frankhuyzen AL (1984) Kappa- and delta-opioid receptor agonists differentially inhibit striatal dopamine and acetylcholine release. Nature 308:278-280.

Murillo G, Mehta RG (2001) Cruciferous vegetables and cancer prevention. Nutr Cancer 41:17-28.

Murphy VA, Wadhwani KC, Smith QR, Rapoport SI (1991) Saturable transport of manganese(II) across the rat blood-brain barrier. J Neurochem 57:948-954.

Na SY, Lee SK, Han SJ, Choi HS, Im SY, Lee JW (1998) Steroid receptor coactivator-1 interacts with the p50 subunit and coactivates nuclear factor kappaB-mediated transactivations. J Biol Chem 273:10831-10834.

Nagatomo S, Umehara F, Hanada K, Nobuhara Y, Takenaga S, Arimura K, Osame M (1999) Manganese intoxication during total parenteral nutrition: report of two cases and review of the literature. J Neurol Sci 162:102-105.

Nagy L, Tontonoz P, Alvarez JG, Chen H, Evans RM (1998) Oxidized LDL regulates macrophage gene expression through ligand activation of PPARgamma. Cell 93:229-240.

Nakane M, Mitchell J, Forstermann U, Murad F (1991) Phosphorylation by calcium calmodulin-dependent protein kinase II and protein kinase C modulates the activity of nitric oxide synthase. Biochem Biophys Res Commun 180:1396-1402.

Nakane M, Klinghofer V, Kuk JE, Donnelly JL, Budzik GP, Pollock JS, Basha F, Carter GW (1995) Novel potent and selective inhibitors of inducible nitric oxide synthase. Mol Pharmacol 47:831-834.

Nakashima S, Ikeno Y, Yokoyama T, Kuwana M, Bolchi A, Ottonello S, Kitamoto K, Arioka M (2003) Secretory phospholipases A2 induce neurite outgrowth in PC12 cells. Biochem J 376:655-666.

Narita K, Kawasaki F, Kita H (1990) Mn and Mg influxes through Ca channels of motor nerve terminals are prevented by verapamil in frogs. Brain Res 510:289-295.

National Academy of Sciences IoM (2001) Dietary Reference Intakes for Vitamin A, Vitamin K, Arsenic, Boron, Chromium, Copper, Iodine, Iron, Manganese, Molybdenum, Nickel, Silicon, Vanadium, and Zinc. Washington DC: National Academy Press.

Neff NH, Barrett RE, Costa E (1969) Selective depletion of caudate nucleus dopamine and serotonin during chronic manganese dioxide administration to squirrel monkeys. Experientia 25:1140-1141.

Newland MC (1999) Animal models of manganese's neurotoxicity. Neurotoxicology 20:415-432.

Nishiya T, Uehara T, Kaneko M, Nomura Y (2000) Involvement of nuclear factor-kappaB (NF-kappaB) signaling in the expression of inducible nitric oxide synthase (iNOS) gene in rat C6 glioma cells. Biochem Biophys Res Commun 275:268-273.

Nomura Y (2001) NF-kappaB activation and IkappaB alpha dynamism involved in iNOS and chemokine induction in astroglial cells. Life Sci 68:1695-1701.

Oates PS, Thomas C, Freitas E, Callow MJ, Morgan EH (2000) Gene expression of divalent metal transporter 1 and transferrin receptor in duodenum of Belgrade rats. Am J Physiol Gastrointest Liver Physiol 278:G930-936.

Oertel WH, Riethmuller G, Mugnaini E, Schmechel DE, Weindl A, Gramsch C, Herz A (1983) Opioid peptide-like immunoreactivity localized in GABAErgic neurons of rat neostriatum and central amygdaloid nucleus. Life Sci 33 Suppl 1:73-76.

Olanow CW (1992) Early therapy for Parkinson's disease. Eur Neurol 32 Suppl 1:30-35.

Olanow CW, Good PF, Shinotoh H, Hewitt KA, Vingerhoets F, Snow BJ, Beal MF, Calne DB, Perl DP (1996) Manganese intoxication in the rhesus monkey: a clinical, imaging, pathologic, and biochemical study. Neurology 46:492-498.

Paganini-Hill A (2001) Risk factors for parkinson's disease: the leisure world cohort study. Neuroepidemiology 20:118-124.

Page G, Peeters M, Najimi M, Maloteaux JM, Hermans E (2001) Modulation of the neuronal dopamine transporter activity by the metabotropic glutamate receptor mGluR5 in rat striatal synaptosomes through phosphorylation mediated processes. J Neurochem 76:1282-1290.

Pal PK, Samii A, Calne DB (1999) Manganese neurotoxicity: a review of clinical features, imaging and pathology. Neurotoxicology 20:227-238.

Papaccio G, Graziano A, d'Aquino R, Valiante S, Naro F (2005) A biphasic role of nuclear transcription factor (NF)-kappaB in the islet beta-cell apoptosis induced by interleukin (IL)-1beta. J Cell Physiol 204:124-130.

Papavasiliou PS, Miller ST, Cotzias GC (1966) Role of liver in regulating distribution and excretion of manganese. Am J Physiol 211:211-216.

Pardridge WM, Eisenberg J, Yang J (1987) Human blood-brain barrier transferrin receptor. Metabolism 36:892-895.

Parent A (1996) Carpenter's Human Neuroanatomy, 9th Edition. Baltimore: Williams & Wilkins.

Parent A, Hazrati LN (1995) Functional anatomy of the basal ganglia. I. The cortico-basal ganglia-thalamo-cortical loop. Brain Res Brain Res Rev 20:91-127.

Parent A, Cicchetti F (1998) The current model of basal ganglia organization under scrutiny. Mov Disord 13:199-202.

Parent A, Cicchetti F, Beach TG (1995) Striatal neurones displaying substance P (NK1) receptor immunoreactivity in human and non-human primates. Neuroreport 6:721-724.

Parkinson J (2002) An essay on the shaking palsy. 1817. J Neuropsychiatry Clin Neurosci 14:223-236; discussion 222.

Pauwels PJ, Opperdoes FR, Trouet A (1985) Effects of antimycin, glucose deprivation, and serum on cultures of neurons, astrocytes, and neuroblastoma cells. J Neurochem 44:143-148.

Pedersen PL (1994) ATP synthase. The machine that makes ATP. Curr Biol 4:1138-1141.

Penalver R (1957) Diagnosis and treatment of manganese intoxication; report of a case. AMA Arch Ind Health 16:64-66.

Pennington JA, Schoen SA (1996) Total diet study: estimated dietary intakes of nutritional elements, 1982-1991. Int J Vitam Nutr Res 66:350-362.

Pentschew A, Ebner FF, Kovatch RM (1963) Experimental Manganese Encephalopathy in Monkeys. A Preliminary Report. J Neuropathol Exp Neurol 22:488-499.

Pisani A, Bonsi P, Centonze D, Gubellini P, Bernardi G, Calabresi P (2003) Targeting striatal cholinergic interneurons in Parkinson's disease: focus on metabotropic glutamate receptors. Neuropharmacology 45:45-56.

Planells E, Sanchez-Morito N, Montellano MA, Aranda P, Llopis J (2000) Effect of magnesium deficiency on enterocyte Ca, Fe, Cu, Zn, Mn and Se content. J Physiol Biochem 56:217-222.

Poinat P, De Arcangelis A, Sookhareea S, Zhu X, Hedgecock EM, Labouesse M, Georges-Labouesse E (2002) A conserved interaction between beta1 integrin/PAT-3 and Nck-interacting kinase/MIG-15 that mediates commissural axon navigation in C. elegans. Curr Biol 12:622-631.

Prensa L, Gimenez-Amaya JM, Parent A (1999) Chemical heterogeneity of the striosomal compartment in the human striatum. J Comp Neurol 413:603-618.

Qin C, Morrow D, Stewart J, Spencer K, Porter W, Smith R, 3rd, Phillips T, Abdelrahim M, Samudio I, Safe S (2004) A new class of peroxisome proliferator-activated receptor gamma (PPARgamma) agonists that inhibit growth of breast cancer cells: 1,1-Bis(3'-indolyl)-1-(p-substituted phenyl)methanes. Mol Cancer Ther 3:247-260.

Rabin O, Hegedus L, Bourre JM, Smith QR (1993) Rapid brain uptake of manganese(II) across the blood-brain barrier. J Neurochem 61:509-517.

Ravenscroft P, Brotchie J (2000) NMDA receptors in the basal ganglia. J Anat 196 (Pt 4):577-585.

Rehnberg GL, Hein JF, Carter SD, Laskey JW (1980) Chronic manganese oxide administration to preweanling rats: manganese accumulation and distribution. J Toxicol Environ Health 6:217-226.

Reichardt LF, Tomaselli KJ (1991) Extracellular matrix molecules and their receptors: functions in neural development. Annu Rev Neurosci 14:531-570.

Reid M, Herrera-Marschitz M, Hokfelt T, Terenius L, Ungerstedt U (1988) Differential modulation of striatal dopamine release by intranigral injection of gamma-aminobutyric acid (GABA), dynorphin A and substance P. Eur J Pharmacol 147:411-420.

Reiner A, Albin RL, Anderson KD, D'Amato CJ, Penney JB, Young AB (1988) Differential loss of striatal projection neurons in Huntington disease. Proc Natl Acad Sci U S A 85:5733-5737.

Reivich M, Kuhl D, Wolf A, Greenberg J, Phelps M, Ido T, Casella V, Fowler J, Hoffman E, Alavi A, Som P, Sokoloff L (1979) The [18F]fluorodeoxyglucose method for the measurement of local cerebral glucose utilization in man. Circ Res 44:127-137.

Rodier J (1955) Manganese poisoning in Moroccan miners. Br J Ind Med 12:21-35.

Roels H, Meiers G, Delos M, Ortega I, Lauwerys R, Buchet JP, Lison D (1997) Influence of the route of administration and the chemical form (MnCl2, MnO2)

on the absorption and cerebral distribution of manganese in rats. Arch Toxicol 71:223-230.

Rosenstock HA, Simons DG, Meyer JS (1971) Chronic manganism. Neurologic and laboratory studies during treatment with levodopa. Jama 217:1354-1358.

Roth JA, Garrick MD (2003) Iron interactions and other biological reactions mediating the physiological and toxic actions of manganese. Biochem Pharmacol 66:1-13.

Roth JA, Feng L, Walowitz J, Browne RW (2000) Manganese-induced rat pheochromocytoma (PC12) cell death is independent of caspase activation. J Neurosci Res 61:162-171.

Roth JA, Horbinski C, Higgins D, Lein P, Garrick MD (2002a) Mechanisms of manganese-induced rat pheochromocytoma (PC12) cell death and cell differentiation. Neurotoxicology 23:147-157.

Roth JA, Feng L, Dolan KG, Lis A, Garrick MD (2002b) Effect of the iron chelator desferrioxamine on manganese-induced toxicity of rat pheochromocytoma (PC12) cells. J Neurosci Res 68:76-83.

Saka E, Iadarola M, Fitzgerald DJ, Graybiel AM (2002) Local circuit neurons in the striatum regulate neural and behavioral responses to dopaminergic stimulation. Proc Natl Acad Sci U S A 99:9004-9009.

Samavati L, Monick MM, Sanlioglu S, Buettner GR, Oberley LW, Hunninghake GW (2002) Mitochondrial K(ATP) channel openers activate the ERK kinase by an oxidant-dependent mechanism. Am J Physiol Cell Physiol 283:C273-281.

Satoh MS, Poirier GG, Lindahl T (1994) Dual function for poly(ADP-ribose) synthesis in response to DNA strand breakage. Biochemistry 33:7099-7106.

Satoh T, Furuta K, Suzuki M, Watanabe Y (1999) Prostaglandin J2 and its metabolites promote neurite outgrowth induced by nerve growth factor in PC12 cells. Biochem Biophys Res Commun 258:50-53.

Schmued LC, Albertson C, Slikker W, Jr. (1997) Fluoro-Jade: a novel fluorochrome for the sensitive and reliable histochemical localization of neuronal degeneration. Brain Res 751:37-46.

Scholten JM (1953) On manganese encephalopathy; description of a case. Folia Psychiatr Neurol Neurochir Neerl 56:878-884.

Schousboe A, Westergaard N, Sonnewald U, Petersen SB, Yu AC, Hertz L (1992) Regulatory role of astrocytes for neuronal biosynthesis and homeostasis of glutamate and GABA. Prog Brain Res 94:199-211.

Schulman IG, Shao G, Heyman RA (1998) Transactivation by retinoid X receptor-peroxisome proliferator-activated receptor gamma (PPARgamma) heterodimers: intermolecular synergy requires only the PPARgamma hormone-dependent activation function. Mol Cell Biol 18:3483-3494.

Selden N, Geula C, Hersh L, Mesulam MM (1994) Human striatum: chemoarchitecture of the caudate nucleus, putamen and ventral striatum in health and Alzheimer's disease. Neuroscience 60:621-636.

Sessa WC, Pritchard K, Seyedi N, Wang J, Hintze TH (1994) Chronic exercise in dogs increases coronary vascular nitric oxide production and endothelial cell nitric oxide synthase gene expression. Circ Res 74:349-353.

Sessa WC, Garcia-Cardena G, Liu J, Keh A, Pollock JS, Bradley J, Thiru S, Braverman IM, Desai KM (1995) The Golgi association of endothelial nitric oxide synthase is necessary for the efficient synthesis of nitric oxide. J Biol Chem 270:17641-17644.

Sheppard KA, Rose DW, Haque ZK, Kurokawa R, McInerney E, Westin S, Thanos D, Rosenfeld MG, Glass CK, Collins T (1999) Transcriptional activation by NF-kappaB requires multiple coactivators. Mol Cell Biol 19:6367-6378.

Shinotoh H, Snow BJ, Chu NS, Huang CC, Lu CS, Lee C, Takahashi H, Calne DB (1997) Presynaptic and postsynaptic striatal dopaminergic function in patients with manganese intoxication: a positron emission tomography study. Neurology 48:1053-1056.

Shoham S, Youdim MB (2000) Iron involvement in neural damage and microgliosis in models of neurodegenerative diseases. Cell Mol Biol (Noisy-le-grand) 46:743-760.

Sidibe M, Smith Y (1999) Thalamic inputs to striatal interneurons in monkeys: synaptic organization and co-localization of calcium binding proteins. Neuroscience 89:1189-1208.

Sloot WN, Gramsbergen JB (1994) Axonal transport of manganese and its relevance to selective neurotoxicity in the rat basal ganglia. Brain Res 657:124-132.

Smith JW, Cheresh DA (1990) Integrin (alpha v beta 3)-ligand interaction. Identification of a heterodimeric RGD binding site on the vitronectin receptor. J Biol Chem 265:2168-2172.

Smith Y, Parent A (1986) Neuropeptide Y-immunoreactive neurons in the striatum of cat and monkey: morphological characteristics, intrinsic organization and co-localization with somatostatin. Brain Res 372:241-252.

Sonnewald U, Qu H, Aschner M (2002) Pharmacology and toxicology of astrocyte-neuron glutamate transport and cycling. J Pharmacol Exp Ther 301:1-6.

Sonnewald U, Westergaard N, Krane J, Unsgard G, Petersen SB, Schousboe A (1991) First direct demonstration of preferential release of citrate from astrocytes using [13C]NMR spectroscopy of cultured neurons and astrocytes. Neurosci Lett 128:235-239.

Spranger M, Schwab S, Desiderato S, Bonmann E, Krieger D, Fandrey J (1998) Manganese augments nitric oxide synthesis in murine astrocytes: a new pathogenetic mechanism in manganism? Exp Neurol 149:277-283.

Stallings WC, Metzger AL, Pattridge KA, Fee JA, Ludwig ML (1991) Structure-function relationships in iron and manganese superoxide dismutases. Free Radic Res Commun 12-13 Pt 1:259-268.

Steiner H, Gerfen CR (1998) Role of dynorphin and enkephalin in the regulation of striatal output pathways and behavior. Exp Brain Res 123:60-76.

Stokes AH, Lewis DY, Lash LH, Jerome WG, 3rd, Grant KW, Aschner M, Vrana KE (2000) Dopamine toxicity in neuroblastoma cells: role of glutathione depletion by L-BSO and apoptosis. Brain Res 858:1-8.

Storer PD, Xu J, Chavis J, Drew PD (2005) Peroxisome proliferator-activated receptor-gamma agonists inhibit the activation of microglia and astrocytes: implications for multiple sclerosis. J Neuroimmunol 161:113-122.

Sun Z, Del Mar N, Meade C, Goldowitz D, Reiner A (2002) Differential changes in striatal projection neurons in R6/2 transgenic mice for Huntington's disease. Neurobiol Dis 11:369-385.

Susin SA, Lorenzo HK, Zamzami N, Marzo I, Brenner C, Larochette N, Prevost MC, Alzari PM, Kroemer G (1999) Mitochondrial release of caspase-2 and -9 during the apoptotic process. J Exp Med 189:381-394.

Szabo C, Dawson VL (1998) Role of poly(ADP-ribose) synthetase in inflammation and ischaemia-reperfusion. Trends Pharmacol Sci 19:287-298.

Takeda A (2003) Manganese action in brain function. Brain Res Brain Res Rev 41:79-87.

Takeda A, Devenyi A, Connor JR (1998a) Evidence for non-transferrin-mediated uptake and release of iron and manganese in glial cell cultures from hypotransferrinemic mice. J Neurosci Res 51:454-462.

Takeda A, Sotogaku N, Oku N (2002) Manganese influences the levels of neurotransmitters in synapses in rat brain. Neuroscience 114:669-674.

Takeda A, Sotogaku N, Oku N (2003) Influence of manganese on the release of neurotransmitters in rat striatum. Brain Res 965:279-282.

Takeda A, Akiyama T, Sawashita J, Okada S (1994) Brain uptake of trace metals, zinc and manganese, in rats. Brain Res 640:341-344.

Takeda A, Kodama Y, Ishiwatari S, Okada S (1998b) Manganese transport in the neural circuit of rat CNS. Brain Res Bull 45:149-152.

Tampo Y, Yonaha M (1992) Antioxidant mechanism of Mn(II) in phospholipid peroxidation. Free Radic Biol Med 13:115-120.

Tholey G, Bloch S, Ledig M, Mandel P, Wedler F (1987) Chick brain glutamine synthetase and Mn2+-Mg2+ interactions. Neurochem Res 12:1041-1047.

Tholey G, Ledig M, Kopp P, Sargentini-Maier L, Leroy M, Grippo AA, Wedler FC (1988a) Levels and sub-cellular distribution of physiologically important metal ions in neuronal cells cultured from chick embryo cerebral cortex. Neurochem Res 13:1163-1167.

Tholey G, Ledig M, Mandel P, Sargentini L, Frivold AH, Leroy M, Grippo AA, Wedler FC (1988b) Concentrations of physiologically important metal ions in glial cells cultured from chick cerebral cortex. Neurochem Res 13:45-50.

Thompson KJ, Shoham S, Connor JR (2001) Iron and neurodegenerative disorders. Brain Res Bull 55:155-164.

Tiffany-Castiglioni E, Qian Y (2001) Astroglia as metal depots: molecular mechanisms for metal accumulation, storage and release. Neurotoxicology 22:577-592.

Tjalve H, Henriksson J (1999) Uptake of metals in the brain via olfactory pathways. Neurotoxicology 20:181-195.

Tjalve H, Henriksson J, Tallkvist J, Larsson BS, Lindquist NG (1996) Uptake of manganese and cadmium from the nasal mucosa into the central nervous system via olfactory pathways in rats. Pharmacol Toxicol 79:347-356.

Torchia J, Rose DW, Inostroza J, Kamei Y, Westin S, Glass CK, Rosenfeld MG (1997) The transcriptional co-activator p/CIP binds CBP and mediates nuclear-receptor function. Nature 387:677-684.

Walowitz JL, Roth JA (1999) Activation of ERK1 and ERK2 is required for manganese-induced neurite outgrowth in rat pheochromocytoma (PC12) cells. J Neurosci Res 57:847-854.

Walz W, Mukerji S (1988) Lactate release from cultured astrocytes and neurons: a comparison. Glia 1:366-370.

Weber S, Dorman DC, Lash LH, Erikson K, Vrana KE, Aschner M (2002) Effects of manganese (Mn) on the developing rat brain: oxidative-stress related endpoints. Neurotoxicology 23:169-175.

Wedler FC, Denman RB (1984) Glutamine synthetase: the major Mn(II) enzyme in mammalian brain. Curr Top Cell Regul 24:153-169.

Wedler FC, Toms R (1986) Interaction of Mn (II) with mammalian glutamine synthetase. In: Manganese in Metablism and Enzyme Function (Schramm VL, Wedler FC, eds), pp 221-238. New York: Academic Press.

Wedler FC, Denman RB, Roby WG (1982) Glutamine synthetase from ovine brain is a manganese(II) enzyme. Biochemistry 21:6389-6396.

Wedler FC, Vichnin MC, Ley BW, Tholey G, Ledig M, Copin JC (1994) Effects of Ca(II) ions on Mn(II) dynamics in chick glia and rat astrocytes: potential regulation of glutamine synthetase. Neurochem Res 19:145-151.

Weiner CP, Knowles RG, Moncada S (1994) Induction of nitric oxide synthases early in pregnancy. Am J Obstet Gynecol 171:838-843.

Weisz A, Oguchi S, Cicatiello L, Esumi H (1994) Dual mechanism for the control of inducible-type NO synthase gene expression in macrophages during activation by interferon-gamma and bacterial lipopolysaccharide. Transcriptional and post-transcriptional regulation. J Biol Chem 269:8324-8333.

Wichmann T, DeLong MR (1996) Functional and pathophysiological models of the basal ganglia. Curr Opin Neurobiol 6:751-758.

Wink DA, Mitchell JB (1998) Chemical biology of nitric oxide: Insights into regulatory, cytotoxic, and cytoprotective mechanisms of nitric oxide. Free Radic Biol Med 25:434-456.

Witholt R, Gwiazda RH, Smith DR (2000) The neurobehavioral effects of subchronic manganese exposure in the presence and absence of pre-parkinsonism. Neurotoxicol Teratol 22:851-861.

Wolters EC, Huang CC, Clark C, Peppard RF, Okada J, Chu NS, Adam MJ, Ruth TJ, Li D, Calne DB (1989) Positron emission tomography in manganese intoxication. Ann Neurol 26:647-651.

Xie QW, Nathan C (1993) Promoter of the mouse gene encoding calcium-independent nitric oxide synthase confers inducibility by interferon-gamma and bacterial lipopolysaccharide. Trans Assoc Am Physicians 106:1-12.

Xie QW, Kashiwabara Y, Nathan C (1994) Role of transcription factor NF-kappa B/Rel in induction of nitric oxide synthase. J Biol Chem 269:4705-4708.

Yamada M, Ohno S, Okayasu I, Okeda R, Hatakeyama S, Watanabe H, Ushio K, Tsukagoshi H (1986) Chronic manganese poisoning: a neuropathological study with determination of manganese distribution in the brain. Acta Neuropathol (Berl) 70:273-278.

Yanai T, Shimo-Oka T, Ii I (1991) Manganese ion elicits a binding activity of placenta vitronectin receptor to fibronectin cell-binding domain. Cell Struct Funct 16:149-156.

You ZB, Herrera-Marschitz M, Nylander I, Goiny M, O'Connor WT, Ungerstedt U, Terenius L (1994) The striatonigral dynorphin pathway of the rat studied with in vivo microdialysis--II. Effects of dopamine D1 and D2 receptor agonists. Neuroscience 63:427-434.

Youdim MB, Ben-Shachar D, Riederer P (1993) The possible role of iron in the etiopathology of Parkinson's disease. Mov Disord 8:1-12.

Yuyama K, Yamamoto H, Nishizaki I, Kato T, Sora I, Yamamoto T (2003) Caspase-independent cell death by low concentrations of nitric oxide in PC12 cells: involvement of cytochrome C oxidase inhibition and the production of reactive oxygen species in mitochondria. J Neurosci Res 73:351-363.

Zhang ZG, Chopp M, Zaloga C, Pollock JS, Forstermann U (1993) Cerebral endothelial nitric oxide synthase expression after focal cerebral ischemia in rats. Stroke 24:2016-2021; discussion 2021-2012.

Zhang ZG, Chopp M, Gautam S, Zaloga C, Zhang RL, Schmidt HH, Pollock JS, Forstermann U (1994) Upregulation of neuronal nitric oxide synthase and mRNA, and selective sparing of nitric oxide synthase-containing neurons after focal cerebral ischemia in rat. Brain Res 654:85-95.

Zheng W, Zhao Q (2001) Iron overload following manganese exposure in cultured neuronal, but not neuroglial cells. Brain Res 897:175-179.

Zwingmann C, Leibfritz D, Hazell AS (2003) Energy metabolism in astrocytes and neurons treated with manganese: relation among cell-specific energy failure, glucose metabolism, and intercellular trafficking using multinuclear NMR-spectroscopic analysis. J Cereb Blood Flow Metab 23:756-771.

Zywicke HA, van Gelderen P, Connor JR, Burdo JR, Garrick MD, Dolan KG, Frank JA, Bulte JW (2002) Microscopic R2* mapping of reduced brain iron in the Belgrade rat. Ann Neurol 52:102-105.

APPENDIX A

EXPERIMENTAL PROTOCOLS

A-1 Western Blot

References: Modified from Molecular Cloning and Dr Tjalkens' protocol

Sample Collection

Preparations:

- ✓ Prepare and label 15ml tubes and 4 sets of 1.7ml tubes.
- ✓ Set heat block to 100°C.
- ✓ Prepare 25ml 2%SDS with 1 cocktail tablet of protease inhibitor & 125ul 0.2M sodium orthovanadate (protein phosphotyrosal-phosphatases inhobitor).
- ✓ Warm up PBS, medium with FBS and 0.25%Trypsin plus EDTA.

Steps:

1. Decant medium from the culture dishes and rinse plate rapidly with PBS.
2. Aspirate excess PBS.
3. Add 1ml 0.25%Trypsin plus EDTA to each $60mm^2$ plate for 10min.
4. Add 1ml medium with FBS to collect the cells in tubes.
5. Centrifuge the tubes at 1500 rpm (500g) 5 min.
6. Aspirate the medium.
7. Wash with PBS.
8. Centrifuge the tubes at 1500rpm (500g) 5min.
9. Add 50ul PBS to each tube and mix well then transfer the samples to 1.7ml tubes.
10. Add 200ul boiling 2%SDS with protease inhibitor (1 tablet/25ml) and 1mM sodium orthovanadate (125ul 0.2M sodium orthovanadate/25ml) to each sample pellet. Boil the sample mix for additional 5 min.
11. To reduce viscosity, the sample may be sonicated briefly at room temperature.
12. Centrifuge the sample for 10,000rpm 10 min,
13. Put the supernatant in another set of 1.7ml tube.
14. Aliquot the samples and store them in -80°C.

Detect Protein Concentration by BCA Method

1. Dilute an aliquot of the sample to 10 fold (5ul in 45ul ddH_2O)
2. Make standard protein.
3. Add 10ul each standard protein and the diluted sample in duplicates into a 96 well plate.

4. Make the BCA protein assay reagent A and B (1:50) master mix (from PIERCE).
5. Add 200ul BCA protein assay reagent A and B (1:50) master mix to each well.
6. Incubate the plate at 37°C for 30 min.
7. Set up the plate reader and collect the data.

Pouring Gels

1. Spray glass plates with ethanol and wipe surfaces clean.
2. Add spacers between the glass plates and insert the plates into the gel apparatus (large plate against the plastic holder).
3. Tighten the screws after checking to see that the glass plates and the spacers are flush on the bottom.
4. Place a piece of parafilm on the foam pad and then set the glass plates on top of this.
5. *Insert the combs into the plates and mark a line below the bottom of the combs to mark the amount of gel needed.*
6. *Prepare the separating gel solution from the table below. For the mini gels, 10 ml / gel.*
7. Add the APS and the TEMED last.
8. Pour the gel using a Pasteur pipet. Try to keep bubbles out of the gel. Once the gel is poured, add ddH_2O or Ethanol. This allows for a smooth straight line to form at the top of the separating gel. This can be stored at 4°C overnight. Add water to the top of the gels and cover with saran wrap.
9. Prepare the stacking gel solution from the table below.
10. After the separating gel has set up (> 30 minutes), remove the water or ethanol from the top of the separating gel by turning the apparatus upside down. Wash with 1.5mM Tris-HCl. Using a paper towel, remove any excess liquid that remains in the area where the stacking gel will be poured.
11. Place the combs in the gel apparatus and pour the stacking gel. **Avoid air bubbles at the bottoms of the combs.**
12. Once the top of the glass plates is reached, pull the comb forward and push them down into the gel so that the tops of the wells are not in contact with air. This keeps the wells from shrinking as the gel sets up.

Sample Preparation

1. Determine the volume of sample needed to load the amount of protein desired (10-100ug total protein). This volume should be kept under 20ul if possible. (the volume = the amount of total protein/ protein concentration).
2. Add 5x loading dye (1/4 sample volume) to each sample.
3. Boil the sample mix for 3-5min, then put them on ice.

Running the Gel

1. Prepare the running buffer. Set up running apparatus. Add running buffer to the middle of the apparatus to check for leaking. Place the apparatus into the running chamber and fill the chamber with the remaining running buffer. Remove air bubbles from the bottom of the plates after the running buffer has been added.
2. Carefully remove the combs from the stacking gel. Aspirate out any liquid remaining in the wells or add buffer and rinse the wells. This removes any unpolymerized acrylamide.
3. Load the samples using gel loading tips (10ul/time). Avoid mixing the samples or moving the chamber once the samples have been loaded.
4. Run the stacking gel at 60V (40 min), 7.5% Gel at 100V (2h), keep the amps below 100. The slower the gel runs the more compact the banding patterns will be. Allow the dye front to run off of the gel. (150 min)

Transferring the Gel

1. Prepare the transfer buffer. Cut the membrane and the filter paper to the appropriate size (7cm x 9cm). Dip the membrane in 100% methanol and Whatman filter paper in the transfer buffer for 1h.
2. Stop the gel and remove the gel apparatus from the running chamber. Clean the chamber thoroughly to remove any residual SDS.
3. Remove the glass plates from the holders. Pry the glass plates apart using the spacer.
4. Remove the gel from the glass and place the gel in transfer buffer and allow to equilibrate for at least 20 minutes.
5. Place the transfer chamber in an ice bucket surrounded by ice. Place a stirring bar in the apparatus and get the running buffer cold.
6. Assemble the transferring apparatus in the following manner. **Important not to let the gel or the membranes dry out at any point from now on during the procedure.**

   Black plastic Sponge Filter Paper Gel Membrane Filter Paper Sponge White Plastic

7. When placing the membrane on the gel, roll over the top with a pipet to remove any air bubbles that are present. This should also be done when placing the filter paper. Remember to keep the sandwich wet at all times.
8. Close the transfer sandwich and place in the transfer chamber. **The black plastic should be on the same side as the black plastic of the transfer apparatus.** The proteins will run from the black to the red.
9. Transfer the proteins at 350mA for 2-3h (for protein smaller than 120kDa) or at 350mA for 4-5h (for protein larger than 120kDa) or 60mA 60V overnight (16h) @4°C. Keep the ice unmelted.

10. When the transfer is done, remove the sandwich from the transfer apparatus. Open so that the membrane is still on top of the gel and cut around the gel so that the membrane is the same size as the gel.
11. Wash the membrane in TBS-T for 10 minutes.
12. Block the background with 5% nonfat dry milk in TBS-T for at least 1 hour. This can be placed in the refrigerator overnight.

Blotting the Membrane

1. The primary antibody should be diluted in TBS-T with 5% nonfat dry milk. Use 10ml per membrane. The primary antibody can be freezer thawed.
2. Remove the membrane from the blocking solution and wash for 15 minutes in TBS-T. Wash 2 x 5 minutes after the 15-minute wash.
3. Prepare the seal-a-meal bags to the proper size or a box for the primary antibody.
4. Place the membrane in primary Ab on the shaker and shake for 1-3 hours @ RT or @4°C overnight.
5. Wash the membrane 3 x 10-15 minutes. The wash steps are essential for reducing the background levels on the blots.
6. Prepare the secondary antibody in TBS-T with 5% nonfat dry milk. Again the dilution of this antibody depends upon which antibody is being used.
7. Incubate the secondary antibody for one hour at room temperature.
8. Wash the membrane in TBS-T 3 x 10-15 minutes.
9. Prepare the ECL reagents. 1:40 (50ul:2ml).
10. Place the membrane in the ECL solution for approximately 30 seconds.
11. Remove the membrane and wrap the membrane in saran wrap. Rub the membrane with a Kimwipe to remove excess ECL reagents. This should be done on the outside of the saran wrap.
12. Place the membrane in the film cassette.
13. Expose and develop the film. Different times should be used to determine the proper exposure.

Stripping the Membrane

1. Submerge the membrane in stripping solution.
2. Incubate at 50°C for 30 minutes with occasional agitation.
3. Wash the membrane 2 x 10-15 minutes in TBS-T. Use large volumes of wash buffer.
4. After the wash block and probe the membrane as described above.

Materials:

1. Acrylamide: (40% stock**)**

- 37.5:1
- Store at 4°C

2. 1.5 M Tris-HCl: pH 8.8
   - 54.45 g Tris-base
   - Adjust pH
   - 300 ml H_2O
   - Store at 4°C
3. 0.5 M Tris-HCl pH 6.8
   - 6.0 g Tris-base
   - Adjust pH
   - 100 ml H_2O
   - Store at 4°C
4. 10% (w/v) SDS
   - 10 g SDS
   - 100 ml H_2O
5. 10% Ammonium Persulfate (APS)
   - 0.1g APS
   - 1 ml H_2O
6. Transfer Buffer
   - 200 ml – 5xRunning Buffer
   - 200 ml - Methanol (20%)
   - H_2O to 1 liter
7. 10x Tris-Buffered Saline (TBS): [4L]
   - 24.2 g Tris Base (20 mM) [96.8g]
   - 8.8 g NaCl (150 mM) [35 g]
   - pH to 8.0 with HCl
   - 1000 ml H_2O [to 4L]
8. TBS-T
   - 1 x TBS
   - 0.2 % Tween-20
9. Stripping Buffer 1000ml ? but good
   - 62.5 mM Tris-HCl pH 6.7 [7.571g]
   - 2% Sodium dodecyly sulfate [20g]
   - 100 mM 2-mercaptoethanol (14.3 M stock) [6.9 ul]

   Stripping Buffer 1000ml , Correct
   - 100mM 2-mercaptoethanol (14.3M Stock) [7ml]
   - 2% SDS [20g]
   - 62.5mM Tris-HCl pH6.7 (FW:157.6) [9.85g]
10. 5x Running Buffer with SDS
    - Tris Base 45g
    - Glycine 216.05g
    - SDS 15g

- ddH_2O 3000ml

11. Lysis Buffer (500ml)
    - Hepes[50mM] 5.957g
    - NaCl [500mM] 14.61g
    - MgCl2[1.5mM] 0.0714g
    - EDTA[1mM] 0.1902g
    - 10%Glycerol 50ml
    - 1%Triton-100 5ml
    - pH 7.5, store @ 4°C
12. Ripa Buffer
    - 1xPBS 500ml
    - 1% NonidetP-40 (Amaresco)(Turgital) 5ml
    - 0.5% Sodium deoxycholate (FW:414.6) 2.5g
    - 0.1%SDS 0.5g
    - Store @ 4°C for 1 year
13. 2xSDS Gel-loading buffer
    - 100mM Tris-HCl (pH6.8)
    - 4%(w/v) SDS
    - 0.2%(w/v) bromophenol blue
    - 20% glycerol
    - 200mM B-mercaptoethanol
    - Aliquot and Freeze @ -20°C
14. 5x SDS Gel-loading buffer 50ml
    - 250mM Tris-HCl (pH6.8) 25ml 500mM Tris-HCl (pH6.8) or 1.97g in 25ml H_2O adjust pH
    - 10%(w/v) SDS 5g
    - 50% glycerol 25ml
    - 0.5%(w/v) bromophenol blue 0.25g
    - 500mM β-mercaptoethanol 1.8ul /50ul (Add before use)
    - Aliquot and Freeze @ -20°C
15. 0.2M Sodium Orthovanadate Stock
    - 0.3678g sodium orthovanadate
    - 10ml PBS.
    - Store at room temperature.

A-2 Isolation of Neonatal Mouse Cortical Astrocytes for Primary Cultures

Reference: Contributed by Jeffrey W. Allen, Lysette A. Mutkus, and Michael Aschner Current Protocols in Toxicology (2000) 12.4.1-12.4.15

Materials:

1. 1-day old C57Bl/6J pups from pathogen free time dated pregnant dams.
2. 70% (v/v) ethanol
3. Complete S-MEM (see recipe)
4. MEM medium with 2x Pen/Strep/Neomycin
5. Astrocyte growth medium (from Invitrogen, cat.# 11095-080) (MEM medium with 10%FBS and 1X PSN)
6. 8000 U/ml DNAse I solution (see recipe)
7. 0.08 (w/v) trypan blue staining solution: 1:4 (v/v) 0.4% trypan blue (Life Technologies) in PBS

Table 12.4.1 Timetable for Preparation of Solutions and Instruments

Time	Preparation procedure
1 or 2 days prior to isolation	Fire polish and Sigmacote Pasteur pipets
	Prepare gelatin solution for coverslips
	Prepare borate buffer, stock DNase I, and poly-L-lysine solutions
	Autoclave glass pipets, surgical instruments, 50-ml beakers with stir-bars, coverslips, and gelatin solution
1 day prior to isolation	Check for birth of pups and determine number of pups
	Treat coverslips with gelatin and poly-L-lysine; store in refrigerator overnight
Day of isolation	Check number of 1-day-old pups (i.e., to determine number of extractions)
	Prepare complete S-MEM and place 25 ml plus 10 ml/extraction on ice in 50-ml conical centrifuge tubes
	Prepare dissociation medium and place in the incubator to warm for 1 hr
	Retrieve rat pups from mother and bring to laboratory
	Proceed with dissection and dissociation

7. Dissecting tools sterile:
   Mayo scissors, 7in. (17.8-mm) length, 50-mm curved blade
   Fine-angled micro-dissecting scissors, 4-inch length, 25-mm blade
   Curved forceps, 4-inch length, full curve, 0.8-mm tip width
   Curved forceps, 4-inch length, full curve, 0.4-mm tip width
   Dumont forceps, pattern no. 5, 110-mm length, 0.1x0.06-mm tip
8. Sterile gauze pads
9. Dissecting microscope or 4x to 8x lighted magnifying lamp
10. 50-ml conical polypropylene tubes, sterile
11. 9-inch Pasteur Pipets
    Cotton plugged and sterile
    Cotton plugged, fire polished, Sigmacote treated
12. 50-ml beaker and 25-mm stir bar, sterile (cover with foil prior to autoclaving)
13. 10-ml glass serological pipets, cotton plugged and Sigmacote treated
14. Laminar flow hood
15. 15-ml conical polystyrene centrifuge tubes, sterile
16. Low-speed centrifuge with a swinging bucket rotor and adapters for 50-ml conical tubes
17. Inverted phase-contrast microscope
18. Tissue culture plates of desired size for culturing astrocytes
19. Coated 18x18-mm coverslips
20. Vacuum source
21. Additional reagents and equipment for counting cells with a hemacytometer

Methods:

1. Gently hold pup with thumb and forefinger around thorax and rinse head and neck of pup with 70% ethanol.
2. Using 7-inch curved Mayo Scissors, decapitate a pup and place the head on a sterile gauze pad. Place body in a plastic bag for disposal.
3. Secure the head by holding down the snout. With fine-angled micro-dissecting scissors, cut the skin along the midline from base of the skull to the eyes. Use 0.8-mm forceps to separate the skin and expose the skull as necessary.
4. With 0.8-mm tip curved forceps, sever the olfactory bulbs at the anterior end of the brain and the spinal cord at the posterior end Sever the cerebellum
5. Gently slip the two sides of 0.4-mm tip curved forceps under the cortices on either side of the brain so that the forceps are straddling the brain.
6. Gently move forceps from side to side and, with a slight back angle, pull up the cortices.
   This will separate the cortices from the rest of the brain, which remains in the

head, but care should be taken not to separate the cortices from each other.

7. Place the cortices in a 35-mm petri dish containing MEM with 2xPSN or S-MEM under a dissecting microscope with the dorsal side up and the anterior (rostral) side facing away.
8. Unfold the cortices and remove any extraneous tissue.
9. With Dumont forceps, gently tease away the meningial coverings on the cortical surface.
10. Flip the cortices up and slightly back to expose the underside of the tissue.
11. Gently remove the darker hippocampal crescents with the curved 0.4-mm forceps.
12. Remove any remaining meninges with Dumont forceps.

    The total time spent removing meninges should be ~10 min. per brain.

13. Place cortices in a sterile 50-ml conical polypropylene tube containing 10 ml of MEM with 2x PSN on ice.
14. Repeat steps 1 to 14 with the remaining pups, placing all cortices in a single 50-ml tube on ice.
15. Carefully remove as much MEM with 2xPSN as possible with a sterile, cotton-plugged 9-in. Pasteur pipet, taking care to retain all of the cortices.
16. Add 12 ml pre-warmed (37°C) dissociation medium to a 50-ml beaker with stir bar and carefully pour cortices into the beaker. Gently triturate the cortices four or five ties using a Sigmacote treated 10-ml glass serological pipet.
17. Stir 10 min. at low speed (60 rpm) on a stir plate in a laminar flow hood.
18. While this is stirring, prepare two 15-ml conical polystyrene centrifuge tubes for each two extractions to be performed. Add 5-ml room temperature astrocyte growth medium to each tube. Also thaw DNase I solution and place it on ice.
19. After 10 min of gentle stirring, remove the beaker from the stir plate and place at a 45-degree angle for 2 to 3 min to allow the nondissociated tissue to collect at the bottom of the beaker.

    Resting the edge of the beaker on a lid from a culture dish works well.

20. Carefully aspirate 10 ml dissociated cells with a Sigmacote-treated 10-ml glass serological pipet.

    Take care not to remove the undissociated tissue pieces.
21. Place 5-ml suspension into each of the first two 15-ml centrifuge tubes containing astrocyte growth medium. Invert the mixture two to three times to mix and then allow tubes to sit undisturbed during the continuing extractions.

    The serum in the growth medium acts to inhibit dispase and prevents overdigestion of the dissociated cells.

    During this time, undissociated tissue will settle to the bottom of the15-ml tube. This undissociated tissue will be placed back into the 50-ml beaker for further dissociation dissociation during the final two extractions.

22. Add another 10 ml pre-warmed dissociation medium to the 50-ml beaker and add 75 ul of 8000 U/ml DNase I solution. Continue to stir for another 10 min.

The removal of dissociated cells and replacement with 10-ml dissociation medium is called an extraction.
DNase I is added after the first extraction to prevent the genomic CAN released by damaged cells from making the dissociation medium too viscous during the on-going digestion. Note that it is added only after the first and is not added again.
DNAse I from pancreas is vulnerable to inactivation by physical damage. Mix all DNase I solutions carefully and do not vortex.

23. Place the 50-ml beaker at an angle for 2-3 min, remove 10 ml dissociated cells, and place 5-ml aliquots into a second pair of 15-ml tubes containing astrocyte growth medium.
24. Repeat extractions until there is only fibrous tissue remaining in the 50-ml beaker.
25. To remove undissociated tissue from the 15-ml tubes, insert a sterile, fire-polished, cotton-plugged, Sigmacote treated 9-in. Pasteur pipet to the bottom of the tube and carefully aspirate the undissociated tissue. Place this tissue back into the 50-ml beaker and perform tow final extractions.
    This is done only during the final two extractions because serum carried over from the completed extractions can inactivate the dispase.

Table 12.4.2 Approximate Surface Area, Plating Density, and Growth Medium Volume for Plates Used in the Production of Primary Astrocyte Cultures

Plate type	Surface area (cm^2)	Seeding density[a]	Growth medium (ml)
35-mm	9.40	1×10^5	2
60-mm	28.27	3×10^5	3
100-mm	78.54	7.5×10^5	7
150-mm	176.71	1.8×10^6	15
96-well	0.32	3.2×10^3	0.1
24-well	1.88	2×10^4	0.5
12-well	3.83	4×10^4	1
6-well	9.40	1×10^5	2

[a]Given as cells per plate or well.

26. Pool dissociated cells and medium from the 15-ml centrifuge tubes into 50-ml conical tubes (one 50-ml tube for each five 15-ml tubes). Centrifuge 10 min at 1000-x g, 4C, in a swinging bucket rotor to pellet the suspended cells.
    Centrifugation at room temperature is acceptable if necessary.
    If astrocytes are to be seeded on coverslips, the coverslips should have been incubating overnight in poly D lysine up until this point.

27. Carefully aspirate medium from the cell pellets.
28. Resuspend in 5-20 ml astrocyte growth medium depending on pellet size. Gently pipet with a Sigmacote treated 10-ml tubes on ice.

29. Allow cells to sit for an additional 5-min and remove any sediment tissue as above. Discard this undissociated tissue.
30. Pool the suspended cells into 50-ml tubes on ice.
31. Gently mix 100ul-cell suspension with 100ul of 0.08% trypan blue staining solution. Allow the cells to take up the trypan blue for 2-5 min.
    Trypan blue is sued to determine cell viability. Intact cells are able to exclude trypan blue while dead or damaged cells retain the dye.

32. Determine total cell number and cell viability with a hemacytometer and an inverted phase-contrast microscope.
33. Look at the correct cell density in the table above to determine what volume to plate the cells. Add Astrocyte growth medium to the final volume of cell stock.
34. Incubate cells in a 37°C, 95% air/5% CO_2, and 95% relative humidity incubator.

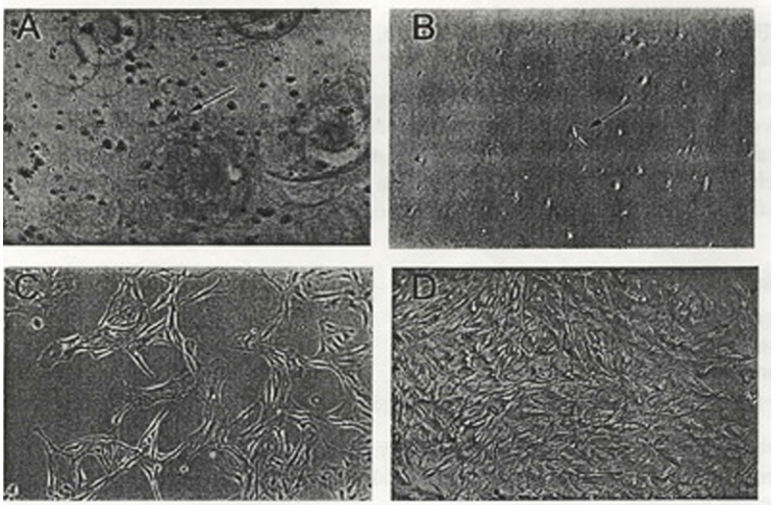

Figure 12.4.1 Primary cultures of neonatal rat astrocytes at various stages of growth (bright-field photomicrographs, 100× magnification). **(A)** 24 hr postisolation but prior to initial medium change. Note the large amount of floating debris. The arrow shows a single attached astrocyte. **(B)** 24 hr postisolation following medium change. Note only a single astrocyte (shown by the arrow) has attached to the cell culture plate in this microscopic field. **(C)** 1 week postisolation. **(D)** At 3 weeks postisolation, the astrocytes are fully confluent.

35. At 18 to 24h after plating, remove old growth medium with a sterile 5 in. Pasteur pipet attached to a vacuum source, and add fresh medium to the volumes as listed in Table 12.42 using a large disposable pipet.
    This is vital in minimizing neuronal, microglial, and oligodendrocyte contamination of cultures. When changing medium, do not completely remove the lid of the culture plates. Instead, use one hand to hold the plate at a slight angle toward you and raise the lid ~45 degree. Change the Pasteur pipet frequently and any time it may have touched anything other than the inside of the culture dishes. A pipet contaminated during medium changes can easily infect the entire culture if it is not changed.
36. Change medium twice per week (e.g., on Tuesday and Friday).

<u>Note:</u> For mouse brain, the dissociation medium is MEM with 2x PSN and 1.5U/ml dispase.

FIRE POLISHING AND SIGMACOTE TREATMENT OF PIPETS FOR CELL ISOLATION

Sigmacote is a prediluted silane-based coating for glass surfaces. It bonds with the uneven surface of glass pipets and provides a smooth hydrophobic barrier. The adherence of cells to the glass surface is greatly reduced, and this minimizes physical damage to the cells. Only pipets used for cell isolation, not routine changing of medium, need to be fire polished and Sigmacote treated. This is most conveniently done in batches of 30 to 50 pipets.

Materials

Sigmacote (Sigma)
9-in. Pasteur pipets
Cotton-tipped swabs
10-ml glass serological pipets, cotton-plugged

1. Fire polish the tip of a 9-in. Pasteur pipet by placing the small end in an open flame from a Bunsen burner for a few seconds. Take care not to make the diameter of the opening too small.

   This will slightly melt the borosilicate glass and will produce a smooth tip to the pipet, which helps prevent damage to the cells. However, if the opening becomes too small, increased shear forces during trituration may lead to increased cell damage.

2. Plug the large end of the Pasteur pipet with cotton removed from a cotton-tipped swab. Use the stick from the swab to push the cotton down to the notch in the neck of the pipet.

   The amount of cotton obtained from a single swab is sufficient for one pipet. With a slight pulling and twisting motion, the cotton is easily removed from the swab.

3. Treat fire-polished Pasteur pipets and 10-ml glass, cotton-plugged serological pipets with Sigmacote by drawing the viscous solution up into the pipet with a portable power pipetter. Do not allow the solution to touch the cotton plug.

   It is not necessary to fire polish or plug the glass serological pipets.

4. Allow the Sigmacote to drain back into the bottle, and allow the pipets to drain and dry completely in a beaker lined with paper towels.

5. Place coated pipets in a metal container and autoclave.

COATING COVERSLIPS FOR ASTROCYTE CULTURE

As a general rule, cultured cells do not adhere well to glass, and thus cell growth on glass coverslips can be difficult. However, many microscopic, histological, or other procedures are necessarily performed on glass, and therefore a procedure for promoting attachment of astrocytes by coating coverslips with gelatin followed by poly-L-lysine is given below.

Materials

2.5% (w/v) gelatin solution (see recipe)
1× poly-L-lysine solution (see recipe)
70% ethanol
H_2O, sterile

18 × 18–mm (no. 2) glass coverslips
Laminar flow hood with ultraviolet light
Sterile forceps
6-well tissue culture plates

1. Rinse 18 × 18–mm (no. 2) coverslips with 70% ethanol and place in an autoclavable container in multiple layers between Kimwipe tissues. Do not crowd coverslips.

   Coverslips must not overlap during autoclaving.

2. Autoclave coverslips.
3. In a laminar flow hood, use sterile forceps to remove coverslips and place them into individual wells of a 6-well tissue culture plate.
4. Add 1.5 ml sterile, room-temperature 2.5% gelatin solution to the surface of each coverslip. Allow gelatin to coat the coverslips for 30 min at room temperature.
5. Aspirate gelatin solution and add 1.5 ml of 1× poly-L-lysine solution to the surface of each coverslip.
6. Incubate plates containing coverslips at 4°C overnight to allow adherence between poly-L-lysine and the gelatin coating.
7. After isolation of cells the following day and ~1 hr before seeding cells, aspirate poly-L-lysine and wash three times with 1.5 ml sterile water.
8. After removing all water, place dishes with coverslips under the ultraviolet light of the laminar flow hood for 30 min to dry the coverslip and to crosslink the poly-L-lysine and gelatin.

   Coverslips are ready for immediate use for culturing astrocytes.

REAGENTS AND SOLUTIONS

Use Milli-Q-purified water or equivalent in all recipes and protocol steps. For common stock solutions, see ***APPENDIX 2A****; for suppliers, see* ***SUPPLIERS APPENDIX****.*

Astrocyte growth medium

900 ml minimal essential medium with Earle's salts (MEM; Life Technologies)
10 ml penicillin/streptomycin (Life Technologies; 100 U/ml penicillin, 100 µg/-liter streptomycin final)
100 ml heat-inactivated horse serum (see recipe; 10% v/v final)
1 ml Fungizone (optional)
Sterilize with a 1-liter sterile filter flask (0.2-µm pore size, cellulose acetate)
Store up to 1 month at 4°C

Penicillin/streptomycin from Life Technologies contains 10,000 U/ml penicillin G and 10,000 µg/ml streptomycin sulfate. Storing penicillin/streptomycin in 10-ml aliquots at –20°C is suggested to avoid repeated freeze-thaw cycles and because it provides the correct amount for 1 liter of medium. (See manufacturer's expiration date.)

Borate buffer

1.24 g boric acid
1.9 g borax
400 ml H_2O
Adjust pH to 8.4 with NaOH
Store at 4°C (stable for many months)

Complete S-MEM

500 ml minimal essential medium with Earle's salts, modified for suspension cultures (S-MEM; Life Technologies)
5 ml penicillin/streptomycin (Life Technologies; 100 U/ml penicillin, 100 µg/l streptomycin final)

continued

Store up to 2 months at 4°C

S-MEM has been modified to contain no Ca^{+2} which can produce cell clumping due to interactions of extracellular matrix proteins.

Penicillin/streptomycin from Life Technologies contains 10,000 U/ml penicillin G and 10,000 µg/ml streptomycin sulfate. Storing penicillin/streptomycin in 10-ml aliquots at –20°C is suggested to avoid repeated freeze-thaw cycles. (See the manufacturer's expiration date.) The use of Fungizone is not recommended.

Filter sterilization of S-MEM is optional.

Deoxyribonuclease I (DNase I) solution, 8000 U/ml

Dilute 15,000 U DNase I from bovine pancreas (type IV; Sigma) in 1.875 ml water. Mix gently; do not vortex. Sterilize with a 0.2-µm syringe filter (cellulose acetate). Store in 100-µl aliquots at –20°C for many months (see manufacturer's expiration date).

DNase I from pancreas is vulnerable to inactivation by physical damage and should not be vortexed.

Dissociation medium

Complete S-MEM (see recipe)
3 U/ml dispase (Life Technologies)

On the day of isolation, prepare 10 ml per brain plus an additional 25 ml (e.g., for 10 brains, add 375 U dispase to 125 ml complete S-MEM). Sterilize with a 150-ml sterile filter flask (0.2-µm pore size, cellulose acetate). Prewarm in a 37°C incubator for 1 hr before use. Discard any unused dissociation medium.

Gelatin solution, 2.5% (w/v)

25 mg gelatin (type A from porcine skin, bloom 300)
100 ml water
Autoclave
Store up to 6 months at room temperature

Heat-inactivated horse serum

Avoid repeated freeze-thaw cycles of horse serum (Life Technologies). To thaw frozen serum, place the bottle in a refrigerator for ~24 to 48 hr. If rapid thawing is needed, place in a water bath that is no warmer than 40°C. Dispense into aliquots in 50-ml tubes and store up to 1 year at –20°C. Thaw at room temperature over a few as hours as necessary.

Thawed serum can be stored for up to 1 week at 4°C, but freezing of aliquots is recommended.

Purchase of horse serum that has been heat inactivated by the vendor is highly recommended.

Poly-L-lysine solution, 1× and 10×

10× stock solution: Dissolve 25 mg poly-L-lysine (Sigma) in 25 ml borate buffer (see recipe). Store up to 2 months at 4°C.

1× working solution: Dilute 5 ml of 10× stock solution into 45 ml borate buffer. Filter sterilize with a 0.2-µm cellulose acetate filter. Prepare fresh each day and keep at 4°C.

Poly-D-lysine is an acceptable substitution for poly-L-lysine and may be preferred due to decreased of digestion of the D isomer by cells (Higgins and Banker, 1998). Regardless of the isomer, the large molecular weight (>300 kDa) preparations should always be used.

A-3 Co-culture PC12 Cells and Primary Astrocytes

Preparations:

- ✓ Wash cover glasses with 70% ethanol. Wipe them dry and have them autoclaved.
- ✓ Laminin Stock Solution (100ug/ml): Put 1ml (1mg/ml) laminin stock solution (from Sigma L2020) in 9ml sterilized PBS. Aliquot in 10 1.7ml tubes. Store at -80°C.
- ✓ NGF Stock Solution (50ug/ml with 2% BSA): Put 0.1g BSA (standard protein) in 5ml ddH_2O, vortex to mix, then sterilize it with a filter (2% BSA). Resolve NGF 100ug (from Calbiochem B49675) in 2ml such sterilized 2% BSA (50ug/ml). Aliquot it and store at -80°C.
- ✓ DMEM-F12 without phenored: Put a bottle of medium in 900ml ddH_2O, rinse the bottle twice. Add 1.2g sodium bicarbanate into the medium. Adjust pH to 7.0 (0.1-0.3 lower than expected PH: 7.2-7.4), add ddH_2O to 1000ml. Filter it in two bottles.

Steps:

1. Six days before co-culture:
    a. Place the cover glasses in the 6 well-plate.
    b. Coat the cover glasses in 6 well-plate with 1ml 5ug/ml laminin (1ml 100ug/ml stock solution in 19ml PBS) overnight.
2. Five days before co-culture:
    a. Aspirate laminin and wash with PBS.
    b. Plate 300,000 PC12 cells per well with 3ml DMEM-F12 with 10% FBS medium.
    c. Put 3ul 50ug/ml NGF (final concentration: 50ng/ml) into each well, grow for 5 days.
3. Three days before co-culture: Plate 20,000 astrocytes onto the inserts placed in a 10cm^2 plate with 5ml DMEM-F12 with 10% FBS medium.
4. One day before co-culture: Infect the astrocytes with adenovirus as follows:

Vector	Stock Solution	Final Concentration
*mt*IκB	$7x10^6$ particles/ml	0.86ul/ml (2.58ul/3ml)
GFP control vector	$5.4x10^6$ particles/ml	1.1ul/ml (3.3ul/3ml)

5. On the day of co-culture:
    a. Wash PC12 cell with PBS.
    b. Put 3ml 10% FBS DMEM-F12 without phenored and PSN medium into each plate.
    c. Treat the cells.

d. Wash primary astrocyte with PBS, directly put the inserts onto the co-culture plate.

A-4 Dopamine and GABA Assay by HPLC

References: Thomas H. Champney, William H. Hanneman and Myesha A. Nichols. γ-Aminobutyric acid, catecholamine and indoleamine determinations from the same brain region by high-performance liquid chromatography with electrochemical detection. Journal of Chromatography, 579(1992) 334-339

Instrument: high-performance liquid chromatography (HPLC) (LC4B, Bioanalytical Systems) with electrochemical detection (ED)

Tissue sample

1. The samples are taken out of freezer, and add 100ul 200ng/ml EPN (in PCA) to each sample. (20ng EPN/ sample, amine internal standard)
2. Sonicate the sample for 2-3 seconds.
3. Draw 10ul for protein assay, dilute by two folds.
4. Centrifuge the sample at 13,000g for 1 min.
5. Wash syringe with 0.1 M parchloric acid (PCA)
6. Draw 25ul **supernatant** of the sample without bubbles.
7. Put the button on ***Loa****d* position, then push the sample into the loop.
8. Push the button to ***Inject*** position and start recording at the same time.
9. Pull chart marker up
10. Set 11 min.

Note: 1. LCEC Analyzer pressure should always in the middle (2500).
2. Double mark your data.
3. Don't forget to take protein sample back with you.

Medium Sample

1. 950ul of the sample is transferred to tubes containing 90ul of 0.4 M perchloric acid.
2. Put the button on ***Loa****d* position, then push 20ul of the standards or samples into the chromatography (HPLC) system loop.
3. Push the button to ***Inject*** position and start recording at the same time.
4. Pull chart marker up
5. Set 11 mins.

GABA Assay of Tissue

1. Add 100ul 150ng/ml epinine (EPN) in PCA to each sample (two punches from striata)
2. Sonicate the sample for 2-3 seconds.
3. Take out 10ul for BCA protein assay.

4. Centrifuge the sample at 13,000g for 1 min.
5. Take out 70ul for DA assay.
6. Add 60ul 70%Ethonal with AVA (aminovaleric acid, 50ng/20ul) to the remaining 20ul sample(1/5th). (Total 80ul, 150ng AVA)
7. Votex well.
8. Take 20ul ($1/20^{th}$) into another 1.7ml tube.
9. Add 20ul derivitizing solution to each tube. (Final: $1/40^{th}$ of the total sample, 18.75ng AVA)
10. Incubate 1 min.
11. Inject 20ul on HPLC.

Materials:

0.4M perchloric acid (PCA):

- 17.6 ml 67-71% perchloric acid (density 1.7kg/L, FW: 100.46)
- ddH_2O to 500ml

A-5 Open Field Activity Chamber

1. Computer Set Up and Data Collection
    a. Click *VersaMax*, if no blue cross, click *configure>animal activity monitor>*two animals
    b. Double click *Versa Map> EXPERIMENT>Set up all test chambers>Sample duration* 1 min *>Primary samples* 15 or 20> *File name> experiment description.*
    c. Click *EXPERIMENT >Set up test chamber*.
    d. Click *EXPERIMENT>Start all experiment*
    e. Insert animals quickly
    f. Click *EXPERIMENT >insert subjects* to begin experiment (screen turn green)
    g. Turn on background noise.
    h. Remove the animals when the screen turns red.
    i. Click *EXPERIMENT > Remove Subjects* to stop the experiment

2. Data Retrieval *VERSADAT>file>open>file generate digiprodata>1>generate* C//*DPR file>Copy to*
3. Data Analysis
    a. Excel DPR open, check where data begin, usually line 57, enter the number where data begins> delimited>next
    b. Move date, subject, and filename to appropriate position.
    c. *Data>SORT>by cage*
    d. Create new worksheet for each parameter
    e. Copy and transpose the data horizontally
    f. To Repeat: *Record as a macro> Stop record*. *Erage>macro>macro*

A-6 Immunohistochemistry

References: Modified from Dr Abbott's protocol

1. Incubate slides in 55°C oven for 15 min. Then cool to room temperature.
2. De-parafinize: 2xXylene, 2x100% ethanol, 1x95% ethanol, 1x70% ethanol, 1xTBS, 5 min each.
3. Antigen retrieval: Boil in 0.01M sodium citrate buffer for 10 min. Add water to original level. Cool to room temperature.
4. Wash 3x5min with 0.05M TBS.
5. Incubate in 0.3%H_2O_2 for 30 min to remove endoperoxidases.
6. Make TrisA/2%BSA. (100ml TrisA+2gBSA)
7. Quick wash the slides with ddH_2O
8. Wash with 0.05M TBS 10 min.
9. Pap pen around tissues.
10. Incubate with Avidin blocking solution for 15 min at room temperature.
11. Wash with 0.05M TBS 10 min.
12. Incubate with Biotin blocking solution for 15 min at room temperature.
13. Wash with Tris A/2%BSA 3x5 min
14. Block with blocking solution: Tris A/2% BSA(2ml) + 10% horse serum(200ul) for 1h.
15. Dilute primary Ab with Tris A/2% BSA(2ml): GFAP 1:400 (2.5ul/ml), TH 1:400 (2.5ul/ml), N-Tyr 1:220 (4.5ul/ml).
16. Pap pen around tissues again. (10 min)
17. Incubate the tissues with the primary Ab at 4°C overnight. (or 1-2h @ RT)
18. Wash with Tris A/2%BSA 3x5 min.
19. Rinse with 0.05M TBS.
20. Wash with Tris A/2%BSA 2x5 min.
21. Add the secondary Ab [Anti-mouse IgG/ Anti-Rabbit IgG (H+L)] 1:200 (5ul/ml) in Tris A/2%BSA, incubate the tissues with the secondary Ab for 1h @ RT
22. Make Avidin/Biotin Complex mix at least 1h before use (one drop of each A & B in 2.5ml of 0.05M TBS) (need 5ml)
23. Wash with Tris A/2%BSA 3x10 min.
24. Rinse with 0.05M TBS.
25. Incubate the tissues in Avidin/Biotin Complex mix for 1h @ RT shaking.
26. Wash with 0.05M TBS 3x10 min.
27. Stain with DAB solution. In 5ml ddH_2O add 2 drops of buffer stock solution, 4 drops of DAB solution, 2 drops of H_2O_2 solution. (Mix after adding each solution.)
28. Staining time varied from different Ab (watch under microscope for the first one): GFAP-1 min, TH-2 min, N-Tyr-3 min.
29. Rinse with ddH_2O.
30. Dehydrate in 1x75%, 1x95%, 1x100% ethanol, 2xXylene, 5 min each. (25 min)

31. Put cover glass on with permount.

Materials:

1. Sample tissue on slides
2. 95% ethanol
   - 100% ethanol 190ml
   - H_2O 10ml
3. 0.05M TRIS Buffer Saline (4L)
   - 6.6g Trizma HCl (26.4g)
   - 1.39g Trizma Base (5.56g)
   - 9g NaCl (36g)
   - 900ml of ddH_2O, pH to 7.6 then bring up to 1L.
4. 10% Triton X
   - 5 ml Triton X-100
   - 45 ml dH_2O
5. 0.3% H_2O_2 (500ml)
   - 10ml 3% H_2O_2 (50ml)
   - 90ml methanol (450ml)
6. TRIS A
   - 200ml TRIS Buffer
   - 4 ml of 10% Triton X
7. TRIS B
   - 200 ml TRIS Buffer
   - 3 ml Goat Serum
   - 4 ml of 10% Triton X
8. Secondary antibody: Vector ABC Kit- 2 drops of Biotinylated Ab in 5ml Tris B.

9. 0.1M Sodium Citrate Stock
   - 29.41g sodium citrate
   - 1000ml ddH_2O
   - pH 6.0

10. Avidin/ Biotin complex: Vector ABC Kit- 2drops of each Avidin & Biotin in 5ml TBS
11. DAB solution
   - In 5ml of ddH_2O
   - 2 drops of buffer stock solution.
   - 4 drops of DAB solution.
   - 2 drops of Hydrogen Peroxide solution.
     mix well after every step.

Notes: When making the TRIS B the type of serum depends on what the antibody was made in.

A-7 TUNEL and Immunofluorescent Antibody Staining

1. Label the slides.
2. Heat oven to 55°C, incubate slides for 15 min. Then cool to room temperature 15 min. (30 min)
3. De-parafinize: 2xXylene, 2x100% ethanol, 1x95% ethanol, 1x70% ethanol, 1xTBS, 5 min each. (35 min)
4. Antigen retrieval: Boil in 0.01M sodium citrate buffer 600ml for 10 min. Add water to original level. Cool to room temperature about 50 min. (60 min)
5. Wash 4x3 min with ddH_2O. (15 min)
6. Wash 1x3 min with PBS.
7. Shake off PBS, circle the slides.
8. Block in Equilibration buffer 10 min.
9. In dark incubate in Reaction buffer or control buffer @ 37°C 45 min.
10. Soak the slides in 1xSSC 15 min to stop the reaction.
11. Wash 5x5 min in PBS.
12. Wash in Tris A 3x3 min.
13. Block 1h in room temperature with 10ml Tris A +2% Serum (200ul serum same as the 2nd Ab).
14. 1st Ab overnight:
    a. rabbit nNOS: 1:200, (50ul/10ml Tris A+2% goat serum).
    b. rabbit Leumorphin: 1:50, (200ul/10ml Tris A+2% goat serum).
    c. rabbit Enkephalin: 1:300, (33.3ul/10ml Tris A+2% goat serum).
    d. goat ChAT: 1:150, (66.7ul/10ml Tris A+2% donkey serum).
15. Wash in TrisA 4x10 min.
16. 2nd Ab Alexafluor 568:
    a. goat anti rabbit 1:1000 (10ul) in Tris A+2% goat serum (made at least half an hour before use).
    b. donkey anti goat 1:1000 (10ul) in Tris A+2% donkey serum (made at least half an hour before use).
17. Wash with Tris A 3x5 min.
18. Mount with [DAPI] antifade 2 drops each slide.
19. Seal the slides with clear nail polish until the slides dry.

Materials:

1xSSC pH 7.0
- 17.53g NaCl
- 8.82g sodium citrate.
- ddH_2O 2000ml, pH 7.0

1xTE pH 7.4
- 10mM Tris-Cl (pH 7.4) (0.5M Tris-Cl pH 7.4 10ml)

- 1mM EDTA (pH 8.0) (0.5M EDTA pH 8.0 1ml)

PBS pH 7.2

- 16.0g NaCl.
- 0.4g KCl.
- 2.3g Na_2HPO_4
- 0.4g KH_2PO_4
- ddH_2O 2000ml, pH 7.2

TUNEL Buffers

Equilibraton Buffer

	2 slides	4 slides	6 slides	8 slides
TE	512ul	1024ul	1536ul	2048ul
5xTT buffer	160ul	320ul	960ul	640ul
25mM$CoCl_2$	48ul	96ul	144ul	192ul

Nucleotide Mix

	2 slides	4 slides	6 slides	8 slides
1mM dUTP	1.5ul	3ul	4.5ul	6.0ul
1mM dATP	3ul	6ul	9ul	12ul
TE	25.5ul	51ul	76.5	102ul

Reaction Buffer

	2 slides	4 slides	6 slides	8 slides
Equilibration Buffer	180ul	360ul	540ul	720ul
Nucleotide Mix	20ul	40ul	60ul	80ul
TdT	4ul	8ul	12ul	16ul

Control Buffer

	2 slides	4 slides	6 slides	8 slides
Equilibration Buffer	90ul	180ul	270ul	360ul
Nucleotide Mix	10ul	20ul	30ul	40ul
TE	2ul	4ul	6ul	8ul

A-8 Isolectin B4 Binding in Brain Slides

Reference: modified from the original protocol of *Localization of Isolectin B4 Binding in Brain Slices or Primary Cultures* from Dr. W. Streit and modified by J.F Bowyer NCTR & D.L. Davies

1. Label the slides.
2. Heat oven to 55°C, incubate slides for 15 min. Then cool to room temperature 15 min.
3. De-parafinize: 2xXylene, 2x100% ethanol, 1x95% ethanol, 1x70% ethanol, 1xTBS, 5 min each. (35 min).
4. Wash 4x with 0.1M NaPB pH 7.4 at least 2-4h to remove any residual formalin.
5. Incubate the slide in blocking solution 1h.
6. Add 5-10ug/ml Isolectin B4 to the blocking solution and incubate the slide at room temperature for 1h, then 4°C overnight.
7. Wash with 3x10 min in 0.1M NaPB pH 7.4.
8. DAB staining for 2 to 4 min.
9. Wash with 3x10 min in 0.1M NaPB PH 7.4.
10. Dry at 50°C for 20min
11. Clear in Xylene and mount cover glass with permount.

Materials:

1. After the brain has been removed after sacrifice and fixation, post fix in formalin less than 2 days before slicing. Make sure brain slices (30 pm or less) have been vibratome cut and stored in PBS pH 7.4 (slices can be stored briefly in PBS containing < 1% formalin for a week)!! Prolonged fixation in formalin will ruin the Isolectin B4 binding.

2. Isolectin B4 is Lectin from Bandeiraea Simplicifolia (BS-l), Sigma L-5391. Isolectin B4 should be stored desicated at -20°C and prepared fresh before use**.** It can be reused 1 time if it is reused within 24 hr of its preparation in our hands. However, this must check out in your own laboratory!

3. 0.1M sodium phosphate buffer (NaPB), pH 7.4
    a. 5.48g NaH_2PO_4, FW 137.99
    b. 22.72g Na_2HPO_4, FW 141.96
    c. 2000ml ddH_2O, pH 7.4

4. Blocking Solution (0.1% Triton X-100, 0.1mM $CaCl_2$, 0.1mM $MnCl_2$ and 0.1mM $MgCl_2$)
    a. 0.004g $MgCl_2$, FW 203.3
    b. 0.004g $MnCl_2$, FW 197.9
    c. 0.004g $CaCl_2$, FW 147
    d. 200ul Triton X-100
    e. 200ml 0.1M NaPB, pH 7.4

Note:

1. The blocking solution have a nasty habit of precipitating so filter the solution with a filter if some ppt. occurs. Excesive ppt. will diminish the effectiveness of the Rx solution.
2. Binding is best to perform on brain slices 30 pm thick in Falcon 24 well tissue culture dishes or 24 well baskets.

A-9 Hoechst & TUNEL Staining in Fixed Cells

Hoechst Staining

1. Wash the cells twice with PBS.
2. Fix with 4% paraformaldehyde 5 min.
3. Permeabilize with 0.1%Triton X100 10 min.
4. Wash with PBS 2x5 min
5. Add Hoechst dye 10uM in PBS, incubate 10 min at room temperature in dark, covered with foil.
6. Wash with PBS 2x3 min.
7. Mount on slides with small drop of Prolong Antifade gel mount (Molecular Probes) (mix 32 drops or 1ml Prolong mounting medium in one brown vial).
8. Do not seal the edge with nail polish until the mounting medium has dried.
9. After sealing, store the slide upright in a covered slide box at –20°C.

TUNEL Staining

1. Wash the cells twice with PBS.
2. Fix with 4% paraformaldehyde 5 min.
3. Permeabilize with 0.1%Triton X100 10 min.
4. Wash with PBS 3x5 min
5. Block with equilibration buffer 10 min.
6. Reaction buffer 30 min at 37°C
7. Soak 1x SSC 15 min to stop the reaction
8. Wash with PBS 3x5 min.
9. Mount on slides with small drop of Prolong Antifade gel mount (Molecular Probes) (mix 32 drops or 1ml Prolong mounting medium in one brown vial).
10. Do not seal the edge with nail polish until the mounting medium has dried.
11. After sealing, store the slide upright in a covered slide box at –20°C.

TUNEL and Hoechst Staining

1. Wash the cells twice with PBS.
2. Fix with 4% paraformaldehyde 5 min.
3. Permeabilize with 0.1%Triton X100 10 min.
4. Wash with PBS 3x5 min
5. Block with equilibration buffer 10 min.
6. Reaction buffer 30 min at 37°C
7. Soak 1x SSC 15 min to stop the reaction
8. Wash with PBS 3x5 min.

9. Add Hoechst dye 10uM in PBS, incubate 10 min at room temperature in dark, covered with foil.
10. Wash with PBS 2x3 min.
11. Mount on slides with small drop of Prolong Antifade gel mount (Molecular Probes) (mix 32 drops or 1ml Prolong mounting medium in one brown vial).
12. Do not seal the edge with nail polish until the mounting medium has dried.
13. After sealing, store the slide upright in a covered slide box at –20°C.

Materials:

TUNEL assay buffers:

Equilibration Buffer:

Component	1x
TE	32 ul
5x Terminal Transferase buffer	10 ul
25mM $CoCl_2$	3 ul
Total	45ul

Nucleotide Mix:

Component	1x
TE	4.25 ul
1 mM dATP	0.5 ul
1 mM Alexa 488 dUTP	0.25 ul
Total	5 ul

Reaction Mix:

Component	1x
Equilibration Buffer	45 ul
Nucleotide Mix	5 ul
TdT Enzyme [or TE for control]	1/0.5 ul
Total	51 ul

APPENDIX B

USEFUL CHEMICALS AND REAGENTS

Chemical Reagent Name	**Application**
rhodamine 110bis(L-aspartic acid amide	Cell permeant pan-caspase substrate
4-amino-5-methylamino-2',7'-difluorofluorescein diacetate (DAF-FM diacetate)	Nitric oxide fluorescent indicator
GW 9662	The specific PPARγ antagonist
1,1-Bis (3'-indolyl)-1-(*p*-trifluoromethylphenyl) methane (DIM-C-pPhCF_3)	The PPARγ agonist
S-Nitroso-N-Acetylpenicillamine (SNAP)	NO donor
(±)-2-Amino-5,6-dihydro-6-methyl-4H-1,3-thiazine (AMT)	A highly selective inhibitor of murine NOS2 (k_i = 4.2 nM)
Hoechst 3342	For nuclear staining
Terminal deoxynucleotidyl transferase-mediated dUTP-biotin nick end-labeling (TUNEL) kit	Detect DNA fragmentation

Acrylamide

Molecular Formula	Molecular Weight	Chemical Properties	Application
C_3H_5NO	71.08	Liquid form is 40% (weight/volume) solution in specially deionized water. Odorless. Readily polymerizes if heated to melting point or if exposed to ultraviolet radiation.	For the production of high molecular weight polyacrylamides. Large quantities of polyacrylamide gel are produced on site for use as a 1) grouting agent. 2) as flocculators (substances that aid the separation of suspended solids from aqueous systems). Smaller quantities of polyacrylamides are used in cosmetic additives. Permanent press fabrics. Electrophoresis, molecular biology applications. Photographic emulsions. Adhesive manufacture.Food processing.

Tris-HCl

Molecular Formula	Molecular Weight	Chemical Properties	Application
$C_4H_{11}NO_3 \cdot HCl$	157.59	Transparent, colorless crystals. Odorless. Soluble in water.	pH Buffer

		Stable under ordinary conditions of use and storage. Burning may produce carbon monoxide, carbon dioxide, nitrogen oxides.	

Tween 20 ™

Molecular Formula	Molecular Weight	Chemical Properties	Application
	1163.92		A surfactant and spreading agent

Lauryl Sulfate (Sodium Dodecyl Sulfate) (SDS)

Molecular Formula	Molecular Weight	Chemical Properties	Application
$C_{12}H_{25}OSO_3Na$ CH3(CH2)11OSOO3Na	288.38	Flammable Solid! Fine, white or slightly yellow powder. Slight fatty odor. Solubility: 10g/100g water	An ionic detergent that is commonly found in household products such as shampoos. The molecule has a tail of 12 carbon atoms, attached to a sulfate group, giving the molecule the amphiphilic properties required of a detergent. In laboratories, SDS is commonly used in gel electrophoresis (SDS-PAGE), where its detergent properties help keep the proteins being studied in a denatured state.

Sodium Citrate

Molecular Formula	Molecular Weight	Chemical Properties	Application
$C_6H_5Na_3O_7$	258.07	White odorless crystals	1.Sodium citrate is used in ice cream to keep the fat globules from sticking together. Citrates and phosphates both have this property. 2. It is also an anti-coagulant. 3. As a buffering agent, it helps maintain pH levels in soft drinks. 4. As a sequestering agent, sodium citrate attaches to calcium ions in water, keeping them from interfering with detergents and soaps.

Ammonium Persulfate (APS)

Molecular Formula	Molecular Weight	Chemical Properties	Application
$(NH_4)_2S_2O_8$	228.19	Off-white crystalline powder. Solubility (2M, H_20): Complete, clear and colorless	A high speed initiator used in polyacrylamide gel electrophoresis

Sodium Orthovanadate

Molecular Formula	Molecular Weight	Chemical Properties	Application
Na_3VO_4	183.91	white to off-white powder. Store at room temperature. Incompatible with strong oxidizing agents.	Sodium orthovanadate should be activated for maximal inhibition of protein phosphotyrosyl-phosphatases.

Glycerol

Molecular Formula	Molecular Weight	Chemical Properties	Application
$C_3H_8O_3$ $CH_2OHCHOHCH_2OH$	92.09	Viscous colourless or pale yellow liquid. Flammable. Stable. Incompatible with perchloric acid, lead oxide, acetic anhydride, nitrobenzene, chlorine, peroxides, strong acids, strong bases.	Widely used as a solvent; as a sweetener; in the manufacture of dynamite, cosmetics, liquid soaps, candy, liqueurs, inks, and lubricants; to keep fabrics pliable; as a component of antifreeze mixtures; as a source of nutrients for fermentation cultures in the production of antibiotics; and in medicine.

Bromophenol Blue Sodium Salt

Molecular Formula	Molecular Weight	Chemical Properties	Application
$C_{19}H_9Br_4O_5SNa$	692	Light pink to purple crystalline powder. pH 3.0 (yellow-green)-pH 3.4 (green)-pH 4.6 (blue) . Slightly soluble in water. Stable under ordinary conditions of use and storage. Incompatible with strong oxidizers	pH indicator, indicating dye for histones, dental cleaning. Tracing dye for acrylamide. Gel electrophoresis.

2-Mercaptoethanol (Thioglycol)

Molecular Formula	Molecular Weight	Chemical Properties	Application
C_2H_6OS, $HSCH_2CH_2OH$	78.13	Clear liquid with disagreeable odor, is produced by synthesis of hydrogen sulphide gas and ehtylene oxide. pH 5.2. Stable under ordinary conditions. Miscible in water and nearly all common organic solvents.	It is a mild reducing agent that is ideal for cleaving disulfide bonds to thiols. It is used for the synthesis of PVC heat stabilizers and as an Intermediate to produce corp protection products,dispersants, fibers, textiles,dyes, phamarceutical products.

VITA

Name: Xuhong Liu

Address: Texas A & M University, 304 Joe H. Reynolds Medical Building,

College Station, TX 77843-1114

Email: xuhongliu@yahoo.com

Education:

2000–2005	Texas A&M University, College Station, TX Ph.D., Toxicology.
1995–1998	Harbin Medical University, Harbin, China M.S., Clinical Neurology.
1989–1994	Harbin Medical University, Harbin, China M.D., Clinical Medicine.

Professional Experiences:

2000–now	Texas A&M University, College Station, TX Research Assistant & Teacher's Assistant
1998–2000	The 2nd Affiliated Hospital of Harbin Medical University, Harbin, China Neurologist and lecturer of Neurology

Publications:

1. Liu X., Buffington J.A., Tjalkens R.B. NF-κB-dependent production of nitric oxide by astrocytes mediates apoptosis in differentiated PC12 neurons following exposure to manganese and cytokines. Molecular Brain Research 141:39-41, 2005

2. Barhoumi R., Faske J., Liu X, Tjalkens R.B. Manganese potentiates lipopolysaccharide-induced expression of NOS2 in C6 glioma cells through mitochondrial-dependent activation of nuclear factor kappa B. Molecular Brain Research 122: 167-179, 2004